

**MTK 19.**

**TUDOMÁNYOS BIZOTTSÁG/LEKTOROK  
SCIENTIFIC ADVISORY BOARD/PEER REVIEWERS**

Bagyinszki Gyula (Budapest)  
Bitay Enikő (Kolozsvár/Marosvásárhely)  
Czigány Tibor (Budapest)  
Dávid László (Marosvásárhely)  
Dezső Gergely (Nyíregyháza)  
Diószegi Attila (Jönköping, Sweden)  
Dobránszky János (Budapest)  
Domokos József (Marosvásárhely)  
Dusza János (Kassa)  
Erdei Timotei István (Debrecen)  
Forgó Zoltán (Marosvásárhely)  
Gobesz Ferdinánd-Zsongor (Kolozsvár)  
Horváth Sándor (Budapest)  
Kakucs András (Marosvásárhely)  
Kelemen András (Marosvásárhely)  
Kovács Tünde (Budapest)  
Kovács Zsolt (Szombathely)  
Markó Balázs (Sopron)  
Máder Patrik Márk (Pécs)  
Máté Márton (Marosvásárhely)  
Pokorádi László (Budapest)  
Radu Sorin Mihai (Petrozsény)  
Réger Mihály (Budapest)  
Roósz András (Budapest)  
Sikolya László (Nyíregyháza)  
Szántó Attila (Debrecen)  
Talpas János (Kolozsvár)  
Tolvaly-Roşca Ferenc (Marosvásárhely)  
Tóth László (Budapest)

**ISSN 2393 – 1280**

# MŰSZAKI TUDOMÁNYOS KÖZLEMÉNYEK

19.

Szerkesztette / Edited by  
BITAY ENIKŐ – MÁTÉ MÁRTON



ERDÉLYI MÚZEUM-EGYESÜLET  
Kolozsvár  
2023

A kötet megjelenését támogatta a Magyar Tudományos Akadémia,  
a Bethlen Gábor Alapkezelő Zrt., és az EME Műszaki Tudományok Szakosztálya.

The publication of this volume was supported by the Hungarian Academy of Sciences,  
by the Bethlen Gábor Fund, and by the TMS – Department of Engineering Sciences,



Copyright © a szerzők/the authors, EME/TMS 2023

*Minden jog a kiadvány kivonatos utánnomására, kivonatos vagy teljes másolására  
(fotokópia, mikrokópia) és fordítására fenntartva.*

*All rights reserved. No part of this publication may be reproduced or transmitted in  
any means, electronic, mechanical, photocopying, recording or otherwise, without the  
prior written permission of the publisher.*

Kiadó/Publisher: Erdélyi Múzeum-Egyesület

Felelős kiadó/Responsible Publisher: Biró Annamária

Szerkesztette/Edited by: Bitay Enikő, Máté Márton

Olvasószerkesztő/Proofreader: András Zselyke (magyar), David Speight (English)

Műszaki szerkesztő/DTP: Szilágyi Júlia

Borítóterv/Cover: Könczey Elemér

Nyomdai munkálatok/Printing-work

F&F International Kft. Kiadó és Nyomda, Gyergyószentmiklós

Ügyvezető igazgató/Manager: Ambrus Enikő

Tel./Fax: +40-266-364171

**Online elérhető/Online available at:**

Magyar/Hungarian

Angol/English

<https://eme.ro/publication-hu/mtk/mtk-main.htm>

<https://eme.ro/publication/mtk/mtk-main.htm>

DOI: 10.33895/mtk-2023.19

DOI: 10.33894/mtk-2023.19



## TARTALOM

### **Bakai Nándor, Zagoráczy Márk Balázs, Rák Olivér, Hillebrand Péter**

*Eszközfejlesztés a virtuális valóság (VR)-technológia felhasználási lehetőségeinek bővítésére, az építéshelyi zuhanásbiztonság területén* ..... 1

### **Bakos Levente Attila**

*Minőségmenedzsment és felelős vállalatirányítás a romániai ipari vállalatok webes kommunikációjában* ..... 6

### **Diós Szabolcs Sándor, Asztalos Gergő Tamás, Husi Géza**

*KUKA KR3 ipari robotegység HMI-tervezése és vezérlése univerzális ipari PC-n Sipy fejlesztőplatform segítségével* ..... 14

### **Dósa János**

*Ipari létesítményekből származó hulladék hő kiaknázásának hatékonysága és ennek lehetséges felhasználása* ..... 22

### **Keresztes Kristóf, Gergely Attila Levente**

*Cserélhető betétes fröccsöntő szerszám tervezése* ..... 32

### **Máté Márton, Gál Károly-István, Tolvaly-Roşca Ferenc**

*Koszinusprofilú lefejtőléccelel gyártott fogaskerékpár szintézise és CAD-vizsgálata* ..... 37

### **Rezes Gábor, Szigeti Ferenc**

*Liftajtók és dekoratív elemeinek védőfóliával való burkolása* ..... 44

### **Szántó Attila, Garai Henrik András, Ádámkó Éva, Sziki Gusztáv Áron**

*Elektromos motorok vizsgálatára fejlesztett mérőrendszer hitelesítése, kalibrálásra* ..... 51

### **Tárkányi Sándor**

*Esettanulmányok az elmúlt 5 év soproni műemlékfelújítási munkáiból* ..... 55

### **Turi Olivér**

*A jászberényi középkori ferences templom barokk átalakítása* ..... 63

**SZERZŐK JEGYZÉKE** ..... 67

## CONTENT

### **Nándor BAKAI, Márk Balázs ZAGORÁCZ, Olivér RÁK, Péter HILLEBRAND**

*Development of Tools for Expanding the Use of Virtual Reality (Vr) Technology in the Field of Construction Site Fall Protection* ..... 1

### **Levente Attila BAKOS**

*Quality Management and Corporate Governance of Romanian Industrial Companies Through Their Web-Based Communication* ..... 6

### **Szabolcs Sándor DIÓS, Gergő Tamás ASZTALOS, Géza HUSI**

*KUKA KR3 Industrial Robot Unit HMI Design and Control with Universal Industrial PC in Sipy Development Environment* ..... 14

### **János DÓSA**

*Review of Possible Waste Heat Sources from Industrial Facilities and Their Potential Use* ..... 22

### **Kristóf KERESZTES, Attila Levente GERGELY**

*Design of an Injection Molding Tool With Exchangable Inserts* ..... 32

### **Márton MÁTÉ, Károly-István GÁL, Ferenc TOLVALY-ROȘCA**

*Synthesis and CAD-Examination of a Cylindrical Gear Pair Derived from a Cosine Profiled Rack* ..... 37

### **Gábor REZES, Ferenc SZIGETI**

*Covering Elevator Doors and Decorative Elements with a Protective Film* ..... 44

### **Attila SZÁNTÓ, Henrik András GARAI, Éva ÁDÁMKÓ, Gusztáv Áron SZIKI**

*Validation and Calibration of a Measurement System for Testing Electric Motors* ..... 51

### **Tárkányi Sándor**

*Case Studies from the Last 5 Years' Restoration Projects of Historic Monuments in Sopron* ..... 55

### **Olivér TURI**

*The Baroque Renovation of the Medieval Franciscan Church of Jászberény* ..... 63

**LIST OF AUTHORS** ..... 67



# DEVELOPMENT OF TOOLS FOR EXPANDING THE USE OF VIRTUAL REALITY (VR) TECHNOLOGY IN THE FIELD OF CONSTRUCTION SITE FALL PROTECTION

Nándor BAKAI,<sup>1</sup> Márk Balázs ZAGORÁCZ,<sup>2</sup> Olivér RÁK,<sup>3</sup> Péter HILLEBRAND<sup>4</sup>

<sup>1</sup> University of Pécs, Faculty of Engineering and Information Technology, Department of Engineering Studies, Marcell Breuer Doctoral School, [bakai.nandor@mik.pte.hu](mailto:bakai.nandor@mik.pte.hu)

<sup>2</sup> University of Pécs, Faculty of Engineering and Information Technology, Institute of Smart Technology and Engineering, Department of Engineering Studies, BIM Skills Lab Research Group, [zagoracz.mark@mik.pte.hu](mailto:zagoracz.mark@mik.pte.hu)

<sup>3</sup> University of Pécs, Faculty of Engineering and Information Technology, Institute of Smart Technology and Engineering, Department of Engineering Studies, BIM Skills Lab Research Group, [rak.oliver@mik.pte.hu](mailto:rak.oliver@mik.pte.hu)

<sup>4</sup> University of Pécs, Faculty of Engineering and Information Technology, Institute of Smart Technology and Engineering, Department of Engineering Studies, BIM Skills Lab Research Group, 3D Printing & Visualisation Centre, [hillebrand.peter@pte.hu](mailto:hillebrand.peter@pte.hu)

---

## Abstract

In the construction industry, the occurrence of work accidents is considered to be a critical issue. With advancements in technology, various innovative tools and methodologies have emerged that may provide solutions to mitigate this risk. One of these technologies could be virtual reality that has the potential to enhance worker safety by providing a controlled environment for practicing relevant safety tasks during safety training. The objective of the research and development was to create a system that links fall protection equipment in the physical environment with the virtual space. This study presents a comprehensive examination of the methodology, outcomes of the tool development, and the evaluation of this system.

**Keywords:** *health and safety, fall protection, virtual reality, AEC industry.*

---

## 1. Introduction

The risk of accidents at work in the construction industry is particularly high. It has been presented in research that between 2001 and 2020, 5% of all accidents at work in Hungary occurred in the construction industry, and in a narrower 5-year period between 2014 and 2018, 17% of accidents were caused by workers falling to a lower-level [1]. This ratio shows that it is of paramount importance to investigate how to prevent accidents at work caused by falls from a height. With the development of technology, several innovations are emerging that could provide solutions to the above-mentioned problem. One of these is virtual reality (VR) technology. Researchers have explored the various possibilities for the use of VR in the construction industry, with a large number of studies focusing on architectural design

support, architectural visualisation, building information modelling (BIM), quality control, and education [2]. In recent years, there have been tool developments [3] and publications that focus on the use of VR technology for fall protection [4]. This paper presents details of a research and tool development project that investigates the feasibility of combining virtual space with real fall protection tools, thereby expanding the application of VR technology for fall protection.

## 2. Introduction of research and tool development

### 2.1. Choosing the right VR and fall protection equipment

The first step of the research was to identify the VR and fall protection tools that could be used to achieve the development objectives. Profession-

al VR devices can typically be divided into two main categories, standalone VR solutions and PC VR solutions. A major advantage of standalone VR solutions is that the applications are run on the device and therefore do not require a computer connection. This solution gives users much more freedom of movement and freedom of action compared to wired PC VR glasses. There are two possible ways to manage the running applications, one is to use controllers and the other is hand tracking. For the hand tracking, devices typically use an infrared camera to determine the position of the hand. From the point of view of the device, this solution has the disadvantage that it is difficult or impossible to apply it to other object tracking in addition to hand tracking.

In the case of PC VR solutions, the VR goggles are connected to a computer by a wire or, in some devices wirelessly, and the application is running on the computer. The VR application is typically handled by controllers as well, but there are some manufacturers that provide various developer solutions for custom accessories. Taking this into account, the Vive PRO VR set from HTC was selected for this research and device development, and a wireless adapter was added to improve its mobility. The product can be extended with a sensor called VIVE Tracker 3.0, which can be used to integrate fall protection devices into virtual space.

One of the most used fall protection devices is a lanyard with a shock absorber, which is easy to learn and requires no prior training. A lanyard with a shock absorber has one end attached to a body or waist strap on the user and the other end attached to a mooring point. Anchoring to the mooring point shall be a twist lock carabiner or screw gate carabiner or scaffold hook carabiner. Looking at the possible devices, it can be concluded that twist lock or screw gate carabiners vary in size between 10 and 15 cm, which is not sufficient to secure the HTC Vive Tracker 3.0, which measures approximately 8 cm. It could not work without affecting the functional operation of the carabiner. Scaffold hook carabiners are significantly larger, averaging 21-35 cm in length, which may be suitable for mounting the sensor. Considering the above parameters, the Portwest FP51 type Y strap equipped with FP 35 type scaffold hook carabiners were selected for the research.

The tools used in this research are shown in [Figure 1](#).



**Figure 1.** Tools used in the research: (1) HTC Vive PRO VR glasses, (2) VIVE Wireless Adapter, (3) SteamVR Base Station 2.0, (4) Portwest FP51 Y sling, (5) Portwest FP35 hook carabiner, (6) CADO AT 150 fixed mooring point, (7) CADO AT 150 fixed mooring point.

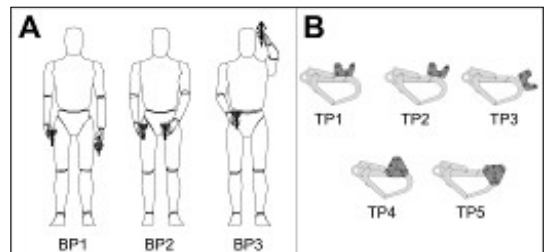


**Figure 2.** Examined (A) body and (B) sensor positions.

## 2.2. Examining possible solutions through 3D analysis

HTC Vive Pro uses the SteamVR Base Station 2.0 to track the spatial movement of the user and determine the position and movement in the virtual space. For this it is using signals reflected from sensors on the VR glasses, controllers and the Vive Tracker 3.0 sensor. The aim of the test was to determine the correct position of the base stations, including the position of the sensor on the carabiner.

The base station can detect in the vertical direction  $110^\circ$  in the horizontal direction  $150^\circ$  at a range of 7m [5]. The size of the "playing field" using two base stations is  $5 \text{ m}^2$ , which can be extended to  $10 \text{ m}^2$  -re using 4 base stations [6].

A three-dimensional analysis of the possible configurations was carried out using ArchiCAD 25 design software, in which the spatial configurations were modelled ([Figure 3.](#)), considering the body positions and sensor positions ([Figure 2.](#)).

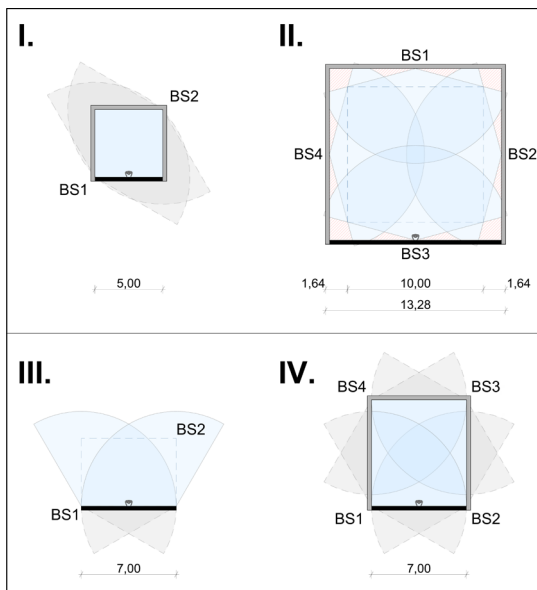


Figure 3. Possible configurations for base stations.

The "camera" tool in the software provides the possibility to set the real position and the exact field of view for the base stations. In addition to the position of the base stations, the analysis also included the visibility of the sensor (Figure 2. B) mounted on the carabiner in the different possible positions of the three body positions (Figure 2. A) that occur during use. For reliable operation, at least three sensors from at least two base stations must be visible on the sensor at the same time. The study recorded the number of sensor visibility from each base station on the left and right hand carabiners for different base station configurations (Figure 3.), in different body and sensor positions (Figure 2.). As a first step in the analysis, the proposed base station positions in the manufacturer's instructions were examined (Figure 3. I., II.). The proposed position of the base stations is defined so that the user should stand in the center of the space, if possible. It is not feasible for this situation as the mooring points have to be fixed to some vertical surface, e.g. a wall. In the case of the four base station set up (Figure 3. II.), there are many areas next to the wall surfaces that are outside of the proposed detection range of the base stations. For the two-base station configuration (Figure 3. I.), it was found that in the examined three body positions, the carabiner, and the sensor on the hand (BS2) are not visible, so there is a risk that the position of the carabiner in virtual space may be inaccu-

rate during its use. Based on the experience of the preliminary study, two configurations (Figure 3. III., IV.) were defined to ensure that the base stations have a proper view of the sensors.

It was found that for configuration III, enough sensors are visible from all three body positions and for different sensor positions (Figure 2. TP1 and TP2). In the other cases, the number of sensors visible was less than three. For configuration IV, all sensor configurations in all body positions ensured that at least three sensors were visible from at least two base stations. Furthermore, by examining the possible positions of the sensors, it was also found that sensors placed on the upper plane of the carabiner (TP1, TP2, TP3) are less likely to be obscured. Looking at the sensor positions TP1, TP2, and TP3, there is no significant difference between them.

### 2.3. Analysis of possible solutions through physical testing

After the analysis in virtual space, the devices were physically tested. The main objective was to determine how the sensor could be attached to the carabiner in a way that would not interfere with the operation of the carabiner, would not prevent the carabiner from being hooked into the mooring point, and would not risk damaging the sensor. During the tests, the attachment of the carabiner to two different mooring points was examined to determine which one might be suitable for future VR development. The first was a CADO AT 180 fix anchor made of a single-point steel plate and the second was a CADO AT 150 fix attachment point with two fixing points. To avoid damage to the Vive Tracker 3.0, a 3D-printed replica of the device was attached to the carabiner for testing (Figure 4.). The physical tests were based on the sensor positions shown in Figure 2.

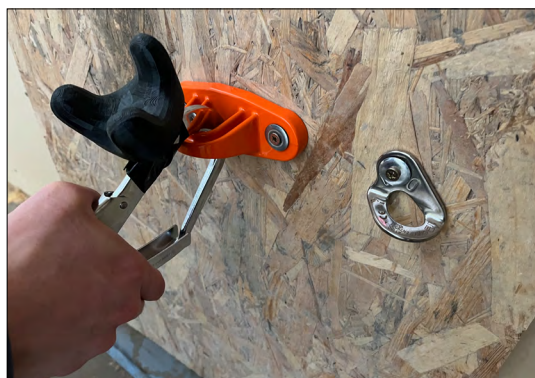


Figure 4. Physical testing.



The testing identified the following statements:

- in the case of TP1, the sensor is highly interfering with the release of the carabiner locking mechanism, but it does not affect the hooking of the carabiner in the anchorage point;
- in the case of TP2, the sensor slightly interferes with the opening of the carabiner, it does not affect the hooking of the carabiner in the anchorage point;
- in the case of TP3, the sensor does not affect the opening of the carabiner, but the sensor may be damaged when the carabiner is hooked;
- in the case of TP4, the sensor is highly interfering with the release of the carabiner locking mechanism, it does not affect the hooking of the carabiner to the anchorage point;
- in the case of TP5, the sensor does not affect the opening of the carabiner, but the sensor may be damaged when the carabiner is hooked;
- for all the attachment methods examined, there is a risk of damage to the sensor due to the rotation of the carabiner after hooking;
- it was also found that the hole in the CADO AT 150 steel plate mooring point was of a size suitable for hooking the carabiner, but too small to allow accurate hooking while wearing VR goggles.

#### 2.4. Description of the tool development

Based on the results of the three-dimensional and physical space tests, an accessory was designed in Shapr3D software to mount the sensor on a carabiner (Figure 5.). A key design consideration was that the accessory should reduce the risk of damage to the sensor and provide adequate space to operate the carabiner's locking mechanism. In addition, in accordance with the manufacturer's instructions [7], it was necessary



Figure 5. 3D model of the designed device.

to ensure that the carabiner should be at least 30 mm from the lower plane of the sensor. The integration of the carabiner in virtual space was done in the Unity development environment using an accurate 3D model of the hook carabiner of the HTC Vive Tracker 3.0 and the attachment accessory.

#### 2.5. Testing the prototype of the device

As part of a non-representative evaluation, 5 people tried the first version of the tool. The feedback from users was consistent: the tool was sufficiently accurate and suitable for integrating the hook carabiner in the virtual space and could be used for future developments.

#### 4. Further objectives of the research

The objectives include the further development of the tool and the solution of the opening mechanism in the virtual space. In addition, the aim is to create simulation courses that combine physical and virtual space for learning and practicing different tasks related to fall protection. Future plans include a detailed study of the potential educational uses of simulation and their validation using scientific methods.



Figure 6. The developed device in operation.

## 5. Conclusions

The study describes the development of tools to link fall protection devices with VR technology. The three-dimensional analyses and physical tests that formed the basis of the development were presented. Based on these results, the development of tools was presented, and further research directions were outlined. As a result of the research, it can be concluded that it is possible to combine VR technology and fall protection devices by using appropriate VR solutions.

## Acknowledgements

Supported by the ÚNKP-22-3-II New National Excellence Program of the Ministry for Culture and Innovation from the source of the National Research, Development and Innovation Fund.

The HTC Vive Pro VR set used for the research was provided by the BIM Skills Lab Research Team.

## References

- [1] Bakai N. et al.: *Az építőipari munkabalesetek megelőzésére és csökkentésére irányuló beavatkozási területek – statisztikai adatelemzéssel történő – meghatározása*. Magyar Építőipar, 3–4. (2021) 90–99.
- [2] S. Safikhani, S. Keller, G. Schweiger, J. Pirker: *Immersive Virtual Reality for Extending the Potential of Building Information Modeling in Architecture, Engineering, and Construction Sector: Systematic Review*. International Journal of Digital Earth, 15/1. (2022) 503–526.  
<https://doi.org/10.1080/17538947.2022.2038291>.
- [3] Bakai N., Etlinger J., Simon D. E., Rác V. N., Rák O., Zagorác M. B., Hillebrand P.: *Application of Virtual Reality Technology for Fall Protection in the AEC Industry*. In: 2022 1st IEEE International Conference on Cognitive Aspects of Virtual Reality (CVR), Budapest, Hungary, 2022, 000035–000036.  
<https://doi.org/10.1109/CVR55417.2022.9967533>.
- [4] Y. Shi, J. Du, C. R. Ahn, E. Ragan: *Impact Assessment of Reinforced Learning Methods on Construction Workers' Fall Risk Behavior Using Virtual Reality*. Automation in Construction, 104. (2019) 197–214.  
<https://doi.org/10.1016/j.autcon.2019.04.015>.
- [5] Tips for Setting up SteamVR Base Station 2.0.  
[https://www.vive.com/eu/support/vive-pro2/category\\_howto/tips-for-setting-up-base-station2.html](https://www.vive.com/eu/support/vive-pro2/category_howto/tips-for-setting-up-base-station2.html) (accessed on 2023. feb. 26.).
- [6] What Things Should I Consider when Installing More than Two SteamVR Base Stations 2.0?  
[https://www.vive.com/eu/support/vive-pro2/category\\_howto/considerations-to-make-when-installing-more-than-two-base-stations.html](https://www.vive.com/eu/support/vive-pro2/category_howto/considerations-to-make-when-installing-more-than-two-base-stations.html)
- [7] HTC\_Vive\_Tracker\_3.0\_Developer\_Guidelines\_v1.1\_06022021 (accessed on 2023. feb. 26).  
<https://developer.vive.com/>



# QUALITY MANAGEMENT AND CORPORATE GOVERNANCE OF ROMANIAN INDUSTRIAL COMPANIES THROUGH THEIR WEB-BASED COMMUNICATION

Levente Attila BAKOS

*Sapientia EMTE, Department of Mechanical Engineering, bakos@ms.sapientia.ro*

---

## Abstract

Contemporary quality management is a more complex issue than first impressions might suggest. In order to continuously assure a certain quality level, it is necessary, albeit far from sufficient, to create optimal technical conditions. Some non-productive activities can also be crucial in quality assurance. We considered the quality manager and the manager for public relations/social responsibility to be of particular importance in this issue. In our research, we examine to what extent the two roles are present in some Romanian organizations. The research sample is 158 companies, of which 92 are companies showing outstanding performance at the national level, and 66 are predominantly small and medium-sized local companies from Transylvania. The data show that there is little difference between the two types of company in the area of social responsibility, while there is a significant difference in the case of corporate governance based on OECD principles. While, at local level, the quality assurance details are somehow hidden, or less visible due to some kind of indolence, the lack of corporate governance is obvious, the companies -if they apply these principles- show transparency, accountability.

**Keywords:** *quality management, quality, corporate governance, corporate social responsibility, Public Relations in industry.*

---

## 1. Introduction

Even the smallest production company is aware that to meet high quality standards it is far from sufficient to properly design the products and production processes. The available workforce, production-supporting processes and the degree of commitment of the management are just few of the factors that directly determine the quality of the products. The concept of quality today is becoming broader than ever. It depends on previously unexamined factors such as the stakeholder identification accuracy, environmental parameters, digitization level, socio-psychological conditions, ethical and legal norms. All these components may contribute to what we mean by quality today. [1]

Total quality management presumes today to improve all processes within the organization – including its supply chain- in order to exceed current and future customer needs. [2] Today,

quality is now not only the direct responsibility of the engineers and managers, but of all people working in the organization. All areas of activity call for attention to dimensions that no one previously considered to be performance factors in industrial systems.

## 2. Quality and leadership

The advanced quality management principles, methods and techniques, developed especially in industrial systems, have become widespread management principles, even in many non-industrial fields. [3] Quality management methods, as theory and practice, have a clear positive and direct impact on product and process innovation. They can also improve indicators such as customer/employee satisfaction or market share. [4]

As we can see, quality assurance is a definitively more complex process than it may first appear.



While quality is primarily the result of an activity (based on the real or induced qualities of the product, shaped in the mind of the consumer), quality assurance is the ability of an organisation to produce a certain level of quality on a continuous and sustainable basis. To achieve this, it is far from sufficient to have the right technical conditions (e.g. proper equipment, carefully made technology design, right machine set-up and skilful operators), it is necessary within an overall supportive organisational environment. In fact, only a fraction of quality management activities and decisions relate to actual technological issues. In real context, several other processes usually require funding and senior management attention to provide a constant quality level. The lack of funding for some non-productive activities means in fact a breach of quality management principles and a lack of management support. Under current standards and concepts, the responsibility for quality assurance lies on the top management of the enterprise in all circumstances. The first evidence of the absence of full commitment is the unwillingness of managers to develop clear job descriptions in the organization (primarily in the quality assurance field). As a starting point for our research, we set out to investigate if there are clearly separated roles defined to support the work of top managers regarding quality assurance. In our assumption, each organization –in order to achieve a constant quality level of its products- must define an organizational chart with clearly visible roles, both for internal and external stakeholders. We investigated the existence of two of key positions regarding the quality management: The Quality Manager and the Public Relations/Social Responsibility Officer/Manager.

### 3. Quality and public relations

Companies operating in industrial environments, by proper CSR communication, can significantly increase their firm-value. [5] Guo et al. demonstrated that this increase in firm's value, even though in lesser extent, is present and enhances the firm's reputation in the industry even when it has to operate in a controversial and conflicting context at a given moment. [6]

While the optimal technical and organisational conditions for the best quality standards are just a small part of the quality management activity, the management must demonstrate and promote these capabilities in many other contexts. If the

measurable technical features of the product are inferior comparatively to competing brands, market success depends on the salespeople, marketers and, not least, those who are managing the reputation and image of the company. It is their job to make the product competitive even if it is not technically so competitive. In such circumstances, the marketing and PR specialist becomes as important a player as the engineers responsible for the production process.

Quality management methods often imply a significant change in organisational culture. Most of the companies around the world try to achieve this upgrade using Japanese or American recipes. Unfortunately, these practices may differ significantly from the domestic organisational culture, containing foreign clichés, slogans and working methods that are difficult to assimilate, especially at the level of the workers. The EFQM quality management model [7], which is a bit closer to the European business culture, is to some extent an exception. However, even when adapting EFQM, it is important to involve both technical managers and communication experts to facilitate the change. Some PR techniques may help the introduction of changes and support to achieve the objectives set. A PR professional, with his knowledge of the art of communication, can facilitate the work of those who are responsible for implementing these modern management concepts. The first condition for QM and PR professionals to work together is that both roles exist within the structure of the organisation. We explicitly sought and examined this in our research. At the same time, we studied a less obvious image-building issue, namely, how quality management and CSR (Corporate Social Responsibility) may contribute. Obviously, it is a blinkered view to classify QM and CSR activities as conscious image-building task, but certainly, there are some connections to it. Empirical studies, through statistical measurements, proved that the emphasis on CSR, TQM and proper Corporate Governance contributes to a high level of sustainability of the organisation [8]. Today, there is no doubt that CSR has a significant role in competitiveness. In a similar study to ours, G&A Institute, found that 92% of companies on the S&P500 list regularly report on their sustainability activities [9]. In our research, we did not find a single multinational company without CSR information on their website. As a rule, the CSR acronym is present on the first page of the website. It is obvious that the CSR activity has measurable impact on financial

results, customer relations, risk management, human resource management, innovation capacity, on anything that has a direct bearing on what we mean today by quality. It is no longer a social desire, but a condition of being on market to demonstrate the responsibility and openness to handle some of issues defined by the community in which the organization acts [10]. The EU institutions [11, 12] the International Organisation for Standardisation ISO [13], and the OECD [14], are formulating recommendations, guiding principles and standards to create a consistent, uniform CSR framework.

#### 4. Corporate governance principles and CSR

There several similarities between the concept of corporate social responsibility and the concept of corporate governance, to such an extent that it is worthwhile to distinguish the two areas in academic analyses. [15] Our research confirmed these similarities on several points, and of course, we succeed to point out some of the differences. The OECD concept of corporate governance (CG) is a more formalised set of governance principles, in a legal sense, in contrast to the CSR concept, which argues for a commitment above the legal framework. Furthermore, CG focuses primarily on internal mechanisms, whereas CSR focuses more on the external environment of the organisation.

Few decades ago, corporate governance was a new topic even for practitioners, but nowadays it is in the focus of the European Union, the OECD, the World Bank and the International Monetary Fund, and its literature is growing exponentially [15]. The OECD (Organisation for Economic Co-operation and Development) is one of the world's most important organisations for economic cooperation between countries, currently with 38 member states, and membership is a matter of prestige. Its aim is to coordinate the best possible economic and social policies for the member states, and addresses specific issues such as corporate governance at the company level. [16] In Romania, the OECD principles of CG is a mandatory standard in the case of state companies. In order to become a full member, the state encourages adopting the CD principles at all companies, being compulsory –setting by the OG109 regulation- [17], to all state companies. Notwithstanding this, CG management is also prevalent in multinational companies, as well as in listed

companies. Today, it is common that prospective business partners, before entering into their first direct contact, inquire about their governance model and about the way this is actually put into practice in site. Actually, this analysis may consist of the examination of all the three mentioned areas (QM, CSR and CG) simultaneously. Through the analysis of QM, it should be relevant to see the level of compatibility of the two organizations regarding quality standards and commitment to quality. In the case of reputation management and CSR it should be interesting to see sensitivity to public interest issues and the level willingness to take conscious responsibility. Last, but definitely not least, the existence a visible CG governance model can reassure that a prospective business partner has a transparent, well-regulated and legally accountable relationship with its stakeholders. It is safe to say that all three aspects and activities are of paramount importance in building a company's image, not only in meeting customers' expectations, but also in building partnerships. In our research, we investigate the extent to which the above three aspects are reflected in the organisation chart of Romanian companies, especially at local small and medium-sized enterprises.

#### 5. Research results

Our research methodology, among the different methodologies of social sciences, falls into the category of content analysis (see e.g. [18]) We proposed to evaluate how the investigated companies reveal their staff for quality management and public relations/corporate social responsibility, based on their website. Data collection took place from August to November 2022. The study sample consists of 158 companies located in Romania. In the first phase of the research, we surveyed large companies. The selection was based on publicly available data from several web sources [19, 20]. We did not necessarily aim at a top-list search, neither by turnover, nor by the profit of the previous years, nor by number of employees. The search criteria for certain types of manufacturing companies was based on their CAEN code (the code system for classifying economic activities in Romania). [21] In spite of the fact that several data were available, it was not our intention to identify the largest industrial companies (measured by any parameter), nor is accurate accounting data relevant to the analysis. The aim is to compare the situation of the leading companies in certain industries with that of

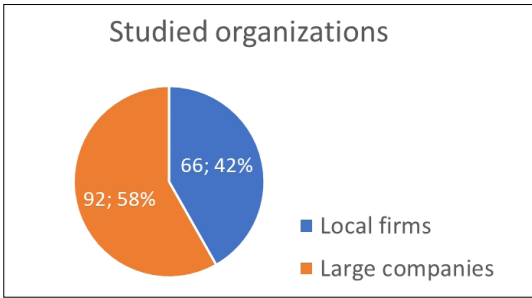


Figure 1. The type of the surveyed companies

companies operating in similar fields in our own region (Mureş and Harghita counties). In the second half of the research, these companies were analysed. These firms, being manufacturing companies, actually are not acting locally, as many of them are present in global markets. Still, due to their size (small and medium-sized companies) and location, we will name them as local companies. Figure 1 gives an indication of the classification of the companies surveyed, according to whether they are major companies at national level or local small/medium sized companies. We can see in the picture, that we have slightly more large companies, as they were relatively easier to identify from the sources.

After identification of firms, we searched for data related to quality management and social responsibility. The search sequence was as follows:

1. Organisation chart
2. CV of managers/ description of the organisational sub-units
3. News feed
4. Body text

As a first step, we looked to see if the organisational chart was available on the website and, if so, whether quality management and corporate social responsibility as separate activities are present on the chart. During the analysis, we found that the organisational chart is generally not publicly available, as only 24 of the 158 companies surveyed had an organisational chart on their website. Where we did not find the chart, or where there was no separate quality management or responsibility evident role, we did a second search to identify the two functions. This time we searched for data on the CVs of the management and/or the description/presentation of certain organisational sub-units. If the first two criteria search did not yield data, we searched for data in the news feeds or the content section of the website. We show the source of our data in figure 2.

The abbreviations CSR and QM in the figure are only labels, as they indicate the research study question in a very narrow sense. The CSR designation was used to refer not only to persons/activities involved in CSR, but also more broadly to everything related to public relations, stakeholder management, lobbying, customer relationship management and other related areas. We decided to use the acronym CSR because we were looking primarily for activities related to the issue of corporate social responsibility. If, during the analysis, we found communication related to only one of the areas listed, i.e. only to image, lobby relations or customer relations, we did not consider the company responsible in a social sense, as we believe, it focuses on only one narrow area, probably driven by self-interest. As far as the term QM

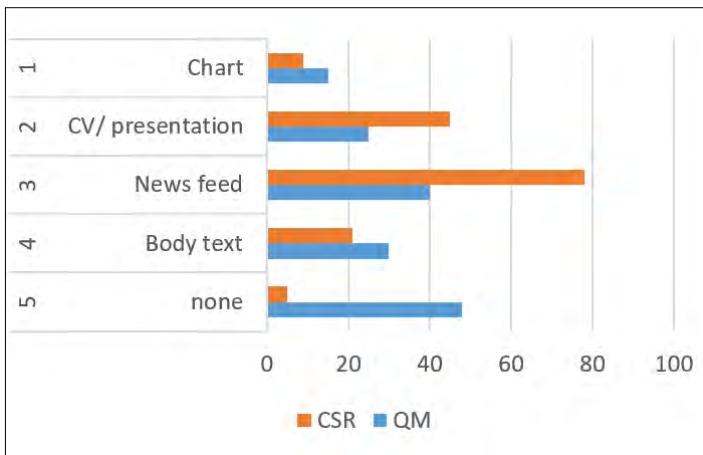


Figure 2. Source of data.

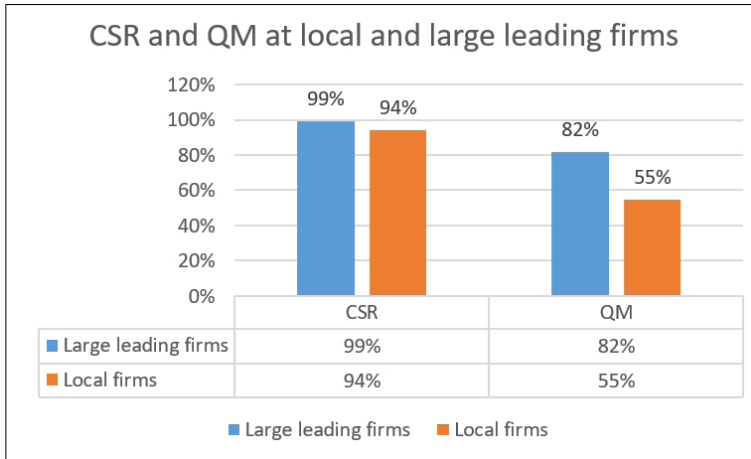


Figure 3. Corporate social responsibility and quality management-

is concerned, we do not necessarily mean QM as used in a technical context. Quality management and control should be focused not only on manufacturing processes, but also on all other activities (from purchasing to after-sales service), as well. The second figure also shows that we have found among the companies surveyed several that did not include any information at all related to quality management or social responsibility. These all were small local companies. Since the main driving force of the research was to understand the situation of local companies, and to compare these companies with market leaders, in the field of quality management, the comparison was mainly made in the above two areas. Figure 3 compares the difference between CSR and QM for the two types of companies, based on the data found on the companies' websites.

The data show that with regard to CSR the difference is less than 5% between the two types of companies. Most of the companies treat their websites as an important tool to show their commitment to social issues. Even for the smaller companies, it seems to be important to indicate that they are active in their social environment, at some level. Most of the studied websites did not present a clear connection between CSR and quality management activities. This is actually a good thing, since this relationship should not even appear; CSR contributes to the overall quality precisely by not linking it to the product or service produced during the core activity.

As for the QM area, as we can see at the right side of the figure 4, there is a significantly greater difference between the two types of companies. The surveyed companies, even some of the market-leading companies - more precisely 18%

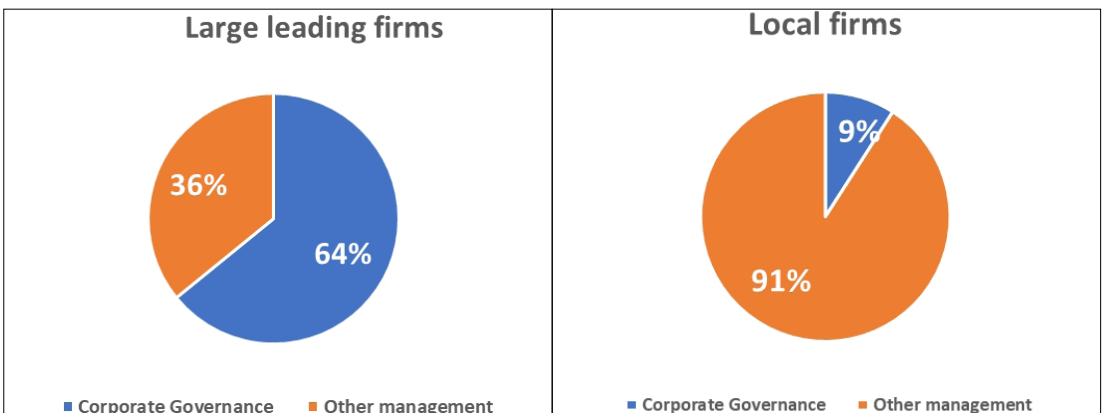


Figure 4. A CG based management at the studied organizations.

of the companies - do not consider it important to promote their quality management activities. This proportion is much higher in the case of local companies, as we found data on QM in only 55% of the sites. This result is fairly surprising if we take in account the fact that, presumably, all companies have a certified quality assurance system. Without them, they would not be able to be present on B2B, B2G markets. A possible explanation for this might be that they consider it self-evident that they have a certified high quality assurance system and there is no need to report on it.

An interesting area of investigation was the presence of OECD principles of corporate governance (CG) in the companies surveyed. We did not specifically look for state-owned companies, since in the case of Romania, according to the Government Decree 109, CG is usually present, and therefore the companies studied are rather multinational, in many cases listed on the stock exchange. **Figure 4** examines the presence of CG based management in the companies studied.

**Figure 4** shows the expected result that corporate governance according to the OECD principle is not really present in local companies. We found signs of this at a rate of less than 10% at the local level. The corporate governance is present in a significantly higher proportion in the case of market leader companies, as 64% of the examined companies clearly apply these principles. During the research, perhaps the most interesting issue is the analysis of the QM and CSR in relation to the existence of visible CG rules at the studied companies. **Figure 5** shows this relationship.

In the figure above, we can see that we found information about CSR and QM, without exception, in companies where corporate governance based on OECD principles is present. In addition to the clearly separated social responsibility and quality management activities, these websites clearly show who the leaders of the organization are. They present the conscious commitment to the adopted values, and there are obvious signs of that in the company's communication. The research also revealed that where there is no CG, the company usually does not have an easily identifiable manager.

We also observed that in the case of important state-owned companies –due to legal requirements –there is a visible organizational chart. In these, usually we found the responsible departments for QM and CSR. In the case of the other examined non-state companies, but among those that we considered large companies, we found that if there is CSR, there is also QM, but the reverse is not always true. As for the sample of local companies, we can see on the right side of **Figure 4**, that there are only really few firms with CG based management. Usually, here neither the management team nor the person responsible for QM and CSR activities are visible. During the research, we did not find a single organizational chart for all the investigated local industrial companies. Here, too, we experienced the same situation to the large companies: if there is CSR, there is also QM, but the reverse is not true here either. At local level, there are very few references related to QM. Still, as we mentioned above,

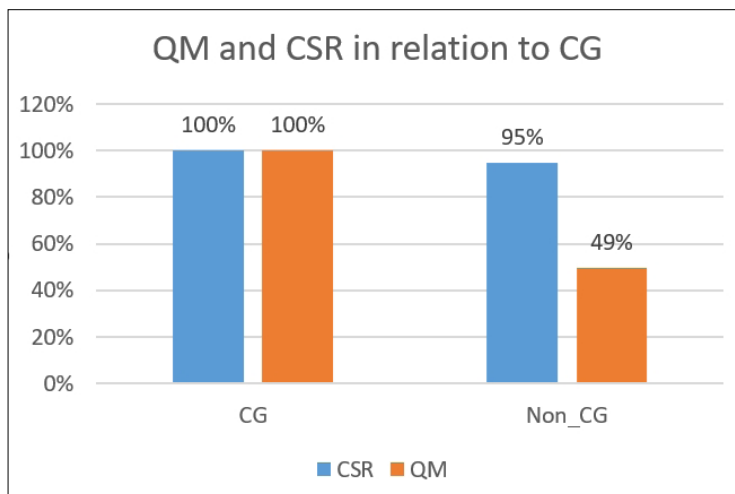


**Figure 5.** Quality management and corporate social i.e., responsibility in relation to CG



they certainly have an advanced certified quality management system, since without ISO9001 and ISO14000 certification - in addition to the sector-specific standards - it is relatively difficult to prevail in the market. The websites of the local firms are usually outdated, or are redirected to the parent company's website. However, in the latter case, almost everything is perfect, so there is usually a significant difference between the information intended for the public shown by the parent company and its subsidiary.

## 6. Conclusions

Contemporary quality management is a more complex issue than it might seem at first impression, since quality assurance today assumes the organization's ability to ensure a certain quality level continuously and sustainably. For this, the creation of optimal technical conditions is far from sufficient (e.g. professional technological planning and proper machine settings), several further activities can also be crucial in quality assurance. It requires substantial senior management attention to sustain these usually non-product activities and to create several jobs to support the quality management processes. One of the essential starting points of our research is the assumption that, in order to ensure comprehensive quality, the top management must establish clearly separated (middle and senior management) roles to achieve this goal. Among these roles, we considered the quality manager and the manager for social responsibility to be of particular importance. In our research, we examined to what extent the two roles/ activities, are reflected in the organization charts of companies located in Romania. We had a particular interest in local small and medium-sized companies. During the content analysis, we examined the websites of the selected companies, and found that the organizational chart of the companies is not usually public, since only 24 of the 158 companies examined (15%) had the chart available on their website. Among these, we found that in 20 cases the QM activity is clearly visible (this is 13% of the entire sample) and in 16 cases the CSR and QM activities appear clearly separately. Looking at the sample of the studied region, we found that there is lack of corporate governance principles (in the sense defined by OECD), the management team and the person responsible for QM and CSR activities are not visible either. We experienced that if there is CSR, there is also QM, but the reverse is not true here either.

We have noticed that there is lack of information referring to QM processes, in spite of the fact that most of them, almost without exception, certainly have a quality management system certified by independent auditors. The websites of the studied local companies are usually outdated, or redirected to the parent company's website. The biggest difference found between local companies and large national-level companies consists of the level of adopting the corporate governance principles. At local level only 9% of the companies have such kind of governance. This situation is totally different regarding our findings related to the existence of QM activities. While, the QM issue is somehow a hidden, or less visible due to some kind of indolence, the CG issue is real; the companies - if they apply these principles- proudly promote it, and there is evidence which proves it in their websites.

## References

- [1] M.-S. Akhmatova, A. Deniskina, D.-M. Akhmatova, L. Prykinac: *Integrating Quality Management Systems (TQM) in the Digital Age of Intelligent Transportation Systems Industry 4.0*. Transportation Research Procedia 63 (2022) 1512–1520.
- [2] Yu G. J., Park M., Hong K. H.: *A Strategy Perspective on Total Quality Management*. Total Quality Management & Business Excellence, 31/1-2. (2020) 68–81.
- [3] K. Canbay, G. Akman: *Investigating Changes of Total Quality Management Principles in the Context of Industry 4.0: Viewpoint from an Emerging Economy*. Technological Forecasting and Social Change, 189. (2023) 122358, <https://doi.org/10.1016/j.techfore.2023.122358>.
- [4] M. García-Fernandez, E. Claver-Cortes, J. J. Tar: *Relationships between Quality Management, Innovation and Performance: A Literature Systematic Review*. European Research on Management and Business Economics, 28/1. (2022).
- [5] Sang-Lin Han, Jong Won Lee: *Does Corporate Social Responsibility Matter Even in the B2B Market?: Effect of B2B CSR on Customer Trust*. Industrial Marketing Management, 93. (2021) 115–123.
- [6] Shuojia Guo, Cheng Lu Wang, Seokyouon Hwang, Fei Jin, Liying Zhou: *Doing Bad by Doing Good? Corporate Social Responsibility Fails when Controversy Arises*. Industrial Marketing Management, 106. (2022) 1–13. <https://doi.org/10.1016/j.indmarman.2022.07.009>.
- [7] EFQM (2019). *The EFQM Model*. Brüsszel: EFQM.
- [8] Talib Hussain et al.: *Examining the Role of Responsible Management, CSR, and TQM in Enhancing Renewable Energy Projects: An Empirical Analysis*. Acta Ecologica Sinica, 2023. <https://doi.org/10.1016/j.chnaes.2023.06.010>

- [9] <https://www.ga-institute.com/index.php?id=9127>
- [10] Braun R.: *Vállalati társadalmi felelősségvállalás*. Akadémiai Kiadó, Budapest, 2015.
- [11] \*\*\* (2001). Green paper - Promoting a European Framework for Corporate Social Responsibility, Commission of the European Communities, Brussels, 18.7.2001, COM(2001) 366 final  
<https://eur-lex.europa.eu/LexUriServ/LexUriServ.do?uri=COM:2001:0366:FIN:EN:PDF>
- [12] European Commission, Executive Agency for Small and Medium-Sized Enterprises, Uptake of Corporate Social Responsibility (CSR) by European SMEs and Start-ups – Executive Summary, Publications Office, 2021.  
<https://data.europa.eu/doi/10.2826/822248>
- [13] <https://www.iso.org/iso-26000-social-responsibility.html>
- [14] <http://mneguidelines.oecd.org/mneguidelines/>
- [15] Auer Á.: *Corporate governance. A felelős társaság-irányítás jelenkori dimenziói*, Dialog Campus, Budapest, 2017.
- [16] OECD (2021), OECD Corporate Governance Factbook 2021, [www.oecd.org/corporate/corporate-governance-factbook.htm](http://www.oecd.org/corporate/corporate-governance-factbook.htm)
- [17] \*\*\* Ordonanța de urgență nr. 109/2011 privind guvernanta corporativă a întreprinderilor publice.
- [18] Krippendorff K.: *Content Analysis: An Introduction to Its Methodology*. Sage Publications, 2019.
- [19] <https://www.zfcorporat.ro/>
- [20] <https://www.topfirme.com/>
- [21] [www.coduricaen.ro](http://www.coduricaen.ro)



# KUKA KR3 INDUSTRIAL ROBOT UNIT HMI DESIGN AND CONTROL WITH UNIVERSAL INDUSTRIAL PC IN SiPY DEVELOPMENT ENVIRONMENT

Szabolcs Sándor DIÓS,<sup>1</sup> Gergő Tamás ASZTALOS,<sup>2</sup> Géza HUSI<sup>3</sup>

<sup>1</sup> University of Debrecen, Faculty of Technology, Department of Mechatronics, Debrecen, Hungary, [dios.szabolcs@eng.unideb.hu](mailto:dios.szabolcs@eng.unideb.hu)

<sup>2</sup> University of Debrecen, Faculty of Technology, Debrecen, Hungary, [gergoasztalos.28@gmail.com](mailto:gergoasztalos.28@gmail.com)

<sup>3</sup> University of Debrecen, Faculty of Technology, Department of Mechatronics, Debrecen, Hungary, [husigeza@eng.unideb.com](mailto:husigeza@eng.unideb.com)

## Abstract

The challenges presented by Industry 4.0 require an innovative, new type of thinking from the engineers. Connecting old machines into a network presents significant problems, as the switch cabinets for these are obsolete and non-upgradeable. This has made developing a solution necessary, that is later universally applicable for scrapped, but mechanically intact robot arms. During the realization of the project such an IoT compatible graphical interface was developed, which can control a KUKA KR3 industrial robot unit and can also Real-Time simulate it in virtual reality. The security functions of the robot are provided by a Pycom SiPy developer panel.

**Keywords:** KUKA KR3, C++, JavaScript, Pycom SiPy, HMI.

## 1. Introduction

At the University of Debrecen, Faculty of Engineering, Department of Mechatronics, in the Cyber-Physical & Intelligent Robot Systems Laboratory, besides education, the testing and validation of research topics is also conducted [1]. One of the main aims of the projects is the complete reimagining of industrial robots and their control systems, as well as realizing the support of new network functions. Old robot units mechanically don't become obsolete, but their control systems do.

In the laboratory students take part in a practical education in the subject of „Robotics Knowledge”, but the distribution of new knowledge also happens here, as any research that is finished has its discoveries added to the lessons. Many of the robots that are found in the laboratory are undergoing refurbishing, just like the robot KR3 that was made by the company KUKA [2]. These units are in a mechanically sound state, with working motor regulating circuitry, but their control

through their original industrial computers is impossible, because they are inoperable and their parts cannot be repaired.

The reasons mentioned above made the development and programming of a new, unique HMI necessary for the KUKA KR3, which makes visualization of 3D position possible in a Real Time environment. The Dead-Man switch was also reimagined, considering the relevant security standard.

## 2. KUKA KR3 Industrial Robot

The KUKA KR3 industrial robot and its variants are six-axis industrial robots designed for precise handling of light payloads.

These are used in small workspaces, for the manufacturing of small parts, with a nominal payload of 3kgs and a maximum reach of 635mm. Its main applications are: arc welding, grinding, assembly, automation in laboratories and the moving and implanting of parts [3].

The structure of the robot can be seen on **figure 1** where the axes, the angular ranges of rotations and also the directions of the rotations are depicted.



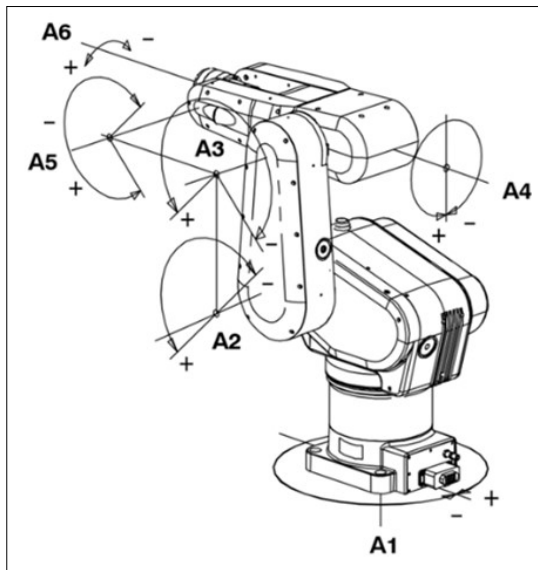


Figure 1. Structure of a KUKA KR3 robot. [3]

The robot itself is a 6R type robot, meaning, that every axis makes a rotational movement possible, resulting in a spherical field of action. It is also important to mention, that the actual field of action is influenced by the axis limitations of the robot unit in question.

1. táblázat. KUKA KR3-axis-mozgástartományok [3]

Maximum angular speeds of robot	Range of motion for axes in (degrees)
Axis 1 (A1) 240°/s	Axis 1: $\pm 180^\circ$
Axis 2 (A2) 210°/s	Axis 2: $-45^\circ / +135^\circ$
Axis 3 (A3) 240°/s	Axis 3: $-225^\circ / +45^\circ$
Axis 4 (A4) 375°/s	Axis 4: $\pm 180^\circ$
Axis 5 (A5) 300°/s	Axis 5: $\pm 135^\circ$
Axis 6 (A6) 375°/s	Axis 6: infinite

An industrial computer is a PC made for use by the industry, that has to meet precise standards, has to provide great reliability, upgradeability and long-lasting technical support, besides being usually more expensive, than everyday consumer electronics.

An industrial PC is first and foremost used for process control and/or data collection or in some cases, if there is distributed processing, as a Front End for another controlling computer.

The control system managing the industrial robot consist of an industrial PC and the HMI control interface.

The above points are general expectations that need to be adhered to by the new control system of the KUKA KR3.

One of the main reasons for this is that although the complete control system is reimaged, in theory it still has to be able to perform the same functions as before, including a DeadMan Switch, Joint, World, Tool, Base coordinate systems, velocity control and axis End-Stops have to be usable.

The KUKA KR3 robot wasn't in sate at the beginning of the project to be used with an HMI, as it was missing one entirely. The robot was only moveable per axis. with the use of Step-Dir commands.

The main problem was presented by the fact, that the control systems or control racks present in the industry are usually company specific, meaning they are not interchangeable or repairable. The real life-cycle is defined by the support of the official manufacturer.

The original KR C3 controller used by the KUKA KR3 (Figure 2) is not being sold anymore and is inoperable. Since it is missing basic functions and the impossibility of a software update, in the case of a working control cabinet, would still present limitations in the performable tasks. The Embedded OS, which is available for it is Windows 95 - an earlier Microsoft development - which had its official support terminated on 31 December 2001. Of the supported ports at that time, the USB 1.0 was also only added with a later OSR 2.1 update, with a data transfer speed of 1,5Mbps. The use of broadband internet was also not possible [5].

Taking the above points into account, we can declare, that the KR C3 industrial control unit does not correspond to the expectations of Industry 4.0, nor to the network communication standards.

In essence, the control cabinet is capable of controlling the KR3 servo-motors, can run its manufacturer HMI, setting speed values and storing programs. In itself the industrial PC elements of it are the same as those of a general use Desktop PC, meaning it has basic hardware elements such as: CPU, RAM, HDD, Motherboard.

The parts cannot be replaced, as these also function as a type of hardware key for the original HMI.

In the original control unit is an MFC expansion card, this handles the I/O s; and also a DeviceNet/ CAN bus to make communication between a teach pendant (KCP2) and the industrial PC possible.

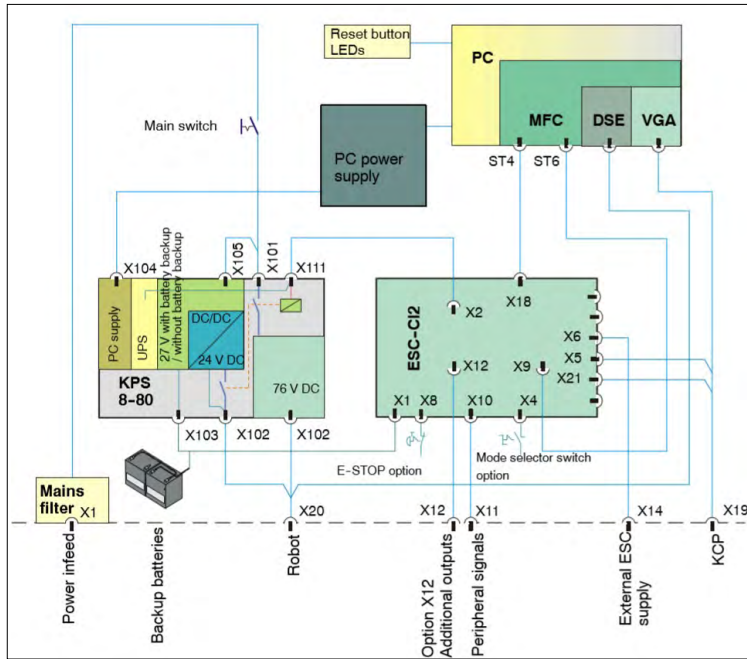


Figure 2. Structure of KR C3 robot controller.

### 3. Control of BLAC Motor

Inside the KUKA KR3 industrial robot there are several servo motors, which all perform rotational movements in every joint of the robot. These motors are all brushless AC motors, meaning that the spools are found on the stator and the magnets on the rotor.

For the precise operation of the servo motor, a HALL sensor is needed, so that the exact position of the motor can be determined at every moment of time. The current for the coils of the motors can be switched with the control of transistors, allowing for the creation of the electromagnetic fields needed for the rotation [6].

In general, BLAC type motors operate with better efficiency, since they are brushless and produce lesser thermal losses (Figure 3).

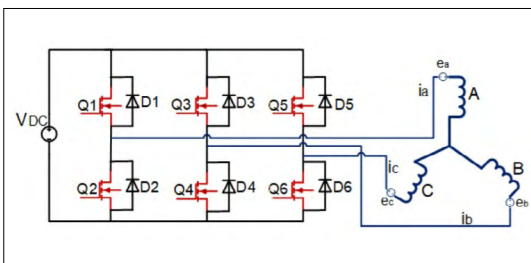


Figure 3. Circuit of BLAC motors. [4]

The outlets of the coils are designated with U, V, W, while those for the HALL sensor are VCC, GND, HU, HV, HW. Data provision regarding the positions from the motor side are made possible by Tamagawa TS5643 N 100 (11/24 bit) encoders [7].

The KUKA KR3 robot arm uses Inertia Dynamics M1701-2221 (FSB series) brakes, that operate with 24V DC current, but not on all 6 axes (A1, A2, A3, A4, A5 applies brakes).

The role of these brakes in the case of industrial robots is to make sure, that if the supply voltage ceases, the position and torque values are kept [8].

In the case of the KR3 robot the former motor controllers were changed out for the industrial



Figure 4. LeadShine ACS606 servo controller [9]

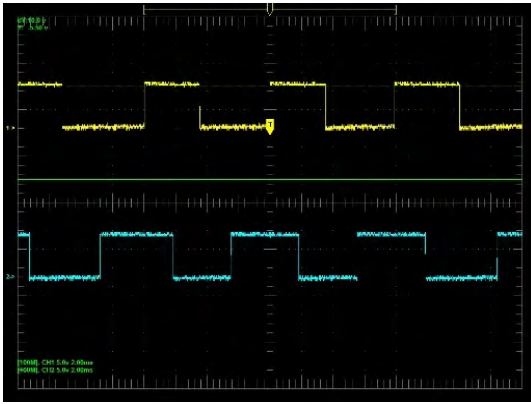


Figure 5. Signals EA+ és EB+ .

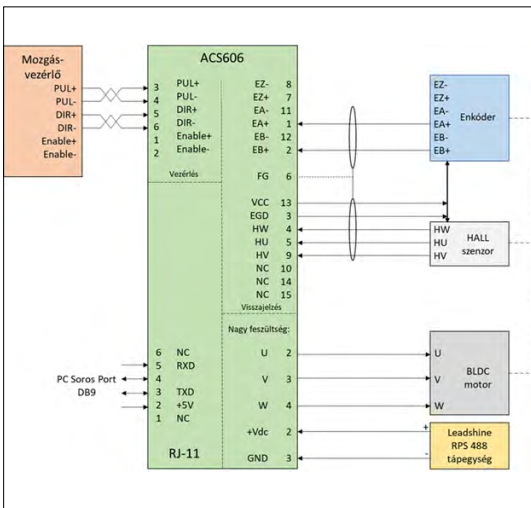


Figure 6. ACS606 servo controller & sensors [9]

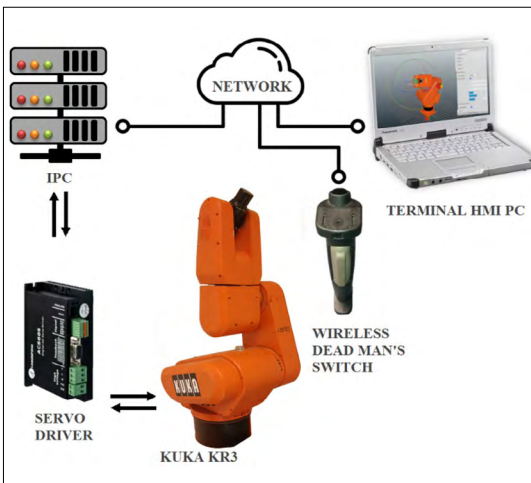


Figure 7. Block diagram of the system.

type Leadshine AC606 [9] servo motor controllers. These are used for multiple axis industrial milling machines, for purposes of production, primarily for brushless (BLAC) motors (Figure 4).

The direct current supplied for the motors by the controller ranges from +18V up to +60V. On the outlets of U, V, W the supplying of current to the motors is made possible. Processing of the positions of each axis controlling motor happens through a 15-pin unique connector.

A rectangular signal is provided on the encoders EA+ and EB+, and on the HALL sensor's HU, HV and HW outlets (Figure 5. ).

At the encoders were validated with an oscilloscope before the new HMI was engineered. The complete rotation of an axis consists of 8192 impulses. In Figure 5 on the X-axis of the oscilloscope is a „t”-time depicted (2ms), while on the Y-axis the current. The RPM set for the motors was 0,915 rotations/minute.

The cable type used for wiring was a twisted pair wire that was routed in a hose.

#### 4. Designing the HMI & Requirements

As was earlier described, most of the elements of the KUKA KR3 are not changeable, as they also function as a sort of hardware key in regards to this system, while the KR C3 control cabinet found in the laboratory was also in an inoperable state. However, during the engineering of our HMI (Human Machine Interface) there were certain points, that, if implemented correctly in our own HMI would mean, that in theory, the original HMI would be reproduced. Therefore, so that the new HMI corresponds to the requirements of Industry 4.0, the system depicted in Figure 7 was developed [7].

To each axis of the robot, one by one a servo controller is connected, depicted in Figure 6. [9] each of these are also connected to a computer. This computer can be an industrial PC as well, just as it was in our case. On this computer a Linux OS is running that was modified so that it could run our own application in real time. Furthermore, it also houses a webserver, on which the 3D model of the KUKA robot, as well as the website responsible for the HMI can be stored, thus providing a flexible solution for the user. Unlike an industrial PC which only has one given hardware key, inside a network we can run our HMI on basically any computer, as long as that computer possesses a JavaScript enabled browser.

If a client wants to connect to the webserver, it first checks whether the Real-Time application is running, afterwards providing the files of the 3D model and the JavaScript program code necessary to run the HMI to the client.

This means, that the Human Machine Interface runs completely on the client, it sends the commands through the network to the Real-Time application, that executes those.

### 5. Industrial Compute Engine

For the realization of the project a one-card computer was selected, which is present as an embedded system during its application. The Strato Pi Base Board [10] was applied together with a Raspberry Pi [11] (Figure 8), that makes RS-232 as well as RS-485 communication possible.

With the help of the extra expansion card, it is now possible to use the Raspberry Pi to complete industrial tasks. The webserver and the Linux OS itself run on the Raspberry Pi, in turn the Strato Pi Base Board [7] sends signals to the servo controllers. Before replacing the old industrial PC, it proved necessary to test the waveforms sent to the motor control electronics.

The motor controller receives a STEP/DIR type signal, that means to every axis there are two corresponding signal cables. On the cable connected to the DIR input, depending on the direction of

the motor steps, either 0V or 5V current is present (Figure 9).

A 5V peak voltage pulse with a 16us period is connected to the STEP input to move a unit in the direction specified by the DIR signal. The step unit depends on the range of motion of the respective axis and the resolution of the position encoder and the gear ratios of the motor.

### 6. Real Time Application

The version number of the Linux kernel of the applied operating system is 5.4.51-v8+, a Preemptive type kernel, which is key for running the application in real time.

The „core” program starts as a system level service, after initializing the network interfaces. The program is based on the principle that the specific position of the axes is given as a digital code, i.e. we know exactly how many steps are allowed due to the digital encoder. After starting it, the „core” program reads the saved maximum position numbers, then the initialization process happens, where it creates the corresponding POSIX socket resources for the network communication. In the background 6 threads are created, each of those corresponding to ‘on’ of the axes of the KUKA KR3 industrial robot. In the event that an inbound connection occurs, a new thread is created that executes it. The threads corresponding to the axes



8. ábra. Strato Pi Base Board & Raspberry Pi [11]

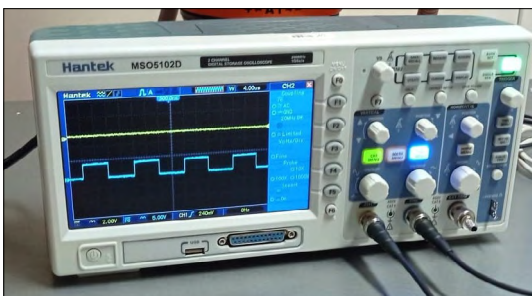


Figure 9. Waveforms sent to motor controllers.

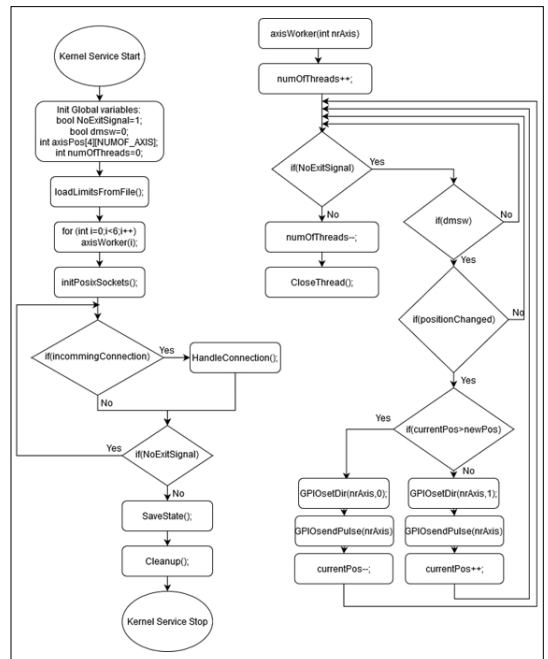


Figure 10. Pycom SiPy Pinout



check whether there is a change in the incoming information compared to that which is stored. Additionally, the state of the DeadMan Switch is also checked, which happens over the network as well (Figure 10.).

### 7. Developing the Dead Man’s Switch

A problem encountered during design was that if the HMI is accessible from anywhere on the network, the robot operator may not always be near the emergency stop button, which is dangerous. Starting from Murphy’s Law, which reads, “What can go wrong, will go wrong” [12], the implementation of a simple emergency stop button accessible from anywhere under the network was necessary.

The solution is provided by Pycom’s SiPy [13] development module, a Micropython-programmable microcontroller based on the Espressif ESP32 chipset (Figure 11).

Inside it are two processors: a network processor, that handles the WiFi radio connection and a main processor that runs a user installed program. Pycom’s SiPy features include ultra-low power consumption, the implementation of a 1Km Wifi radio between Pycom devices, and Sig-Fox communication with other IoT devices.

The wireless Dead Man’s Switch only turns the power on or off from the SiPy panel.

The program running on the microcontroller will definitely try to connect to the real-time application on the network, which will detect the status of the connection and the MAC address of the device (Figure 12).

### 8. 3D KUKA KR3 HMI

One of the basic conditions of the HMI was to display the given robot unit in 3D. There were several reasons for this, one of which was to make it easier to track changes in the positions of individual axes and to allow easier user coordination.

The 3D model of the KUKA KR3 industrial robot arm was designed in 3D CAD (Computer Aided Design) program.

One solution to this is provided by SketchUp [14] which allows us to model 3D spatial shapes with a low polygon number, making it not only easier to slice 3D models during 3D printing, but also to design different simulation models.

The HMI interface was produced with the help of the JavaScript based ThreeJS 3D graphical engine. The functions of the HMI, such as calculations of coordinates, positioning of the robot, has

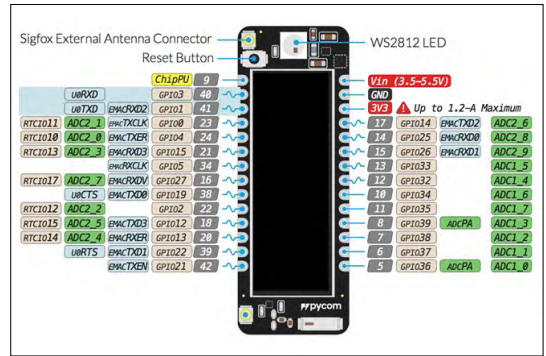


Figure 11. Pycom SiPy Pinout. [13]



Figure 12. Pycom SiPy Deadman Switch.

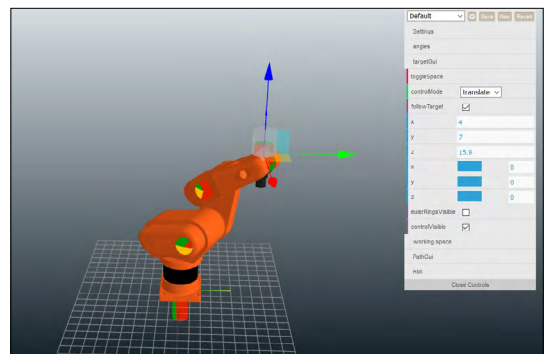


Figure 13. KUKA KR3 3D HMI.



14. ábra. 3D vs Real KUKA KR3 HMI

also been written in JavaScript, as such the HMI runs in its entirety on the client computer (Figure 13).

Through the HMI the sending of signals towards the real KR3 industrial robot is possible, thus that will follow the position designated in the HMI. Positions can be reached through the velocities allowed by the robot's settings (Figure 14).

During the tests, the used client PC was an industrial Panasonic Toughbook CF-C2, with 8 GB DDR3 RAM, Intel Core i5 4300U CPU.

The Cyber-Physical & Intelligent Robot Systems Laboratory previously provided opportunities for other types of research tasks as well. Whether it was image analysis for detection of specific elements in work stations [15], creation of virtual environments [16] or conducting measurements related to singularities [17]. In addition to the aforementioned, the HMI design and control task mentioned above further strengthens this laboratory.

## 9. Conclusion

This project was fully realized and everything within it was also fully engineered. The KUKA KR3 industrial robot had its HMI engineered, for which a 3D model of the robot unit was also made that was integrated into a virtual reality environment. For the Dead Man's switch a SiPy controller developed by Pycom was used, while for the PC a Linux based OS, a once-card computer, a Strato Pi Base Board and Raspberry Pi were applied.

With the help of the 3D KUKA KR3 HMI, we can exactly track the changing of positions and also make the coordination of the real KUKA KR3 possible. As further possibilities for development, the integration and 3D modeling of a gripper tool for the virtual reality environment were considered.

## Acknowledgements

Project no. TKP2020-NKA-04 has been implemented with the support provided from the National Research, Development and Innovation Fund of Hungary, financed under the 2020-4.1.1-TKP2020 funding scheme. Special thanks to the University of Debrecen, Faculty of Technology, Cyber-Physical & Intelligent Robot Systems Laboratory, and Roland Décei.

## References

- [1] Erdei T. I., Molnár Zs., Obinna N. C., Husi G.: *Cyber Physical Systems in Mechatronic Research Centre*. MATEC Web on Conferences, 126. (2017) 1006. <https://doi.org/10.1051/mateconf/201712601006>
- [2] Erdei T. I., Molnár Zs., Husi G.: *Robot Visual and Virtual Control Technology in Industrial Environment*. WoS (Web of Science) (SIMS), Narvik, NORWAY- IEEE, Jun 21-24, 2016. <https://doi.org/10.1109/SIMS.2016.7802902>
- [3] KUKA KR3 | Eurobots, [Online]. Available: <https://www.eurobots.net/kuka-robots-kr-3-p248-en.html> [Accessed on: 10.08.2021].
- [4] Flah A., Lassaad S.: *Overview on BLAC and BLDC Motors: designs and Mathematical Modeling*. International Journal of Powertrains, 10/2. (2021) 204–215. <https://doi.org/10.1504/IJPT.2021.117470>
- [5] Win95 - INDIANA University [Online]. Available: <https://kb.iu.edu/d/aezf> [Accessed on: 12.10.2021].
- [6] K. R. GmbH, „KR C3 User Manual,” 11 november 2003. [Online]. [Accessed on: 06.06.2021].
- [7] L. Tamagawa Seiki Co., „Rotary Encoders,” 20.09.2021. [Online]. Available: [https://www.tamagawa-seiki.com/assets/img/downloads/pdf/rotaryencoder/1228N58EJ\\_shusei3.pdf](https://www.tamagawa-seiki.com/assets/img/downloads/pdf/rotaryencoder/1228N58EJ_shusei3.pdf).
- [8] FSB Series, Spring Applied Brakes | Inertia Dynamics, Altra Industrial Motion Corp., 2019. [Online]. Available: <https://www.idicb.com/products/spring-applied-brakes/type-fsb>. [Accessed on: 01.10.2021].
- [9] User's Manual For ACS606 Digital AC Servo Drive, 2009. [Online]. Available: <http://www.leadshine.com.ua/pdf/acs606.pdf>. [Accessed on: 03.10.2020].
- [10] Sfera Labs S.r.l. Strato Pi Base User Guide Revision 024 [Online]. Available: <https://www.sferalabs.cc/files/strato/doc/stratopi-base-user-guide.pdf> [Accessed on: 11.01.2021].
- [11] Raspberry Pi Ltd. Raspberry Pi 3 Model B Plus [Online]. Available: <https://static.raspberrypi.org/files/product-briefs/Raspberry-Pi-Model-Bplus-Product-Brief.pdf> [Accessed date: 11.01.2021].

- [12] Spark N. T.: *A History of Murphy's Law*. Periscope Film (21 May 2006). ISBN 0-9786388-9-1
- [13] Pycom Ltd. „SiPy Datasheet” [Online]. Available: [https://docs.pycom.io/gitbook/assets/specsheets/Pycom\\_002\\_Specsheets\\_SiPy\\_v2.pdf](https://docs.pycom.io/gitbook/assets/specsheets/Pycom_002_Specsheets_SiPy_v2.pdf) [Accessed on: 15.10.2021].
- [14] 3D CAD - SkechUp” [Online]. Available: <https://www.sketchup.com/> [Accessed on: 18.10.2021].
- [15] Kapusi T. P., Erdei T. I., Husi G., Hajdu A.: *Application of Deep Learning in the Deployment of an Industrial SCARA Machine for Real-Time Object Detection*. Robotics, 11/4. (2022) 69. <https://doi.org/10.3390/robotics11040069> .
- [16] Erdei T. I., Krakó R., Husi G.: *Design of a Digital Twin Training Centre for an Industrial Robot Arm*. Applied Sciences, 12/17. (2022) 8862. <https://doi.org/10.3390/app12178862>
- [17] Erdei T. I., Husi G.: *Singularity Measurement in the Cyber-Physical and Intelligent Robot Systems Laboratory*. International Review of Applied Sciences and Engineering, 11/2. (2020) 82–87. <https://doi.org/10.1556/1848.2020.20001>



# REVIEW OF POSSIBLE WASTE HEAT SOURCES FROM INDUSTRIAL FACILITIES AND THEIR POTENTIAL USE

János DÓSA

*University of Petroșani, Faculty of Mechanical and Electrical Engineering, Department of Mechanical, Industrial Engineering and Transportation, Petroșani, Romania. iondosa@upet.ro*

---

## Abstract

The aim of the paper was to review the main reusable sources of heat from industrial facilities and to analyze the most efficient way in which they can be exploited. In order to carry out some case studies, examples were chosen from fields of industry in which energy consumption is very high, namely the energy and mining industries. It was shown that although there are large amounts of energy that can be recovered, they are generally low temperature heat sources. Their efficient recovery can be achieved with the help of heat pumps, but due to the final temperature of the heat source, which is around 70 °C, they can be used mainly as heat sources for heating or hot water. This use greatly limits the research and projects for the reuse of these secondary energy resources, therefore future research should focus on obtaining higher temperatures, but also on the production of steam from these sources. The production of steam would facilitate an increase in projects for the recovery of these secondary energy resources for industrial use, which would lead to a superior valorization of them.

**Keywords:** *waste heat, secondary energy resources, heat recovery, primary energy source savings.*

---

## 1. Introduction

The guideline drawn by the EU from a sustainable development point of view is concretized by the European Green Deal which stated that we are striving to be the first climate-neutral continent.

The starting point of the strategy is that climate change and environmental degradation are an existential threat to Europe and the world. To overcome these challenges, the European Green Deal will transform the EU into a modern, resource-efficient and competitive economy. The major goals of the Green Deal can be summarized as follows: no net emissions of greenhouse gases by 2050; economic growth decoupled from resource use; no person and no community left behind.

An important part of the action plan is a set of proposals to make the EU's climate, energy, transport and taxation policies fit for reducing net greenhouse gas emissions by at least 55% by 2030, compared to 1990 levels.

It is also not accidental that two of the featured initiatives are energy related: REPowerEU and EU action to address energy crisis.

Basically, this is the mainframe in which Europe's industry will be functioning in the future.

## 2. Industry and power demand

The current state of the European Union from an energy point of view will be analyzed in the following section.

In [figure 1 \[1\]](#) can be seen that the primary energy consumption of the EU, compared to 2005, dropped. Also, the impact of the COVID pandemic can be clearly noticed.

Another important aspect is that the use of hard coal and brown coal dropped consistently, and as a result, in order to meet the energy demand use of natural gas, petroleum and nuclear energy grew. The overall tendency is the decrease of the primary energy consumption.

The gross electricity production as presented in [figure 2](#) highlights that fossil fuels were again the leading source for electricity generation. The second source is nuclear, but hydro power and green energy is also in the top.

From a heat recovery point of view in order to show the current state of the use of renewable resources, data presented in [figure 3](#) are important.



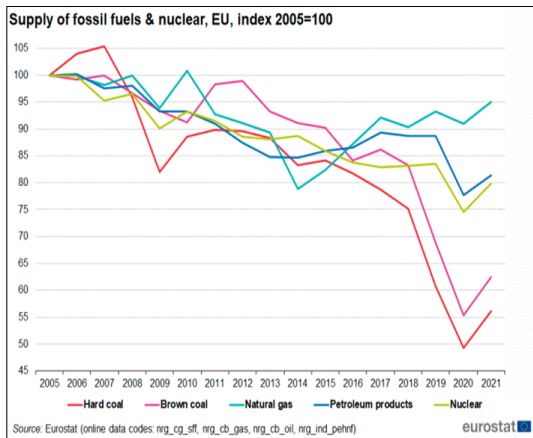


Figure 1. Primary energy supply. [1]

Renewables inland consumption (calculated) in the EU		2017	2018	2019	2020	2021
TJ	Geothermal	283 521	284 082	288 813	288 822	284 292
TJ	Solar thermal	190 137	179 916	194 823	187 583	190 553
TJ	Ambient heat (heat pumps)	456 113	486 381	520 765	553 193	630 597
TJ	Biogases	581 985	580 288	592 251	614 908	625 835
kt	Biogasoline	3 839	4 118	4 356	4 339	4 811
kt	Biodiesels	12 951	14 532	14 731	15 072	15 718
kt	Bio jet kerosene	0	0	0	0	0
kt	Other liquid biofuels	1 350	1 382	1 499	1 484	1 362
TJ	Primary solid biofuels	3 869 241	3 984 029	4 057 549	4 025 668	4 359 881
kt	Charcoal	517	528	500	444	437
TJ	Renewable municipal waste	397 656	390 913	395 136	399 661	409 465
TJ	Non-renewable municipal waste	393 219	386 537	390 248	395 068	399 305
TJ	Industrial waste (non-renewable)	185 722	195 742	202 075	206 295	207 573

Source: Eurostat (online data code: nrg\_cb\_rw)

Figure 3. Renewables inland consumption. [1]

Gross electricity production in the EU, GWh		2017	2018	2019	2020	2021
Anthracite		4 103	4 013	680	715	636
Coking coal		11 164	8 805	13	81	64
Other bituminous coal		316 143	286 535	205 613	154 218	190 144
Sub-bituminous coal		3 170	2 394	1 554	572	389
Lignite		301 921	291 618	241 259	195 292	226 128
Brown coal briquettes		2 329	2 132	1 799	1 510	1 663
Coke oven gas		7 770	7 204	7 166	6 237	6 117
Gas works gas		1 939	1 803	1 734	1 250	142
Blast furnace gas		20 844	20 866	19 455	16 343	20 053
Peat		5 243	5 922	5 161	3 137	2 502
Oil shale and oil sands		9 912	9 380	4 318	2 247	3 444
Natural gas		525 178	490 689	569 312	560 997	551 784
Refinery gas		6 550	7 158	6 955	6 622	6 310
Liquefied petroleum gases		452	237	232	147	145
Gas oil and diesel oil		10 518	9 704	10 274	10 087	10 461
Fuel oil		28 737	25 614	24 894	21 345	23 388
Petroleum coke		2 280	1 577	621	517	465
Solid biofuels		74 261	76 252	80 560	82 959	92 752
Biogases		55 648	55 096	54 991	55 766	52 603
Industrial waste (non-renewable)		2 750	2 925	2 942	2 639	2 573
Renewable municipal waste		18 739	19 335	19 011	18 873	19 573
Non-renewable municipal waste		18 218	18 838	18 584	18 334	18 797
Hydro		322 463	370 234	345 643	375 487	374 849
Pure hydro power		281 813	326 819	306 478	331 709	330 758
Mixed hydro power		22 720	27 044	23 276	25 838	27 915
Mixed hydro power - pumping		10 187	9 981	9 494	10 367	10 355
Pumped hydro power		17 931	16 372	15 889	17 940	16 177
Geothermal		6 715	6 655	6 726	6 717	6 538
Wind		312 313	320 616	367 118	397 799	386 866
Solar thermal		5 883	4 867	5 683	4 992	5 176
Solar photovoltaic		102 052	108 200	118 202	140 125	158 588
Tide, wave, ocean		522	480	499	509	503
Nuclear		759 383	761 943	765 338	683 512	731 701
Heat from chemical sources		1 172	1 099	1 038	1 089	1 105
Other fuels (including non-specified)		22 551	20 860	19 848	19 560	16 081
<b>Total (excluding pumped hydro)</b>		<b>2 932 807</b>	<b>2 916 698</b>	<b>2 881 840</b>	<b>2 761 371</b>	<b>2 885 010</b>

Source: Eurostat (online data codes: nrg\_ind\_pehcf, nrg\_ind\_pehnl)

Figure 2. Gross electricity production. [1]

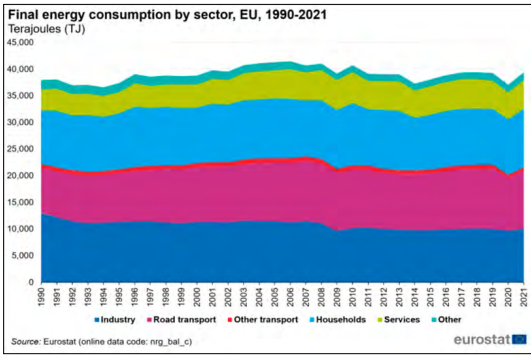


Figure 4. Final energy consumption by sector. [2]

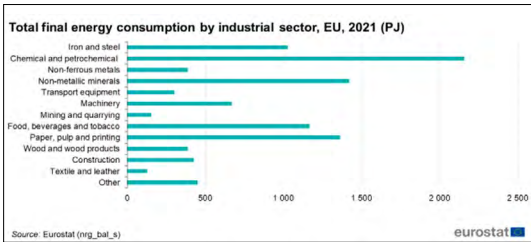


Figure 5. Final energy consumption by sector. [3]

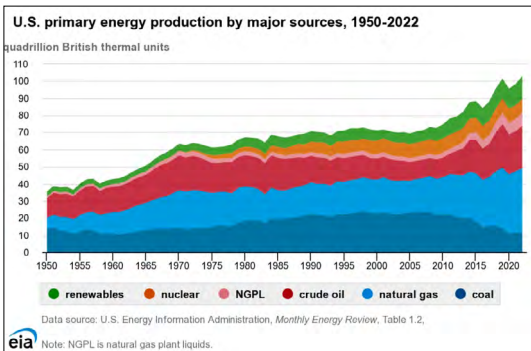


Figure 6. Primary energy consumption U.S. [4]

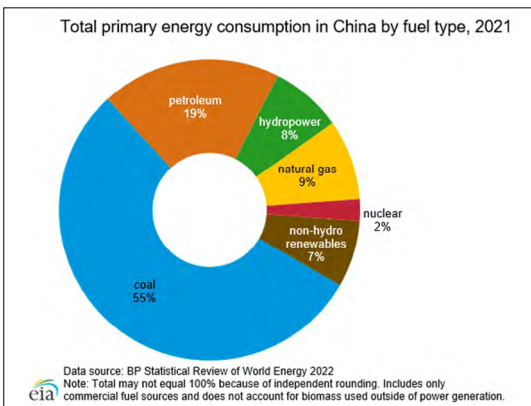


Figure 7. Primary energy consumption China. [5]

In the first place is the primary solid biofuel consumption followed by biogases.

Is important to notice that use of heat pumps also has an important share that is increasing over time. Renewable and non-renewable municipal waste, as well as non-renewable industrial waste have their share, but there is room for improvement.

Regarding the use of final energy, figure 4 shows that there are three major energy consumers: industry, road transport and households.

While heat recovery in road transport can be technically challenging, and the large share of household is due to their large number (which makes heat recovery usually economically inefficient), it means that from energy recovery point of view we should focus on industry.

The Energy-Intensive Industries cover a broad range of sectors such as chemicals, steel, paper, plastics, mining, extraction and quarrying, refineries, cement, wood, rubber, non-ferrous metals, glass and ceramics.

Their share in the final energy consumption is presented in figure 5 mutatja be [3].

Some discussions must take place regarding the data presented in figure 5, as the numbers are absolute values, and they must be analyzed from energy-intensity point of view. Therefore, the share of a certain industry in the overall consumption will be analyzed.

For example, the mining industry is far more energy-intensive than can be inferred on the basis of figure 5.

Its current status is due to the fact that the mining industry in Europe almost no longer exists as a result of the closure of most of the mines.

In order to have a complete picture, data on energy production and consumption in the case of the USA and China will be presented.

Figure 6. ábrát shows that ,compared to figure 1, the data are almost the same. In figure 7 the large share of coal in the primary energy consumption of China cannot be overlooked.

A more complex picture is presented in figure 8 [6], regarding energy consumption by source and sector in the case of the USA.

Data in figure 8 is consistent with data in figure 4 as major end user sectors are transportation, industry and residential (household).

Comparing data in figure 5 with data in figure 9 reveals that in China the share of the mining industry in total energy consumption is greater than in the case of EU (figure 5). and in recent

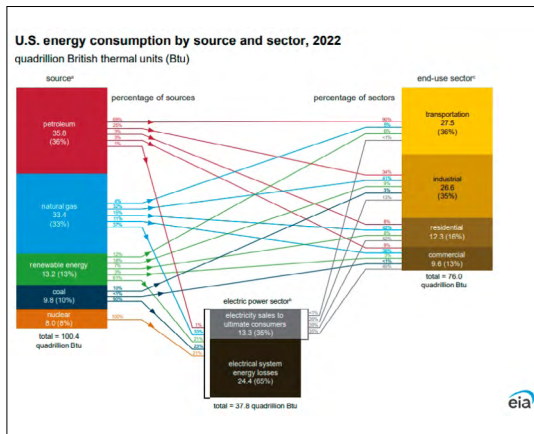


Figure 8. Energy consumption by source and sector. [6]

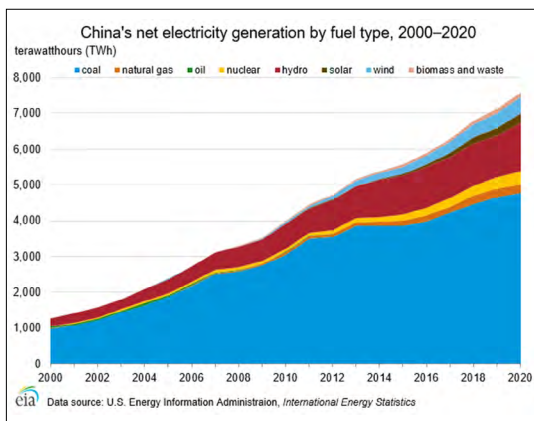


Figure 9. Net electricity generation by fuel type (China). [5]

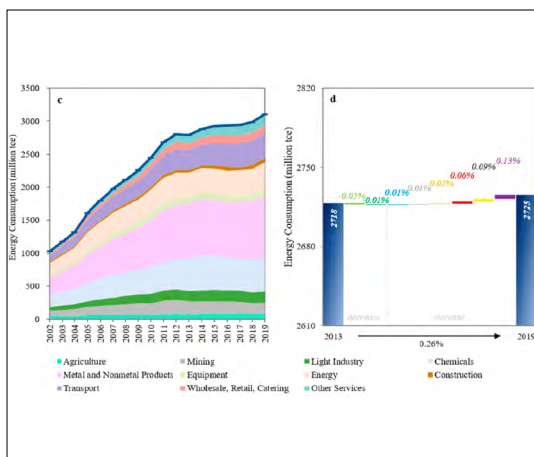


Figure 10. Energy consumption by industry sector (China) [7]

years this energy consumption is quite constant as China still has its mining industry.

Moreover, energy consumption in the mining industry is on the third place, which shows that mining is an energy-intensive industry.

Another important aspect is that in figure 10 the energy industry is also presented as major consumer, being in the first place in terms of share of total energy consumption. In case of the EU and the USA the share of energy industry is not listed.

Conclusively due to the weight of industrial consumption as presented above, and within it the share of the energy and mining industry, in the following, recoverable heat sources within them will be identified and evaluated from the magnitude and efficiency of recovery point of view..

### 3. Waste heat sources in industry

Waste heat recovery is not a new topic, and consequently such heat sources have already been mapped out [8].

A short enumeration will be helpful in the process of discovering the most promising recoverable heat source from heat recovery point of view.

Some of the most typical waste heat sources and their potential for energy recovery are [8]:

- process exhaust air (flue gas) between 30% to 90% can be utilized;
- waste heat from cooling systems - between 35% to 95% can be utilized as process heating supply;
- air compression facilities – up to 90% of electrical capacity can be recovered;
- ventilation technology – 35% to 90% can be utilized for fresh air preheating.

#### 3.1. Waste heat in energy industry

The waste heat sources enumerated above can be found in all industrial sectors.

As stated above, the energy sector and mining industry were chosen in order to evaluate possibilities of waste heat recovery.

In order to highlight the very high potential of the industrial waste heat from a heat recovery point of view two types of waste heat sources were considered:

- waste heat from cooling systems;
- waste heat from air compression.

##### 3.1.1. Amount of waste heat from condenser cooling

There are many studies in literature regarding the operation of a thermal power plant. The amount of heat released into the environment by



condenser cooling is 66% according to Gajendra [9] while according to Kale in [10] the loss is 34%. In other works, heat rejected by the condenser was found to be between 39,11% to 42,87% [11], and 45,02% to 45,98% [12] depending on power plant load.

These figures are high, and in absolute values are around 200 MW for data listed in [11] [12].

Assessment of the available heat that can be recovered from condenser cooling waste heat can be made using data gathered during heat balance calculations.

In figure 11 the schematic of a 200 MW thermal power plant is presented.

The steam turbine that works within this power plant is a condensing type turbine and was designed to operate at 3,000 rpm, 13 MPa pressure, and 545 °C temperature with one steam reheat to a temperature of 545 °C at a pressure of 2.44 MPa. The exhaust pressure of steam is 0.0034 MPa. The turbine has seven bleeder connections for regenerative feed water heating. Maximum temperature of feed water is 242 °C. From the outlet of the High Pressure Turbine (HPT) steam is directed to the re-heater at a pressure of 2.89 MPa and 350 °C. Steam is returned to the Reheat Turbine (RT) having a higher temperature. The Low Pressure Turbine (LPT) is of a double-flow design.

Steam for the turbine is provided by Pp-330/140-P55 type steam generator, a once-through coal-fired boiler [13].

An energy audit was carried out for this power plant and, as regulations require for heat balance calculations, measurements were carried out for at least 3 different loads. The loads for performance tests were fixed to 460 t·h<sup>-1</sup> - 70%, 560 t·h<sup>-1</sup> - 85% and 640 t·h<sup>-1</sup> - 94% (steam flow rate).

Data in table 1 shows the huge amount of heat available as waste heat and rejected by the condenser in the environment.

In order to be able to choose the appropriate heat recovery method, besides the amount of available heat the temperature of heat source is also important.

In table 2 the cooling water temperatures are presented.

The subject of another case study will be analyzed: a 150 MW rated output power plant.

The schematic of this power plant is presented in figure 12.

This power plant is equipped with K 160-130-2PR-2 type steam turbine, presented in the schematic diagram of the 150 MW unit (figure 12).

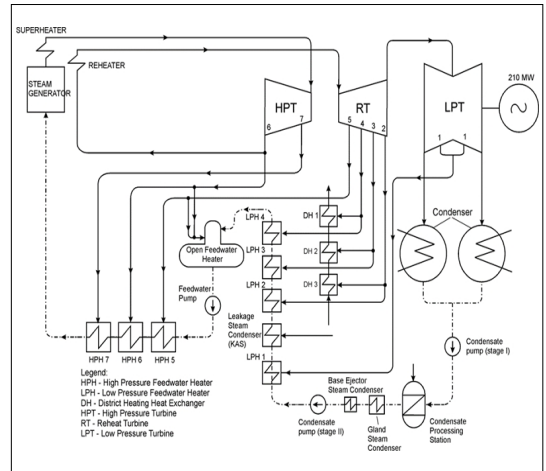


Figure 11. Schematic of the 200 MW power plant [11]

Table 1. Condenser loss

Load	Heat rejected by condenser Pcd, MW
70%	209.291
85%	259.989
94%	261.675
Average loss	243.652

Table 2. Cooling water temperatures

Load	Cooling water temperature at condenser inlet, °C	Cooling water temperature at condenser outlet, °C
70%	26.00	32.74
85%	27.93	36.43
94%	26.19	35.15

This turbine is a condensing type turbine with uncontrolled bleed, designed to operate at 12.8 MPa pressure, and 540 °C temperature, with one steam reheat to a temperature of 540 °C at a pressure of 3.41 MPa. The exhaust pressure is 0.0038 MPa. At the listed steam parameters and a cooling water temperature of 12 °C, the calculated power of the turbine can reach 170 MW.

It also can deliver up to 175 MW (150 Gcal·h<sup>-1</sup>) of thermal energy from an unregulated bleeder at 150/70 °C or 130/70 °C in the district heating network.

Abbreviations used in figure 12 are: HPT – high pressure turbine; RT – reheat turbine; LPT – low pressure turbine; CP, CP-1, CP-2 – condensate

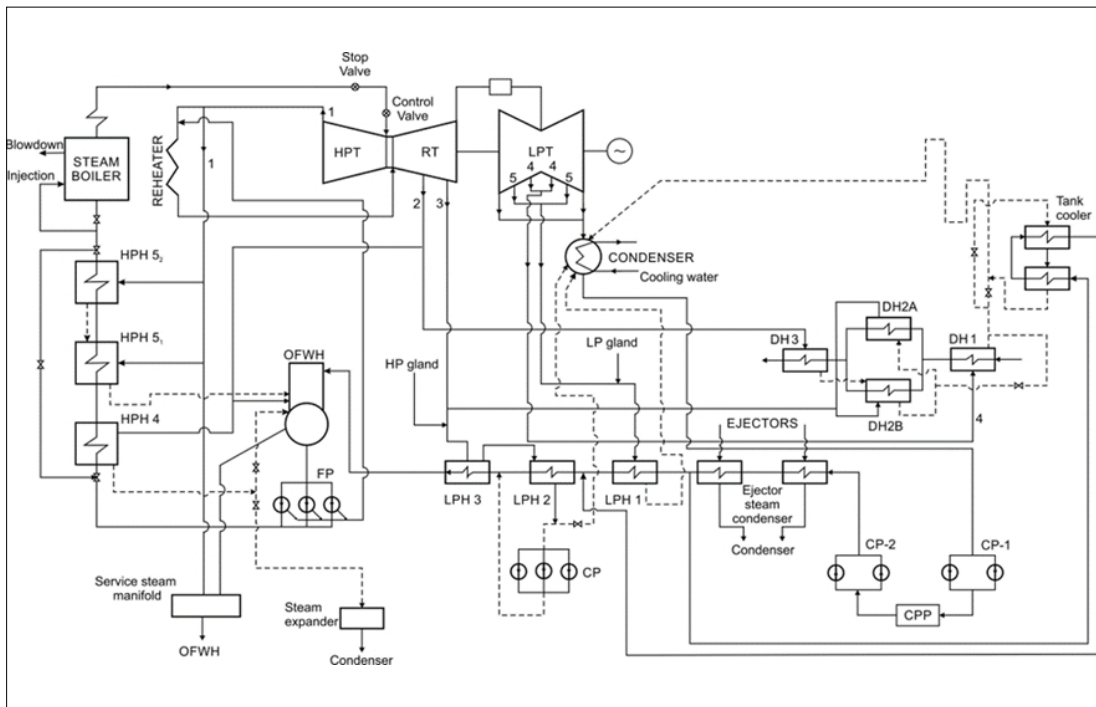


Figure 12. Schematic of 150 MW power plant. [12]

pumps; LPH – low pressure feedwater heater; HPH – high pressure feedwater heater; FP – feedwater pump; DH – district heating heat exchanger; CPP – condensate polishing plant.

The turbine has five bleeder connections for regenerative feed water heating to 235.4 °C. From the High-Pressure Turbine (HPT) steam enters the reheater at a pressure of 3.12 MPa and 350.7 °C temperature, from which it is returned to the Reheat Turbine (RT). The Low-Pressure Turbine (LPT) is of a double-flow design.

Steam for turbine is a coal-fired boiler, with 540 t·h<sup>-1</sup> rated steam output, at a pressure of 13.85 MPa and 541°C for live steam and 471.4 t·h<sup>-1</sup> at 2.96 MPa and 541°C temperature for reheat steam. Feed water parameters at steam generator rated load are: pressure 18.8 MPa, temperature 235.4 °C.

The loads for performance test, for this power plant, were fixed to 115 MW, 130 MW and 150 MW power output for condensation operation.

Data in [table 3](#) shows the amount of heat available as waste heat rejected by the condenser for the 150 MW power plant. The amount of heat is close to the value in [table 1](#).

The temperature of the cooling water for the 150 MW power plant is presented in [table 4](#).

Table 3. Condenser loss

Load, MW	Heat rejected by condenser P <sub>cd</sub> , MW
115	185.380
130	216.480
150	262.759
Average loss	221.540

Table 4. Cooling water temperatures

Load	Cooling water temperature at condenser inlet, °C	Cooling water temperature at condenser outlet, °C
70%	19.2	30.84
85%	21.44	34.62
94%	24.69	40.32

### 3.1.2. Waste heat from turbocompressor cooling

Modern compressors employed today in the mining industry are rotary-screw compressors, but in the case of high air requirements and necessity of uninterrupted compressed air production, turbocompressors are also used. Choosing a

turbocompressor instead of a rotary-screw compressor is due to their high compressed air yields, and in addition, the turbocharger adapts well to the changing compressed air demand since the operating point of the turbocompressor moves, as for any such machine or pump, so no control is required if there is no major variation in the compressed air demand.

In the heyday of mining, the mines in Jiu Valley were all equipped with turbocompressors, and sometimes even up to three turbocompressors were in use.

This type of turbocompressor consists of seven stages, arranged in three bodies, the first two bodies having two rotors and the last having three. Cooling is performed by means of two intercoolers (Figure 13) and a final cooler, each of which is interchangeable.

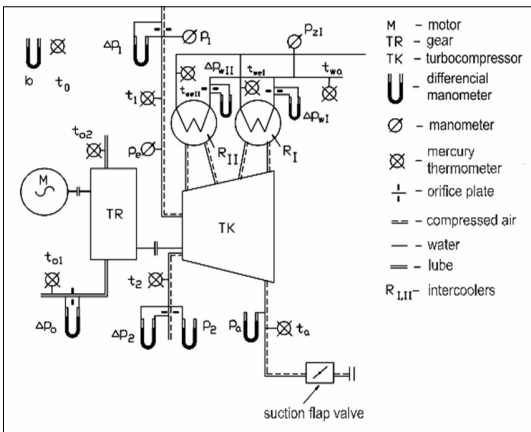


Figure 13. Schematic of the turbocompressor. [15]

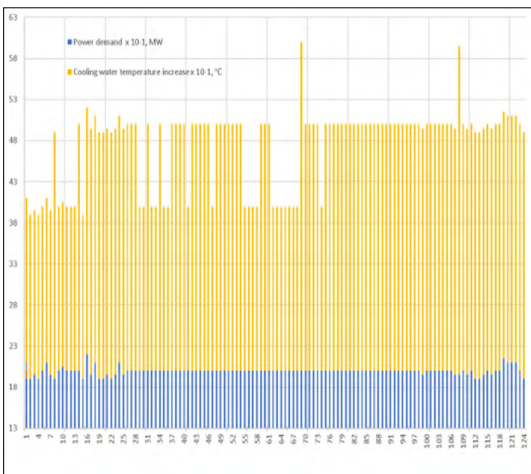


Figure 14. Measured data. [15]

Rated characteristics according to operation manual [14]:

Inlet air flow rate	16000 m <sup>3</sup> ·h <sup>-1</sup> ;
Inlet pressure	1 bar
Inlet temperature	20 °C;
Outlet pressure	8 bar
Turbocompressor speed	9980 rpm;
Motor speed	1500 rpm
Air temperature at final cooler outlet	40 °C;
Cooling water temperature at inlet	25 °C;
Cooling water flow rates:	
– through final cooler	55 m <sup>3</sup> ·h <sup>-1</sup> ;
– through intercoolers:	95 m <sup>3</sup> ·h <sup>-1</sup> ;
– through oil cooler	20 m <sup>3</sup> ·h <sup>-1</sup> ;
Rated motor power	1800 kW;
Motor efficiency	0.9;
Gear efficiency	0,95.

In order to accurately calculate the amount of waste heat, 124 measurements were made [15].

Measurement data is presented in figure 14.

Inlet temperature of the cooling water can vary from 15 °C in colder months (March), while in the summer months it can reach 28 °C. In winter even lower temperatures can be reached.

The temperature increase of cooling water is between 2-4 °C (2.75 °C average) and it is consistent with the motor power, which is directly proportional to the change in compressed air demand.

At a flow rate of the cooling water of 170 m<sup>3</sup>·h<sup>-1</sup> the inlet temperature was measured at the outlet of the cooling tower, while the outlet temperature of the cooling water was measured at the inlet of the cooling tower.

Therefore, amount of received heat is:

$$\begin{aligned}
 Q &= m \cdot c \cdot \Delta t = \rho \cdot V \cdot c \cdot \Delta t = \\
 &= \frac{997.05 \cdot 170 \cdot 4.186 \cdot 2.75}{3600} = \\
 &= 541,99 \text{ kW}
 \end{aligned}
 \tag{1}$$

where: Q – amount of heat, kW; V – volumetric flow rate, m<sup>3</sup>·h<sup>-1</sup>; Δt – temperature difference, °C, c – specific heat capacity of water at 25 °C, kJ·kg<sup>-1</sup>·K<sup>-1</sup>, ρ – density of water, kg · m<sup>-3</sup>.

As can be seen, the amount of waste heat is very high, 542 kW, and all this is released into the environment. Not to mention that, high cooling water temperatures can lead to inadequate cooling of the turbocompressor, which negatively affects its efficiency. Another disadvantage resulting from inadequate cooling is that hot compressed air

raises the temperature in the quarry, which has a negative effect on humans.

Basically, if we solve the problem of waste heat recovery, we will be able to solve the problem of proper compressor cooling as well, and will be able to extract a desired amount of heat, assuring that way the proper cooling of the turbocompressor. Solving these problems can bring huge energy savings.

The biggest challenge in this case, in terms of waste heat usage, is that the temperature of the water is very low, so that it cannot be used as it is in other technological processes.

### 3. Efficiency of waste heat recovery

To better understand the amount of waste heat available, some calculation can be carried out.

Heat demand of an average household can be met usually by installing a 28-kW boiler for heating and hot water delivery.

Assuming that we can recover all the heat rejected by the condenser which theoretically is 221,540.0 kW we can provide heating for 7912 households, and if we consider recovering the heat from the turbocompressor cooling water, we can provide heat for 19 households.

Waste heat recovery can be conducted through various waste heat recovery technologies, but their applicability depends on the temperature of the source.

In examples listed above the temperature of the heat source is everywhere between 10 °C for winter time and as high as 40 °C in summer. That means that the waste heat is a low temperature heat source.

For low temperature heat sources, the mechanical vapor compression, water-water type [16] heat pumps (figure 15) are suitable for harnessing energy. They can use waste heat from water with temperatures under 40 °C, and deliver heat at temperatures between 50 to 80 °C while a COP (coefficient of performance) in the range of 2.5 – 5.0.

Usually, a heat pump extracts heat from a source, such as the surrounding air, geothermal energy stored in the ground, or nearby sources of water.

In order to evaluate the efficiency of heat recovery let's assume that we recover heat from the cooling water of condenser of the 150 MW power plant.

As hot water is usually delivered using pipelines, losses can occur, so we set the required heat delivery for the heat pump to  $Q_i = 700$  kW, a value

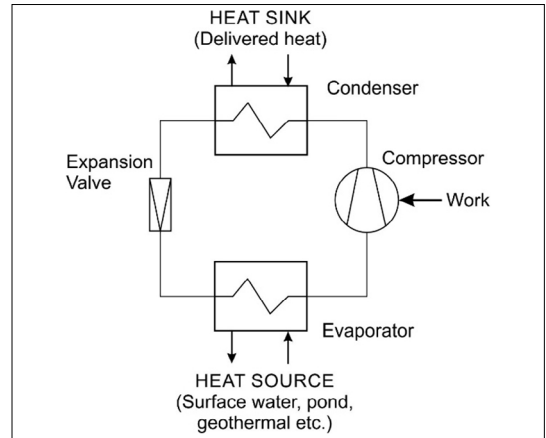


Figure 15. Vapour compression heat pump.

close to the maximum capacity of heat pumps employed today.

Additional data for calculation are:  $T_i = 70$  °C – temperature of delivered hot water,  $T_a = 5$  °C – ambient temperature,  $\Delta T_c = 5$  °C – temperature difference required for heat transfer in condenser (heat delivery),  $\Delta T_0 = 5$  °C – temperature difference required for heat transfer in evaporator,  $\Delta T_{sr} = 10$  °C – temperature difference for sub-cooling, mechanical efficiency  $\neq 0.9$ , employed refrigerant R717 (ammonia).

It must be stated that the ambient temperature will be the average temperature in the evaporator taking into account that at outlet of evaporator water temperature must be above 5 °C to prevent freezing, and the inlet temperature is the condenser outlet temperature. In order to compare the efficiency of using waste heat as heat source, a heat pump using the heat source a body of water is calculated first, considering heat source temperature 5 °C, this will represent a basis of comparison.

Data in table 4 regarding cooling water temperatures were measured during summer.

Results are presented in table 5 and figure 16.

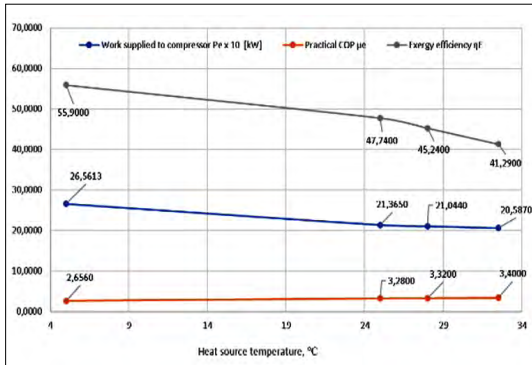
In addition, primary energy resources savings brought by a heat pump can be calculated using equation [17]:

$$\Delta E = \left( 1 - \frac{\eta_{CT}}{\mu_e \cdot \eta_{sis}} \right) 100, (\%) \quad (2)$$

where  $\mu_e$  is the practical COP (coefficient of performance);  $\eta_{sis} = 0,35$  – efficiency of electricity production in the national power grid;  $\eta_{CT} = 0,85$  – energy efficiency of hot water production in heat-only boiler stations.

**Table 5.** Heat pump efficiency

Heat source temperature, °C	Work supplied to compressor $P_e$ , kW	Practical COP $\mu_e$	Exergy efficiency $\eta_E$
5	265.613	2.656	55,90
25	213.648	3.28	47,74
28	210.437	3.32	45,24
32.5	205.635	3.40	41,29

**Figure 16.** Work supplied, practical COP and exergy-efficiency of heat pump.

Data presented in **figure 16** reveals that the exergy efficiency of the heat pump varies from 55.90 to 41.29 % for the studied temperature range.

COP of the heat pump increases with the temperature of the heat source up to 3.40 while the work supplied to compressor decreases from 265.613 kW to 205.87 kW. The primary energy resources savings calculated with equation (2) varies from 8.56 % to 28.57 %.

Hot water can be produced locally by small boiler units with energy efficiencies around 85% or obtained from cogeneration plants having up to 80% energy efficiency.

In order to compare these values with exergy efficiency of heat pump, exergy efficiency of boiler units and cogeneration plants must be established. Literature provides data on cogeneration plants showing that exergy efficiency can vary from 23% to 30.7% [18][19], while exergy efficiency of boilers can be between 16% to 25% [20].

## 4. Conclusions

A great amount of waste heat is available in industry, as in the examples provided, it can be seen that the value of the heat rejected by the power plant condenser is 243.652 MW for the 200 MW power plant and 221.540 MW for the 150 MW

power plant. The heat that can be recovered from turbocompressor cooling is 542 kW.

A major problem linked to this waste heat is that it is a low temperature heat source.

Using heat pump technology in order to recover waste heat is a very good solution as the COP of heat pump is between 2.65 and 3.40, while the exergy efficiency is between 55.90 and 41.29 %.

Using heat pump technology can lead to important primary energy savings varying from 8.56 % to 28.57%, higher values for high heat source temperature.

Unfortunately, the temperature of delivered heat is around 70 °C, which limits its usage to heating or hot water supply. As industrial facilities are located usually far away from human settlements, heat needs to be delivered, and that can dramatically decrease the overall efficiency of recovery (depending on distance).

This shortcoming can be eliminated by creating industrial parks near these secondary heat resources.

Another solution could be that research should be developed in the direction of increasing the temperature of the recovered heat source (waste heat to steam solutions), increasing the possibility of using it in different directions, within the framework of industrial facilities.

## References

- [1] [https://ec.europa.eu/eurostat/statistics-explained/index.php?title=Energy\\_production\\_and\\_imports](https://ec.europa.eu/eurostat/statistics-explained/index.php?title=Energy_production_and_imports) (letöltve: 2023. március 3.)
- [2] [https://ec.europa.eu/eurostat/statistics-explained/index.php?title=Energy\\_statistics\\_-\\_an\\_overview#Final\\_energy\\_consumption](https://ec.europa.eu/eurostat/statistics-explained/index.php?title=Energy_statistics_-_an_overview#Final_energy_consumption) (letöltve: 2023. március 3.)
- [3] [https://ec.europa.eu/eurostat/statistics-explained/index.php?title=Final\\_energy\\_consumption\\_in\\_industry\\_-\\_detailed\\_statistics#The\\_largest\\_industrial\\_energy\\_consumers\\_in\\_the\\_EU](https://ec.europa.eu/eurostat/statistics-explained/index.php?title=Final_energy_consumption_in_industry_-_detailed_statistics#The_largest_industrial_energy_consumers_in_the_EU) (letöltve: 2023. március 3.)
- [4] <https://www.eia.gov/energyexplained/us-energy-facts/> (letöltve: 2023. március 3.)
- [5] <https://www.eia.gov/international/analysis/country/CHN> (letöltve: 2023. március 3.)
- [6] <https://www.eia.gov/energyexplained/us-energy-facts/images/consumption-by-source-and-sector.pdf> (letöltve: 2023. március 3.)
- [7] Jiali Zheng, Gengzhong Feng, Zhuanzhuan Ren, Nengxi Qi, D'Maris Coffman, Yunlai Zhou, Shouyang Wang: *China's Energy Consumption and Economic Activity at the Regional Level*. Energy, 259. (2022) 124948. <https://www.doi.org/10.1016/j.energy.2022.124948>



- [8] <https://www.waste-heat.eu/about-waste-heat/waste-heat-sources> (letöltve: 2023. mácius 10.)
- [9] Gajendra Kumar Gaurav, Nitu Singh, Bijo Francis: *Exergy Analysis of a Thermal Power Plant*. Proceedings of Recent Advances in Interdisciplinary Trends in Engineering & Applications (RAITEA) 2019.  
<https://www.doi.org/10.2139/ssrn.3366867>
- [10] Rajesh Kale, Krishnakumar Dipak Pilankar: *Energy and Exergy Analysis of Steam and Power Generation Plant*. International Journal of Engineering Research & Technology (IJERT), 5/6. (2016)  
<https://www.ijert.org/research/energy-and-exergy-analysis-of-steam-and-power-generation-plant-IJERTV5IS060478.pdf>
- [11] Dosa Ion, Petrilean Dan Codrut: *Efficiency Assessment of Condensing Steam Turbine*. Journal Advances in Environment, Ecosystems and Sustainable Tourism, 2013, 203–208.  
<http://www.wseas.us/e-library/conferences/2013/Brasov/STAED/STAED-00.pdf>
- [12] Sorina Anutoiu, Ion Dosa, Dan Codrut Petrilean: *Steam Turbine Efficiency Assessment, First Step towards Sustainable Electricity Production*, MATEC Web Conf. 342 04007 (2021),  
<https://www.doi.org/10.1051/mateconf/202134204007>
- [13] Technical Instructions and Operation Manual for K 200-130-1 turbine.
- [14] Operation Manual of TK-R 16/8 turbocompressor.
- [15] Dosa I.: *Research on Energetics of Thermal and Fluid Dynamic Processes in Mining Pneumatic Installations*. Ph. D. thesis in Engineering; Speciality: Mining machines and installations; University of Petrosani, 1999.
- [16] Radcenco, V. et. al.: *Processes in Refrigeration Equipment*. Didactică și Pedagogică Publishing House, Bucharest, 1983, 372–390.
- [17] Berinde, T., Berinde, M.: *Energy Audits in Industrial Processes*. Tehnica Publishing House, Bucharest, 1985.
- [18] Mehmet Kanoglu, Ibrahim Dincer: *Performance Assessment of Cogeneration Plants, Energy Conversion and Management*. 50/1. (2009) 76–81.  
<https://www.doi.org/10.1016/j.enconman.2008.08.029>.
- [19] S.C. Kamate, P.B. Gangavati: *Exergy Analysis of Cogeneration Power Plants in Sugar Industries*. Applied Thermal Engineering, 29/5–6. (2009) 1187–  
<https://www.doi.org/10.1016/j.applthermaleng.2008.06.016>.
- [20] R. Saidur, J. U. Ahamed, H. H. Masjuki: *Energy, Exergy and Economic Analysis of Industrial Boilers*. Energy Policy, 38/5. (2010) 2188–2197.  
<https://www.doi.org/10.1016/j.enpol.2009.11.087>.



# DESIGN OF AN INJECTION MOLDING TOOL WITH EXCHANGABLE INSERTS

Kristóf KERESZTES,<sup>1</sup> Attila Levente GERGELY<sup>2</sup>

*Sapientia University of Transylvania, Faculty of Mechanical Engineering, Târgu Mures, Romania*

<sup>1</sup> [keresztes.kristof@student.ms.sapientia.ro](mailto:keresztes.kristof@student.ms.sapientia.ro)

<sup>2</sup> [agergely@ms.sapientia.ro](mailto:agergely@ms.sapientia.ro)

---

## Abstract

The aim of this work was to design an injection molding tool with replaceable inserts. The tool design is made for a BOY 15S injection molding machine. Based on the interpretation and comparison of the simulation results of the filling process, we optimized the plastic part design, the runner system and the location of the gates and cavities in order to maximize productivity and efficiency while minimizing cost. In the process of the tool design, we also considered the potential problems regarding the manufacturing process of the tool.

**Keywords:** *injection molding, tool design, optimization, simulation.*

---

## 1. Introduction

### 1.1. The basics of injection molding

The basic principle of injection molding is the "injection" of a low viscosity plastic melt into a closed cavity. This is done through a narrow passage. Low viscosity is essential for a fast and complete filling of the mold. Complete filling (for thermoplastics) is also facilitated by high injection pressure. Due to the fundamental nature of the injection molding process, the cooling process of the melt only lasts a few seconds at most and results in a final product of high dimensional accuracy. In addition, the advantage of injection molding is that it allows the production of complex shaped parts that require no further machining other than the removal of plastic that has solidified in the runner system.

### 1.2. The injection molding machine

The injection molding machine is responsible for melting the plastic (usually in the form of granules) and injecting it into the mold. It is also responsible for opening the mold along the parting plane and operating the ejection system. Its mechanism is optimized for fast and efficient injection molding and ejection of the product after solidification.

The mold is designed for the BOY 15S injection molding machine located at the University of Sapientia EMTE Târgu Mures, Faculty of Mechanical Engineering.

### 1.3. The injection molding tool

The injection molding tool is the component that allows the shaping of the part. It contains the runner system and the mold cavities that are filled to create the part. The type of tool used depends on the part. The production of more complex parts requires more complex tooling, so it is important to think cost-effectively from the very first steps of part design. The mold designed in this article has a simple, two-plated design (**Figure 1**).

It is also the tool's task to convey the melt from the nozzle of the injection molding machine to the mold cavity, this is done by means of the inlet / runner system.

The opening through which the plastic melt enters the mold cavity from the runner system is called the gate. The size and position of the gates have a profound influence on the quality of the final product. It can sometimes make the difference between a perfect and a defective part, so correct sizing and positioning is of particular importance.

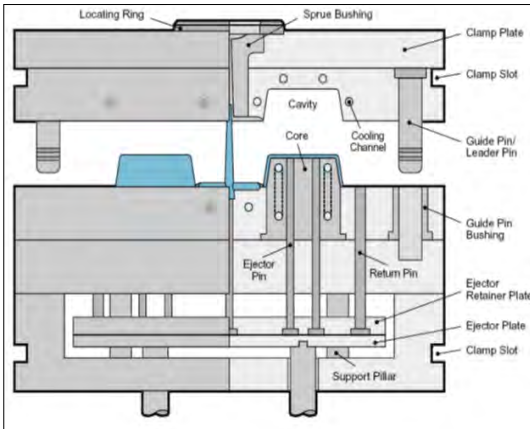


**Figure 1.** Construction of a two-plated injection mold tool. [1]

## 2. Methodology

Autodesk Inventor was used to create the assembly model of the plastic part, inserts and tool housing, and to perform the stress analysis. The plastic flow of the melt was simulated using SolidWorks Plastics. The parameters required to run the simulations were chosen from the table of the parameters of the BOY 15S injection molding machine.

In the calculations, at each step, we chose the less favorable parameter of either polyethylene or polypropylene, therefore the results provide a significant safety factor.

### 2.1. Tool housing

In designing the tool housing, the selected components were based on the simple two-plated tool structure. The correct movement of the two tool halves during tool opening and closing process is ensured by pins and corresponding bushings, the 3D models of which were downloaded from the online parts catalogue of Meusburger GmbH & Co KG.

### 2.2. Inserts

The design process of the inserts consists of several steps. The first step is to design the shape of the mold cavity, which is determined by the plastic part. When designing the plastic part (and therefore the mold cavity as well), it is important to avoid shapes that are problematic for injection molding. Examples include right-angled corners, thin recesses, sections with staggered wall thicknesses, etc.

## 3. Results

### 3.1. Cavity filling simulations

To perform the simulations, a plastic component model is needed. This model forms the final product.

#### 3.1.1. Determining the optimal gate position

The first result of the evaluation of the simulations is the determination of the optimal gate position. This was chosen based on the number and size of air pockets and weld lines that appear in the simulations, since these are manifested as aesthetic defects in the final product [2]. The overall quality of the filling process was also taken into consideration.

In determining the optimal gate position, injection pressure, and a gate dimension were kept constant so that the quality of the filling process could be studied as a function of gate position.

In addition to the results of simulations with different barrier positions, cost-effective design also played an important role in this decision.

**Figure 2** shows the final gate position. This will ensure that the melt front fills the model's protrusions longitudinally, which helps to eliminate weld lines. [3]

#### 3.1.2. Determining the optimal plastic part model

The plastic part model represents a keychain with the logo of the Sapientia University of Transylvania. The prominent parts of the 3D model create a number of geometric corners, which present difficulties for the injection molding process. In the optimization process of the model, the priority was to change these problematic shapes

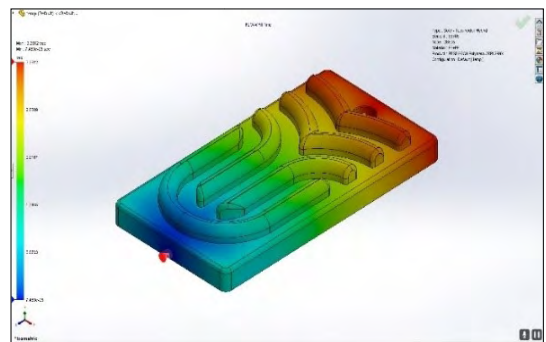


**Figure 2.** Optimal gate position for symmetrical filling.

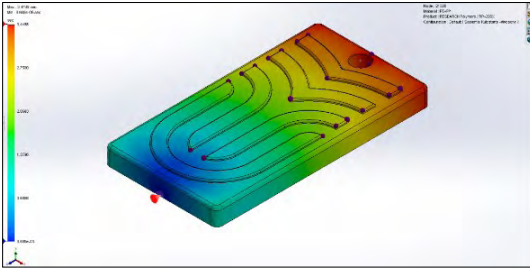


**Figure 3.** Optimized model with reduced and chamfered protrusions.

in such a way that the deviation from the original part was minimized (Figure 3).

The simulations helped in the optimization of the plastic part model to ensure that the cavity is fully filled. This was done by modifying the geometric features that result in air pockets and weld lines. [3]

## 3.2. Design of the injection molding tool

### 3.2.1. Design of core and cavity retainer plates

Due to the interchangeable inserts of the mold, the space required for the insert must be provided in the two mold halves, which measure  $80 \times 100$  [mm  $\times$  mm]. The inserts have a thickness of 15 mm, and they are positioned 13 mm deep in the two retainer plates to ensure full contact of the inserts - and only the inserts - during the closing of the tool.

The ejector rods must penetrate the moving side of the core retainer plate to allow ejection of the plastic part. This can be achieved by drilling holes, but this would mean that different holes would have to be drilled to accommodate different inserts (which have varying rod sizes and placements). As one of the main concerns is to facilitate the interchangeability of the inserts, this solution is not ideal.

In order to make the moving side of the tool suitable for different inserts, a through-slot must be designed in the core retainer plate. The dimensions of this slot are slightly smaller than the size of the insert, as shown in figure 4. This is done to achieve a shoulder that provides a support surface for the insert.

To verify the functionality of the mold base, stress analysis was performed. The maximum load is known due to the injection molding machine parameters (50 tons). The analysis was performed using AutoDesk Inventor Stress Analysis (Figure 5). The material used in the simulations is AISI 1045 steel. The mechanical properties of this

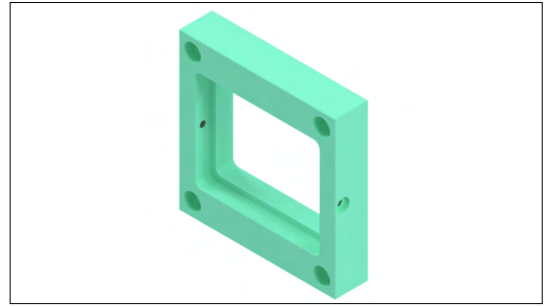


**Figure 4.** More retainer plate machined for insert accommodation and ejection system operation.

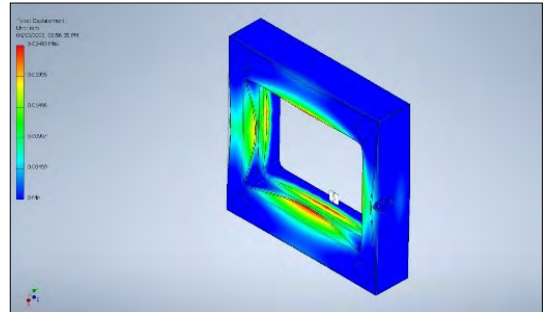


**Figure 5.** Deformation of the moving side mold base under 50 tonnes of load force (AutoDesk Inventor Stress Analysis).



**Figure 6.** Side view of the parting plane (marked with a blue line at the bottom of the part).

material can be found in the AutoDesk Inventor material catalogue. The Young's Modulus of AISI 1045 is around 200 GPa.

The maximum deformation at 50 tonnes of closing force did not exceed  $25 \mu\text{m}$ , as it is shown in figure 5. This value is low enough to be considered negligible for injection molding.

### 3.2.2. Determining the parting plane

When designing an injection molding tool, it is important to consider the position of the parting plane. Since cost-effective design is a major objective, the part's base plane has been chosen as the parting plane (Figure 6). This offers several advantages.

Primarily, it ensures that the part remains in the moving side of the mold during mold opening, thus making part ejection possible. Next, the position of the parting plane means that only one of the inserts needs to be machined, reducing production costs and time. There is one drawback to the choice of this particular parting plane: the edges of the part that are in the parting plane cannot be rounded, nor chamfered.

### 3.2.3. Runner system and cavity design

The inlet channel diameter was chosen to be 2 mm, as this diameter is suitable for injection molding all the listed plastics for the designed mold (Table 1), since the maximum flow path is 70 mm (from the nozzle to the gates).

The relationship between the diameter of the sprue and the diameter of the runner system channels is given by the following formula:

$$D_{previous} = D_{next} \cdot \sqrt{n} \quad (1)$$

where  $n$  is the number of channels in the junctions,  $D_{previous}$  is the diameter before the junction and  $D_{next}$  is the diameter after the junction.

The runner diameter calculated from the size of the sprue is 2,82 mm. Since the sprue channel is tapered (0,5° taper angle), the value obtained is the average diameter. Among the sprues distributed by Meusburger GmbH, one can be found with an average diameter of 2,91 mm. This is sufficiently close to the calculated value.

The positioning of the cavities is determined by the factors previously mentioned: the chosen gate position and the dimensions of the base plates. Since the dimensions of the insert are 80 x 100 [mm x mm], four cavities can be placed leaving a sufficiently thick (6 mm) wall between the tool cavities and the outside of the insert (Figure 7).

The volume calculated from the 3D model of the designed plastic part is 2.35697 cm<sup>3</sup>, so the volume of the four cavities is 9.42788 cm<sup>3</sup>. The combined volume of the inlet manifold and runner system is 3.80619 cm<sup>3</sup>, so the volume of polymer melt required for one injection molding cycle is 13.23407 cm<sup>3</sup>. The maximum injection volume per cycle is 96 cm<sup>3</sup>.

### 3.2.4. Determining the dimensions of the gates

When designing the gates, the aim is to minimize the size of the gate. The reason for this is to make the removal of plastic solidified in the gates easier from the product of the injection molding cycle.

**Table 1.** Maximum flow path of plastics in a 2 mm diameter channel [4]

Plastic	Max. flow path in a 2 mm diameter channel [mm]
Polyethylene (LDPE)	720
Polyethylene (HDPE)	400
Polypropylene	870
Polystyrene	670
Polyamide 66	560
Polyamide 6	510
ABS	370

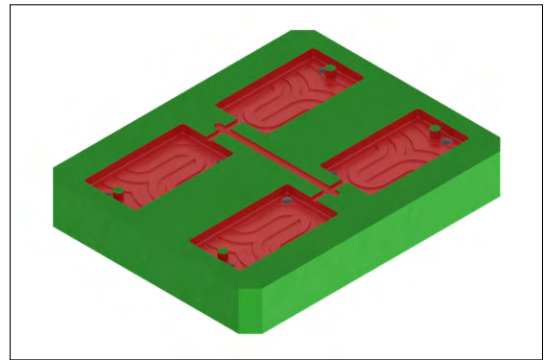


**Figure 7.** Model of the moving side insert.

The limiting factors are the maximum shear rate and the calculated pressure drop at the gates. These values depend on the used plastic [5].

In the first step, the maximum shear rate was considered: [5]

$$\dot{\gamma} = 6 \cdot \dot{V} / (w \cdot h^2) \quad (2)$$

where  $\dot{\gamma}$  – shear rate [1/s],  $\dot{V}$  – volume flow [cm<sup>3</sup>/s],  $w$  – gate width [m] and  $h$  – gate height [m].

The final dimensions of the barriers are:  $w=2$  mm,  $h=0,75$  mm. The resulting shear rate:  $\dot{\gamma}=17645.426$  1/s. Among the different polyethylene and polypropylene types, the lowest maximum shear rate value was found to be that of HDPE and LDPE: 40000 1/s [6], which is not exceeded by the calculated result.

Next, the calculated pressure drop across the entire runner system was investigated. From the results of the simulations, the pressure drop is found to be less than 75 MPa. The used injection molding machine is able to produce more than twice the calculated pressure ( $P_{max} = 168$  MPa).



### 3.2.5. Ejection system design

The ejector rods used in this design are cylindrical and have a flat face. In order to calculate the minimum diameter, we had to determine the force required for ejection using formula (3) [5]. The value of this force is 1970 N (rounded up).

$$F = \mu \cdot \cos(\Phi) \cdot E \cdot CTE \cdot (T_2 - T_1) \cdot A_{eff} \quad (3)$$

where  $\mu$  – coefficient of friction,  $E$  – Young's Modulus [Pa],  $CTE$  – coefficient of thermal expansion [ $1/^\circ\text{C}$ ],  $A_{eff}$  – shrinkage area of the plastic piece [ $\text{m}^2$ ],  $\varepsilon$  – material specific elongation,  $\Phi$  – taper angle of the wall of the tool cavity that is stressed during the shrinkage of the plastic [ $^\circ$ ].

Knowing the force required to eject the parts, the minimum diameter required to resist the shearing force by the plastic parts can be calculated. [5]

$$\Omega_{ejectors} > 2 \cdot \frac{F_{ejection}}{\sigma_{max} \cdot h} \quad (4)$$

where  $\Omega_{ejectors}$  – circumference of the face of the ejector rods [m] (shear line),  $\sigma_{max}$  – yield strength [Pa] and  $h$  – wall thickness of the plastic part at the point of contact with the ejector rod [m].

The resulting minimum total circumference of the ejector rods is 41.042 mm. The designed inserts have 8 ejector rods, so the minimum diameter of one ejector rod is 1.63301 mm. Including a safety factor, the rounded value is 3 mm; such ejector rods are available from Meusburger GmbH, which simplifies sourcing and obtaining the part.

The ejector rods were also checked for deflection: their stress was 34.83725 MPa, while the maximum allowable value was 2.86467 GPa.

The shape of the plastic part limits the positioning of the ejector rods, which can only come into contact with the plastic part where its surface is flat (Figure 8.).

## 4. Conclusions

We have successfully completed the design of an injection molding tool with exchangeable inserts. Thanks to the mold's design, it will be possible to injection mold different plastic parts without the

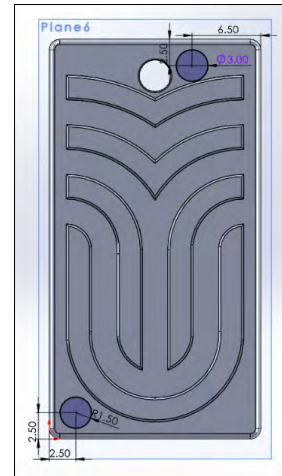


Figure 8. Positioning of ejector rods on the plastic part.

need for the lengthy and costly process of changing the tool. Thanks to the implementation of several safety factors, the tool will be suitable for analyzing the injection molding process of different types of plastics.

This has been the first step towards enabling students at our University to study the injection molding process with an industrial injection molding machine.

## References

- [1] Mikó B.: *Műanyagfröccsöntő szerszám tervezése és gyártása*. Budapest, 2006. 1–6.
- [2] Seow L. W., Lam Y. C.: *Optimizing Flow in Plastic Injection Molding*. Journal of Materials Processing Technology, 78/3. (1997) 333–341. [https://doi.org/10.1016/S0924-0136\(97\)00188-X](https://doi.org/10.1016/S0924-0136(97)00188-X)
- [3] Mehdi M.: *Intelligent Optimization of Mold Design and Process Parameters in Injection Molding*. Springer. Springer International Publishing, Cham, 2019. <https://doi.org/10.1007/978-3-030-03356-9>
- [4] Dunai A., Macskási L.: *Műanyagok fröccsöntése*. 2003. 357–358.
- [5] Kazmer O. D.: *Injection Molding Design Engineering*. Hanser Gardner Publications Inc, München, 2016. 176–178, 265–273.
- [6] Maximum of Shear Stress and Shear Rate. 2021.



# SYNTHESIS AND CAD-EXAMINATION OF A CYLINDRICAL GEAR PAIR DERIVED FROM A COSINE PROFILED RACK

Márton MÁTÉ,<sup>1</sup> Károly-István GÁL,<sup>2</sup> Ferenc TOLVALY-ROȘCA<sup>3</sup>

*Sapientia Hungarian University of Transylvania, Faculty of Technical and Human Sciences, De-partment of Mechanical Engineering, Targu-Mures, Romania*

<sup>1</sup> [mmate@ms.sapientia.ro](mailto:mmate@ms.sapientia.ro),

<sup>2</sup> [gal.karoly@ms.sapientia.ro](mailto:gal.karoly@ms.sapientia.ro),

<sup>3</sup> [tferi@ms.sapientia.ro](mailto:tferi@ms.sapientia.ro)

---

## Abstract

The problematic of gear profiles has again come to the fore during the power demands imposed by technical development. Most of nowadays gears have involute profile due to its numerous advantages. The most important is that that axis distance variation does not affect the transmission ratio. According to [1], a cosine gear drive has a lower slip coefficient and the contact and bending stresses by charge are significantly lower compared to an involute gear. This paper presents a study regarding the generation synthesis of a cosine profiled gear pair, using a single cosine profiled rack, in a CAD environment. The profile of the generating rack and the mathematical computations of the equations of gearing were performed in a Mathcad environment. The tool models were created in Autodesk Inventor. Then it was implemented in Autodesk AutoCAD and using its special programming language (Auto lisp), a simultaneous subtraction-rolling method was used to obtain a realistic simulation of the meshing of the cut gear with the rack. Implementing the generated gears in Autodesk Inventor environment, tests were performed in order to compare the cosine profile of the generated gears with the profile of the involute gears. In the near future, we intend to exploit the results obtained and compare the transmission quality of the involute gears with the cosine gears.

**Keywords:** *cosine profile, involute, CAD, Mathcad, Autolisp, cosine profiled rack, gear.*

---

## 1. Introduction

In terms of tooth profile, gears can be classified as involute, bolt, cycloid or circle arc shaped. The most widely used profile is the involute profile due to its numerous advantages among which the following must be emphasized: the transmission ratio is not affected by the variation of the axis distance, and the manufacturing technology is simple, robust and at reasonable costs. Certainly, the involute gear has also drawbacks such as the limited load capacity and the susceptibility to interference and undercut. Thanks to the appearance of numerical controlled machine tools, the area of special tooth profiles has been vigorously extended.

The use of cycloid profiled gears in today's machinery is significantly uncommon – the area of implementation being confined to the mechanical clock industry and some special gear pump

constructions. It must be mentioned here that cycloidal gears have the advantage of zero relative slipping between the tooth flanks which results in neglectable mechanical wear, lubrication is not a prerequisite in any circumstances of exploitation, and the contact ratio is certainly greater than for the involute, bolt or circular arc toothed gears.

Bolt gears are the oldest type of gears. This type of gear has made a major comeback in clock mechanisms, cycloidal drives and lifting equipment. Cyclo-drives consist of a wheel having the teeth as circular section equiangular disposed rods and a cycloid profiled counter gear.

There exists also the possibility of designing the spur gears with circular arc profiled teeth. Their field of application comprises concrete mills, compressors, elevation systems and others. In the US machinery the endowment of plastic gears with circular arc profiled teeth is considered the

most appropriate. These present certain advantages due to their rigidity, resulting in high load transmission capacity and silent functioning by a corresponding lubrication. The efficiency of the transmission is superior to non-grinded involute gear transmissions [2].

## 2. The cosine-rack generated gear pair

### 2.1. The elements of the involute rack

For easier further application, the basic profile is defined for the module  $m=1$  mm. The standard profile angle is set at  $\alpha=20^\circ$ . To increase the rigidity of the dedendum zone, the root fillet is set to  $\rho_{of}=0.38 \cdot m$  (Figure 1). The definition of the cosine rack is based on the values of the standard involute rack, excepting the profile angle and the linear flank form [2].

### 2.2. The design of the cosine generating rack

The equations of the cosine rack profiles are written to the frame  $O_{Si} X_{Si} Y_{Si}$ ,  $i \in \{1, 2\}$ .

Respecting Litvin’s criterion, a gear pair’s generating racks must match like a template and counter-template. Thus, the blue rack generates part 1, while the green rack part 2 of the gear pair. (Figure 2). Their common profile is the ABCDEFG cosine curve, shown in red. The equation of the profile is sought in the form:

$$y_{s1}(x) = a \cos(bx), \tag{1}$$

where

$$a = a_s = b_s = (h_o^* + c_o^*)m, \\ \text{and } h_o^* = 1, c_o^* = 0.25.$$

The implementation of the cosine curve needs the pitch of the rack ( $p = \pi m$ ) which must be synchronized with the period of the function. Using the periodicity of the cosine function it can be written, that:

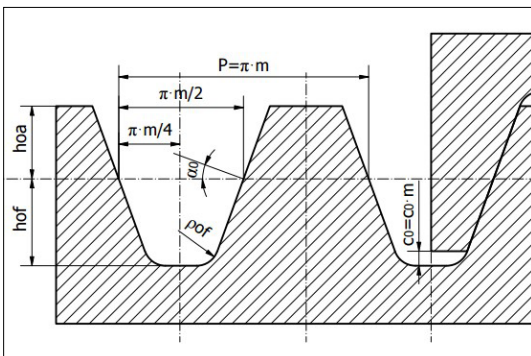


Figure 1. Standard basic profile.

$$y_{s1}(x) = y_{s1}(x + p) \\ \Rightarrow a \cos(bx) = a \cos b(x + p) \tag{2}$$

After transforming the sum above in a product, the result is:

$$\sin\left(bx + \frac{pb}{2}\right) \sin\left(\frac{bp}{2}\right) = 0 \tag{3}$$

Equation (3) must be true for any  $x$ , thus:

$$\sin\left(\frac{bp}{2}\right) = 0 \tag{4}$$

The solution of the trigonometric equation in canonic form (4) is:

$$\frac{pb}{2} = (-1)^k \arcsin(0) + k\pi, k \in \mathbb{Z} \tag{5}$$

So we get

$$b = \frac{2k\pi}{p} = \frac{2k\pi}{\pi m} = \frac{2k}{m} \tag{6}$$

The next possible value results in for  $k=1$ , thus:

$$b = \frac{2}{m} \tag{7}$$

Although the profile angle of the cosine rack is variable, its nominal value is defined on the pitch line. This choice allows the comparison with a standard involute rack of,  $\alpha_0=20^\circ$ . Based on Figure 1, the cosine rack profile angle is defined by the pitch line-point tangent of the cosine curve and the perpendicular to the  $x$  axis.

Exploiting the geometric sense of the derivative, one gets

$$\operatorname{tg} \varphi = \operatorname{ctg} \alpha_c = \frac{dy}{dx} \Big|_{(x=-\frac{\pi m}{4})} = -ba \sin bx \tag{8}$$

After performing the computation we obtain:

$$\alpha_c = \frac{\pi}{2} + \operatorname{arctg}(-2.5) \approx 21^\circ 48'$$

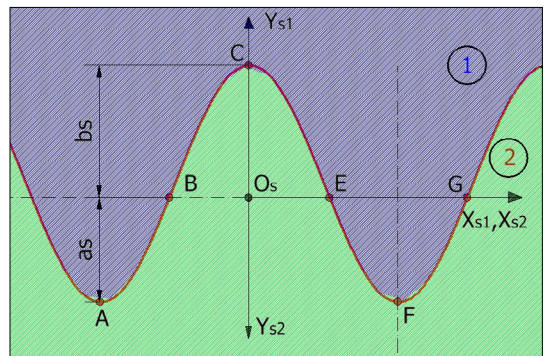


Figure 2. The common profile of the rack pair.

The symmetry axis of the tooth gap of the element 1 generating rack is axis  $y_{S1}$  as can be seen in **Figure 2**. Thus, the explicit equation of the rack 1 results in:

$$y_{S1}(x_{S1}) = a \cos\left(\frac{2}{m} x_{S1}\right) \tag{9}$$

The axis  $y_{S2}$  is the symmetry axis of the tooth of the element 2 generating rack. Let us observe the template-counter template principle in the build-up of the two racks. Thus, the equation of rack 2 results in:

$$y_{S2}(x_{S2}) = -a \cos\left(\frac{2}{m} x_{S2}\right) \tag{10}$$

If admitting the translation of a half pitch, to overlap the symmetry axis of the tooth gap with the axis  $y_{S2}$  it must accept

$$x_{S2} = x_{S2}^* + \frac{\pi m}{2}.$$

As following  $y_{S2}^*(x_{S2}^*) = a \cos\left(\frac{2}{m} x_{S2}^*\right)$ , thus

one gets the equation of the profile of rack 1. By this calculus it was proven that the principle of the pattern- counter pattern persists and the two racks not only present the same profile, but they are congruent, exactly as in the case of involute racks.

### 2.3. The synthesis of a cosine gear pair

The generating principle of the cosine gear pair by conjugate generating racks is presented in **figure 3**. On the left are presented the used frames in their initial positions while on the right, in a position that corresponds to an arbitrary moment of the generation process. The indices of the axes have the following significance: zero is the index of the fixed frame, 1 and 2 the indices of the generated wheels while indices s1 and s2 are the indices of the corresponding rack.

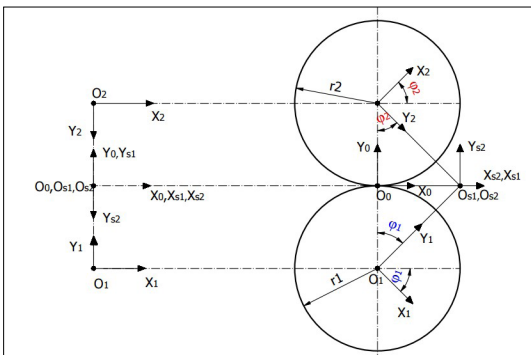


**Figure 3.** Generating geometry of a gear pair.

The transformation of coordinates between the involved frames is given by the following matrix equations:

$$\begin{aligned} \mathbf{r}_1 &= \mathbf{M}_{10} \mathbf{M}_{0s1} \mathbf{r}_{s1} \\ \mathbf{r}_2 &= \mathbf{M}_{20} \mathbf{M}_{0s2} \mathbf{r}_{s2} \\ \mathbf{M}_{1s1} &= \mathbf{M}_{10} \mathbf{M}_{0s1} \\ \mathbf{M}_{2s2} &= \mathbf{M}_{20} \mathbf{M}_{0s2} \end{aligned} \tag{11}$$

In this paper the detailed form of the matrices is omitted; although, if performing the computing, the structural identity of  $\mathbf{M}_{10}$  and  $\mathbf{M}_{20}$  is obvious.

### 2.4. The equations of gearing

The equations of gearing are written for wheels 1 and 2 which are contacting their racks. The relative velocities result from the position vectors and angular velocities shown in **figure 4**. [7]

The expressions of the relative velocities become:

$$\begin{aligned} \mathbf{v}_{s1}^{(1,s1)} &= \mathbf{v}_{s1}^{(1)} - \mathbf{v}_{s1}^{(s1)} = \\ &\boldsymbol{\omega}_{O1}^{(1)} \times \mathbf{r}_{s1} + \mathbf{A}_1 \times \boldsymbol{\omega}_{O1}^{(1)} - \omega_1 r_1 \mathbf{i}_{s1} \\ \mathbf{v}_{s2}^{(2,s2)} &= \mathbf{v}_{s2}^{(2)} - \mathbf{v}_{s2}^{(s2)} = \\ &\boldsymbol{\omega}_{O2}^{(2)} \times \mathbf{r}_{s2} + \mathbf{A}_2 \times \boldsymbol{\omega}_{O2}^{(2)} - \omega_2 r_2 \mathbf{i}_{s2} \end{aligned} \tag{12}$$

### 2.5. The generation of conjugate profiles with a common rack

Due to the fact that the validity of the template-counter template principle was demonstrated in subsection 2.2, a cosine gear pair can be machined with a unique rack, admitting  $\xi=0$  profile shifting. Thus, the equation of the rack coincides with those given in subsection 2.2.

The matrix transformation equations used for the meshing are as follows:

$$\begin{aligned} \mathbf{M}_{1s} &= \mathbf{M}_{10} \mathbf{M}_{0s} \\ \mathbf{M}_{1s} &= \mathbf{M}_{10} \mathbf{M}_{0s} \end{aligned} \tag{13}$$

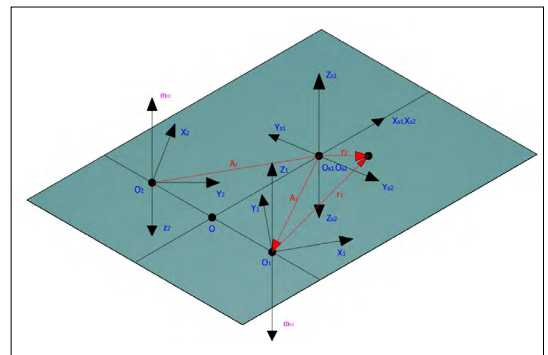


**Figure 4.** The scheme of coupling involving two different racks

Angular velocity vectors and their moments related to the origin  $O_s$  are as follows:

$$\omega_{O1s}^{(1)} = \begin{bmatrix} 0 \\ 0 \\ -1 \end{bmatrix}; \mathbf{A}_{1s} = \begin{bmatrix} -r_1\varphi_1 \\ -r_1 \\ 0 \end{bmatrix};$$

$$\omega_{O2s}^{(2)} = \begin{bmatrix} 0 \\ 0 \\ -1 \end{bmatrix}; \mathbf{A}_{2s} = \begin{bmatrix} -r_2\varphi_2 \\ r_2 \\ 0 \end{bmatrix}; \tag{14}$$

If substituting column vectors (14) in velocity expressions (12) one gets the relative velocity column vectors related to the frame of the rack:

$$\mathbf{v}_s^{(s1)} = \begin{bmatrix} -y_s \\ x_s - r_1\varphi_1 \\ 0 \end{bmatrix}$$

$$\mathbf{v}_s^{(s2)} = \begin{bmatrix} y_s \\ x_s + r_2\varphi_2 \\ 0 \end{bmatrix} \tag{15}$$

In this model it is to remark that both profiles are simultaneously in contact which means that if  $M$  is the contact point, then  $\mathbf{n}_1 = \mathbf{n}_2$ , thus, the equations of gearing become:

$$\mathbf{v}_s^{(s1)} \cdot \mathbf{n}^{(1)} = 0$$

$$\mathbf{v}_s^{(s2)} \cdot \mathbf{n}^{(2)} = 0 \tag{16}$$

The cosine profile's normal vector is written using the parametric form (9) (Figure 5):

$$\mathbf{n}(u) = \begin{bmatrix} \frac{2a}{m} \sin\left(\frac{2}{m}u\right) \\ 1 \\ 0 \end{bmatrix} \tag{17}$$

To get the first gearing equation expression (15) and (17) are replaced in equation (16):

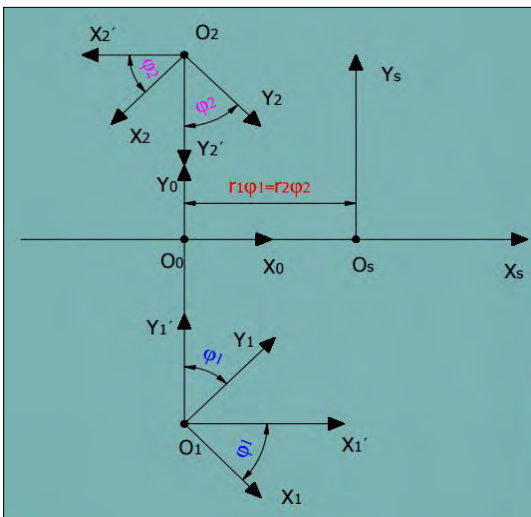


Figure 5. Machining with a unique rack.

$$-y_s \frac{2a}{m} \sin\left(\frac{2}{m}u\right) + (x_s - r_1\varphi_1) \cdot 1 = 0 \tag{18}$$

This leads to the following solution:

$$\varphi_1(u) = \frac{2}{mz_1} \left( x_s - y_s \frac{2a}{m} \sin\left(\frac{2}{m}u\right) \right) \tag{19}$$

Similarly, the second gearing equation is:

$$y_s \frac{2a}{m} \sin\left(\frac{2}{m}u\right) - (x_s - r_2\varphi_2) \cdot 1 = 0, \tag{20}$$

whose solution is presented in the following expression:

$$y_s \frac{2a}{m} \sin\left(\frac{2}{m}u\right) - (x_s - r_2\varphi_2) \cdot 1 = 0, \tag{21}$$

Implementing equations above in the Mathcad environment, the resulting left (red) and the right (blue) tooth gap profile's shapes are drawn in figure 6.

Transposing the coordinates of the contact points gained with the function of gearing  $\varphi = \varphi(u)$  in the fixed frame using the matrix equations  $\mathbf{r}_{0i} = \mathbf{M}_{0si} \mathbf{r}_{si}$ ,  $i \in \{1; 2\}$ , the lines of actions are obtained. These are represented in figure 7.

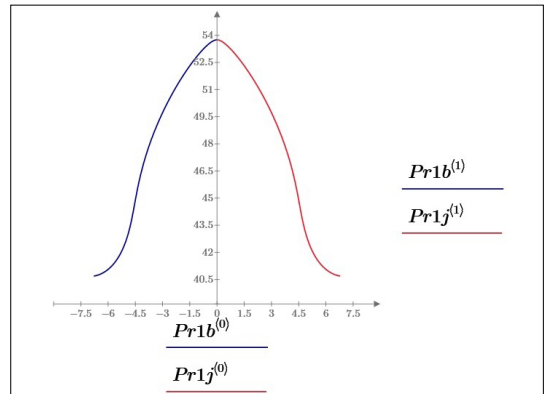


Figure 6. Tooth gap profiles.

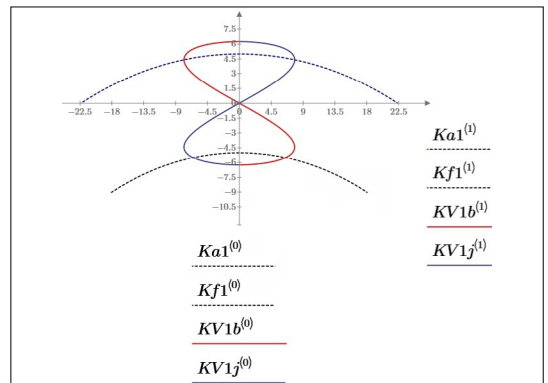


Figure 7. Lines of actions for the left and right tooth profiles.



The real segments of action are comprised of the addendum circle and the inner circle arcs (radius of the inner circle is considered here greater than the dedendum circle radius by  $c_0^*m$ ).

### 3. Simulation of the gearing

In order to simulate the gearing and meshing process, first the solid model of the generating rack must be built up.

Model initial data was considered as follows:  
 $m = 5 \text{ mm}; h_0 = 1; c_0 = 0.25; z_1 = 19; z_2 = 27; b = 2/5$   
 $a = (h_0 + c_0)m = 6.25 \text{ [mm]}$  (22)

Using the deduced equations with initial data in the Mathcad environment, the generated cosine profile is shown in **figure 8**.

The 3D rack model was realized in Autodesk Inventor environment, using the coordinates of the profile points (**figure 9**). The simulation of manufacturing was performed in the Autodesk AutoCad environment because the Inventor environment cannot handle 3D solid object subtraction. Using the AutoCad programming space, an Autolisp [3-5] program was realized which simultaneously performs the rolling and subtraction.

### 4. Comparative study

Investigations were carried out on the gear pair realized with the common rack. An involute gear pair defined by similar initial data (number of teeth, module, axis distance) was also modelled.

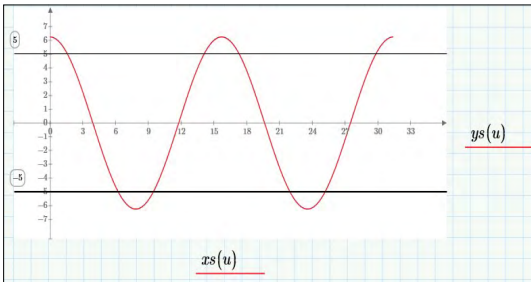


Figure 8. Generating rack’s cosine profile.

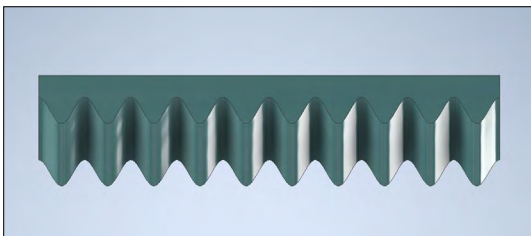


Figure 9. Solid model of the generating rack.

In order to obtain valid data, the profile shifting coefficient was set to  $\xi = 0$ . To increase the profile precision of the cosine rack, the maximum possible number of profile points (500 points) was considered, and spline fitting functions were defined by them. Using the Autolisp programming environment the solid models of cosine gears with  $z_1 = 19$  and  $z_2 = 27$  teeth were obtained. The precision value for the subtraction was set at 0.2 mm, due to the very high hardware demand of this operation (a complex operation consisting of step by step subtraction and surface regeneration). **Figure 12** shows the linear traces drawn by the generating rack on the tooth surface [3].

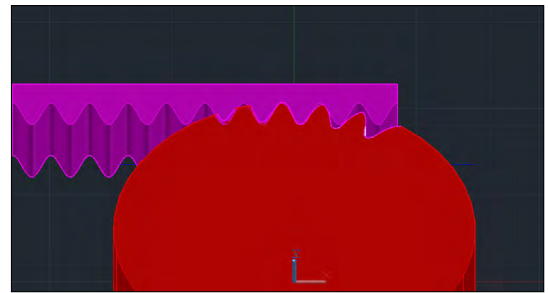


Figure 10. The subtracting operation through the rolling process.

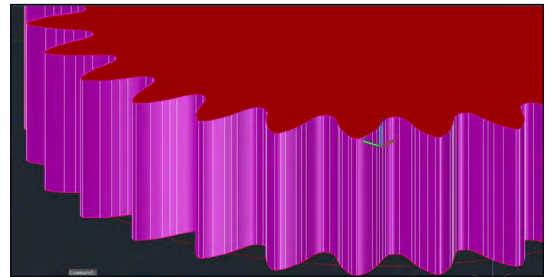


Figure 11. Gear generated in the AutoCad environment

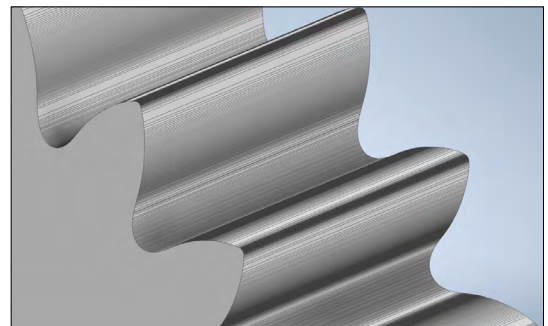


Figure 12. Traces of the generating rack on the tooth surface.

**4.1. Graphical validation of the mathematical model**

Firstly, the matching of the mathematically deduced and the 3D modelled profiles was examined.

Figure 13 shows a perfect match of the profile deduced with the use of the equation of gearing in the Mathcad environment with the profile realized by CAD-simulation. Thus, the validation of the analytical formulae defining the mathematical model has been confirmed.

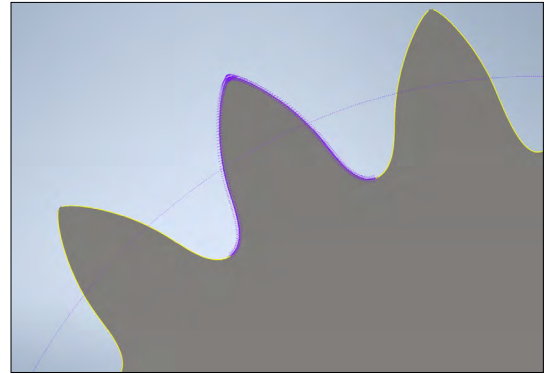


Figure 13. Proofing of the mathematical model

**4.2. The influence of tooth number on tooth profile form**

As is well known, involute profile curvature depends on the tooth number, due to the variation of the basic circle radius. This conclusion remains valid for the cosine gears too, as can be seen in figure 14.

It shows the profile of the tooth of  $z=19$  gear (magenta) set on the symmetry axis of the tooth of  $z=27$  gear (yellow), to realize a visual geometric comparison. If looking on the profiles from the pitch circle out to the addendum circle, one can observe that profiles defining the  $z=19$  tooth approach each other faster at the addendum, thus, the tooth tip sharpens faster. Now if looking on the profiles from the pitch circle to the root circle, the observed tendency is the decreasing of the dedendum width teeth number. (see the magenta profiles) That decrease causes the weakening of the tooth root.

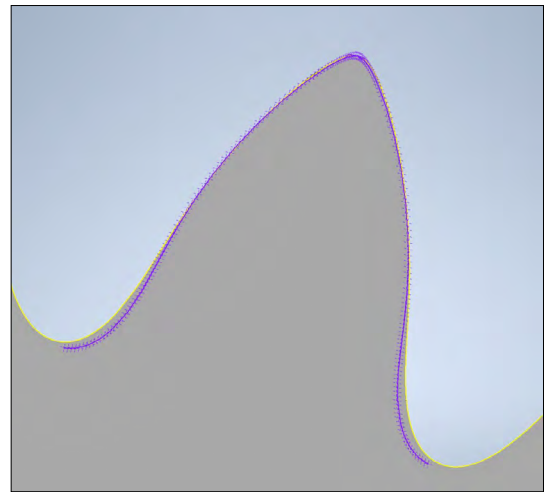


Figure 14. The influence of tooth number on the shape of the profile

**4.3. Comparison of involute and cosine profiles**

The involute profiles of the involute gear pair were drawn in the Mathcad environment. They consist of an involute arc and a root fillet. The last is a looped involute drawn by the tip of the generating edge of the involute rack (if considering a simplified rectilinear rack tooth). The profiles were overlapped using the axis  $y$  as symmetry axis of the tooth together with their pitch circle points. The calculus of the involute profile can be found in a very large number of publications thus it is omitted here.

Figures 16 and 17 show the profile comparison in the CAD environment. In both cases the involute tooth root fillet curve produces a weaker tooth root than the cosine tooth root. If analyzing the tip geometry, it is obvious that cosine gear tip width in both cases is smaller than involute tip width.

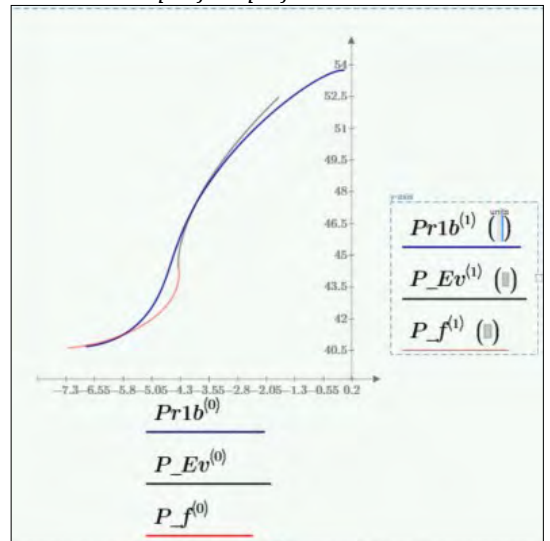


Figure 15. The cosine and involute profiles.

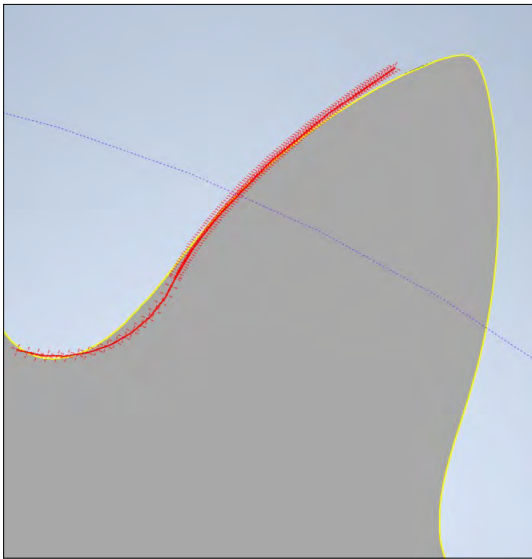


Figure 16. Case of  $Z=19$ .

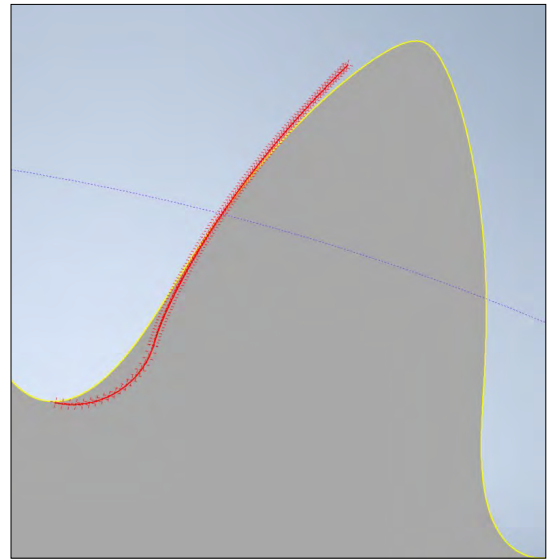


Figure 17. Case of  $Z=27$ .

## 5. Conclusions

The synthesis of a cosine gear pair requires identical generating racks thus their cutting with a single cosine planning comb is possible.

Tooth number has a significant influence on the tooth profile shape.

Root width increases with the number of teeth. The cosine gear tooth root's rigidity is always higher than that of the involute tooth. This will probably lead to a more extended lifetime of the gear pair.

At small tooth numbers, cosine gears are susceptible to tip sharpening.

## References

- [1] Shanming Luo, Yue Wu, Jian Wang: *The Generation Principle and Mathematical Models of a Novel Cosine Gear Drive*. Mechanism and Machine Theory, 43 (2008) 1543–1556.
- [2] Pálfi K., Prezenszky T., Csibi V., Antal B., Gyenge Cs., Balogh F.: *Fogazott alkatrészek tervezése, szerszámai és gyártása*. Gloria Kiadó, Kolozsvár, 1999.
- [3] Tolvaly-Roşca F.: *A számítógépes tervezés alapjai: AutoLisp és Autodesk Inventor alapismeretek*. Erdélyi Múzeum-Egyesület, Kolozsvár, 2009. <https://doi.org/10.36242/mtf-07>
- [4] Máté M.: *Hengeres fogaskerek gyártószerszámai*. Erdélyi Múzeum-Egyesület, Kolozsvár, 2016. <https://doi.org/10.36242/mtf-12>
- [5] Hollanda D.: *Aşchiere și scule*. Reprografia. I.I.S.Tg.Mureş, 1994. 234–240.
- [6] Szeniczei L.: *Az általános fogazás*. Nehézipari Műszaki Könyvkiadó, Budapest, 1958. 49–50.
- [7] Máté M.: *Az egyenesfogú metszőkerék szer számkapcsolószögének optimalálása*. Műszaki Tudományos Füzetek – FMTÜ I. (1996) 12–15. <https://doi.org/10.36243/fmtu-1996.03>



# COVERING ELEVATOR DOORS AND DECORATIVE ELEMENTS WITH A PROTECTIVE FILM

Gábor REZES,<sup>1</sup> Ferenc SZIGETI<sup>2</sup>

<sup>1</sup> University of Nyíregyháza, Institute of Technical and Agricultural Sciences, Nyíregyháza, Hungary, [rgaborezes@gmail.com](mailto:rgaborezes@gmail.com)

<sup>2</sup> University of Nyíregyháza, Institute of Technical and Agricultural Sciences, Nyíregyháza, Hungary, [szigeti.ferenc@nye.hu](mailto:szigeti.ferenc@nye.hu)

## Abstract

In today's world, in order to maintain competitiveness, all companies strive to meet deadlines and sell their products to their customers in the best possible quality. Also, they want to produce these products as cheaply as possible. This is no different in the elevator industry. At Wittur Hungária Kft., we produce thousands of elevator doors or their decorative elements every year, which must be provided with a protective film on a painted or structured surface, thus ensuring that the customer receives the quality product they expect. The main reason for the design of the machine is to speed up and automate the foiling process, while increasing productivity and reducing costs. Therefore, we set out to design a machine with which we can make the work of the workers easier and faster, since this operation is currently carried out manually, and we also ensure a consistent quality with the least possible human intervention.

**Keywords:** *elevator, foiling machine, machine design, finite element method, automation.*

## 1. Limitations of Current Technology and Advantages of Planned Development

Currently, our company relies on a completely manual process for foiling elevator doors and decorative elements. This requires the worker to guide the foil by hand and cut it manually to size. The process is further complicated by the fact that the worker must walk alongside the stand, causing discomfort and fatigue. The new foiling machine will not only streamline the process and improve productivity, but it will also enhance ergonomics and raise the standard of work.

The limitations of our current technology also make it difficult to apply foil to wider or taller elements that hang off the table. To ensure full coverage, extra foil must be used, and the element must be moved several times, significantly slowing down the foiling process. With the new machine, we can overcome these limitations and achieve faster and more precise foiling.

The current manual foiling process only allows for one element to be covered at a time. However,

with the new design, up to four elements can be foiled in a single cycle, resulting in increased productivity and reduced operation time (**Table 1.**).

Currently, the quality of the foiling process is inconsistent, often resulting in wrinkled or stuck film and unnecessary film usage. Workers may also cover elements at an angle, requiring multiple foils and increasing costs while also harming the environment. The new machine will improve the quality of foiling by ensuring precise and even coverage while reducing the amount of film used.

**Table 1.** *Current technology*

Technology parameters	Current foiling	Machine foiling to be introduced
Productivity	2 pcs/min	3-4 pcs/min
Maximum width	795 mm	1000 mm
Maximum element length	2450 mm	3300 mm



### 1.1. Detailed presentation of current technology

To begin the manual foiling process, the worker places the item on the foiling table and positions it in front of the foil roll. The worker must ensure that an adequate amount of protective foil is applied to both the top and sides of the element, using both foils for larger elements. Next, the worker pulls the foil over the element and smooths it along the edges, repeating this process for larger elements until they are completely covered. Once the element is covered, excess film is cut by hand using a scalpel, and the film is then smoothed on the other side of the element (Figure 1.) [1].



Figure 1. Current technology.

## 2. Creation of the construction of the new machine

The construction of the new foiling machine began with the tallest and widest door produced by the company, which measures 3020 mm in height and 930 mm in width. To ensure that the machine can accommodate elements of all sizes, it has been designed with slightly larger dimensions (Figure 2) [2]. This will ensure that the protective film can be applied to elements of any size without any issues.

### 2.1. The design and requisitioning of the table

To assess the feasibility of the new foiling machine, a thorough analysis of its structural integrity using the finite element method was conducted. The analysis was performed under different loading conditions, including the weight of several elevator doors and other potential loads [3].

In order to simplify the calculations, in this part of the study I have not shown the assembly to be presented later but during the verification, the load resulting from the weight of the specific kit as a distributed load was taken into account as a distributed load (Figure 3) [3].

The analysis revealed that the rack is not overloaded even when both specific kits are located in the center of the rack, with a maximum tension of:  $3.68 \text{ N/mm}^2$ . Furthermore, as shown in Figure 4 [3] the deflection of the structure barely reaches 0.1 mm.

In examining the results (Table 2) it is notable that the average panel (Figure 5) [3], has almost the same maximum compressive stress ( $4.26 \text{ N/mm}^2$ ) as the largest panel ( $4.27 \text{ N/mm}^2$ ) (Figure 6) [3].

This may seem counterintuitive, but it is possible because the larger panel lies on a larger

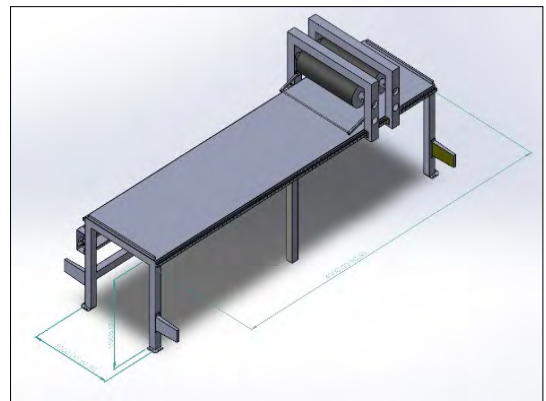


Figure 2. Foiling machine.

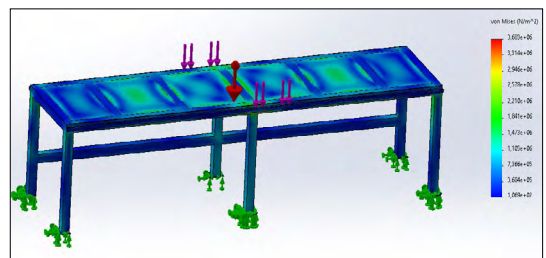


Figure 3. Table load at idle.

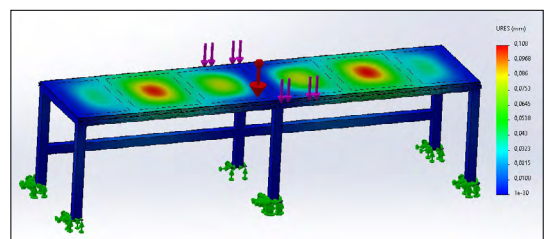


Figure 4. Table deflection in idle.



surface, and its weight can be distributed over a larger area, placing the load on more stiffening ribs, which in turn reduces the load on individual elements.

Additionally, when subjected to another load case where four 80-kilogram individuals sit on the structure (Figure 7) [3] the data shows that the structure is not critically loaded.

**Table 2.** The stresses of the table in the case of different loads

	Average elevator door	The largest elevator door
Pressure tension	4.27 N/mm <sup>2</sup>	4.26 N/mm <sup>2</sup>
Displacement / bending	0.18 mm	0.112 mm
	Load at idle	In the case of other loads
Pressure tension	3.68 N/mm <sup>2</sup>	4.27 N/mm <sup>2</sup>
Displacement / bending	0.108 mm	0.18 mm

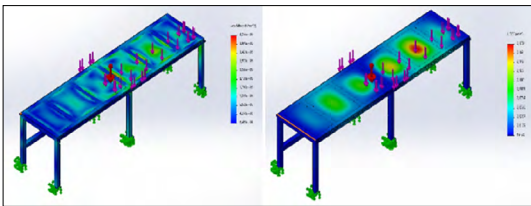


**Figure 5.** For an average lift door load.

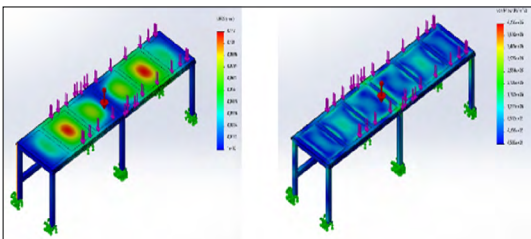


**Figure 6.** For the largest lift door load.

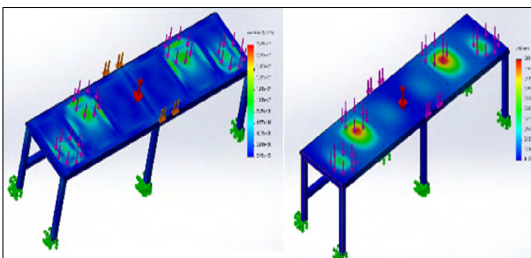


**Figure 7.** In case of other loads.

## 2.2. Specific kit design and loads

The specific kit's purpose is to guide and secure the foil, and it will also house the roller responsible for smoothing the foil (Figure 8) [2].

The loads on the specific kit include its own weight, the foil roll support shaft, bushings, and bearings, as well as the weight of the foil roll and the force required to pull it down.

To determine the force needed to peel off the foil, a spring-loaded force meter was used at various pull-off angles. The force required was found to be 15 N, with a maximum force of 20 N. Therefore, the maximum force of 20 N when calculating the loads was accounted for.

The maximum compressive stress on the specific kit was 1.032 N/mm<sup>2</sup> (Figure 9) [3]. However, due to its dimensions, it is over-insured. In later versions, we will strive for weight reduction while maintaining its strength. Although the kit is relatively long, the largest deflection in the middle is still less than 0.01 mm (Figure 10) [3] which is within more than an acceptable range.

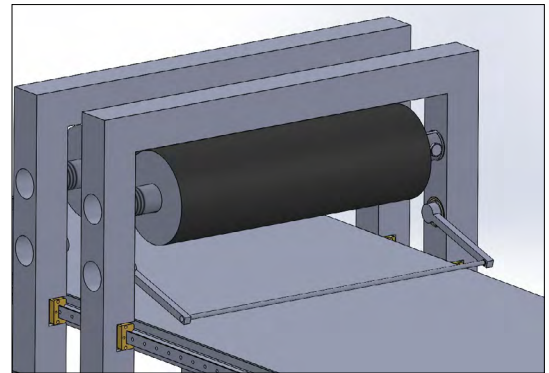


**Figure 8.** Specific kit.

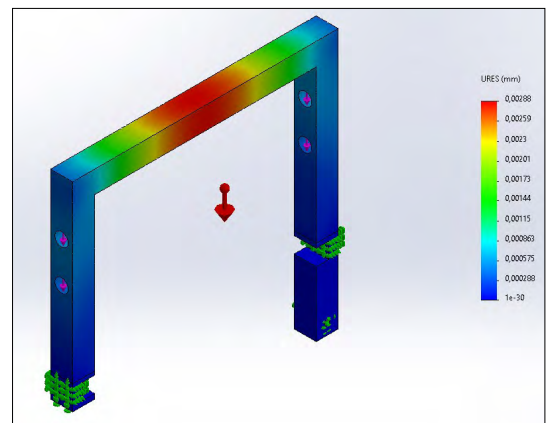


**Figure 9.** Specific kit's bending Figure

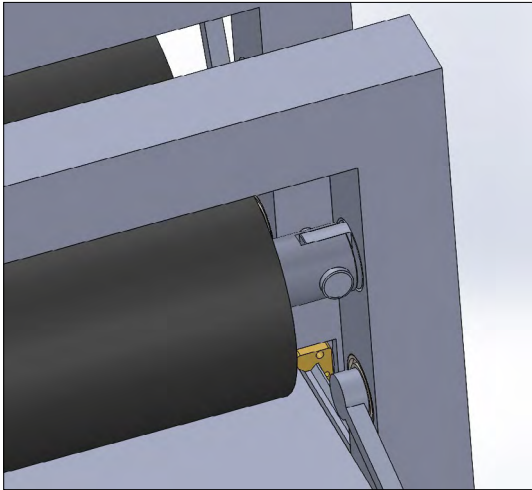


Figure 10. Rotating shaft

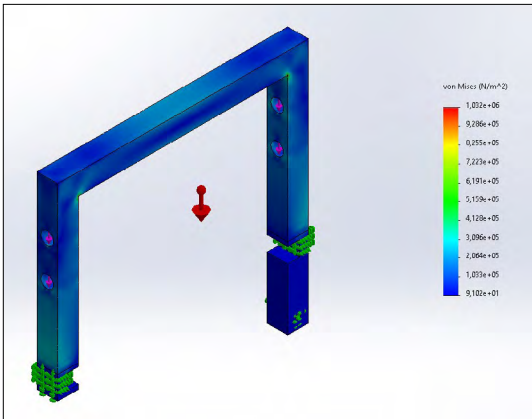


Figure 11. Specific kit's pressure tension Figure

### 2.3. Operation of the specific kit

The worker places the item to be foiled on the table, guides the foil under the smoothing roller, and threads it between the clamping jaws on the table. The operator then starts the machine, which unrolls the film from the roll by capturing it. The smoothing roller moves with the specific kit to smooth the foil. Once the covering is complete, the worker cuts the film that extends beyond the element and removes the element.

To increase productivity, two specific kits are placed on both sides of the machine, which move together. After foiling one element, the worker threads the foil on the other side and starts the specific kit in the other direction by pressing a button, foiling the next element.

To replace the coils, a rotating shaft was implemented (Figure 11) [2]. One end of the shaft is equipped with a joint that can be easily folded out to change the coils, and the other end has an easily removable clamping ring.

### 2.4. Specific kit inserts

The specific-kit-inserts are essential to facilitate the connection of the linear carriages to the specific kit. If the assembly consisted only of hollow sections, the carriage would only be able to rest on the wall thickness of the hollow section, which would not allow for safe and stable movement of the carriage.

The specific-kit-insert 02 (Figure 12) [2] will contain the necessary surfaces to grasp the ball nut. This part will be connected to the ball screw and ball nut, transferring the necessary movement for foiling. The specific-kit-insert 01 (Figure 13) [2] will assist in guiding the opposite side.

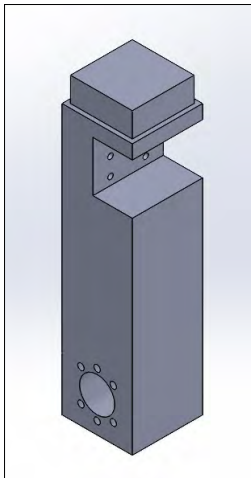


Figure 12. Specific-kit-insert 02.

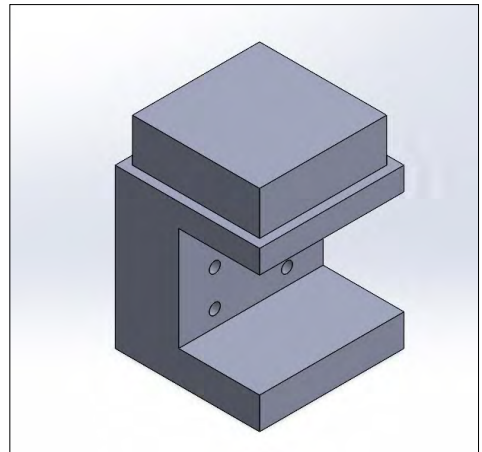


Figure 13. Specific-kit-insert 01

### 3. Dimensioning of linear line and linear carriage

The specific kit slides on the linear wire with the help of linear carriages. The linear carriages are fastened to the specific kit with 6 pcs M10 screws, thus ensuring a connection with adequate strength (Figure 14) [2].

The linear wire is loaded by the weight of the specific kit when idling, but during foiling, pulling off the foil also exerts some force on the linear wire (Figure 15) [2].

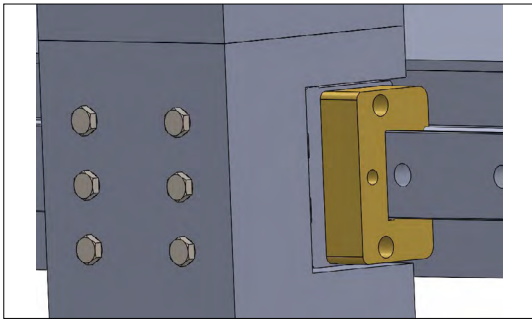


Figure 14. Kit insert and linear carriage.

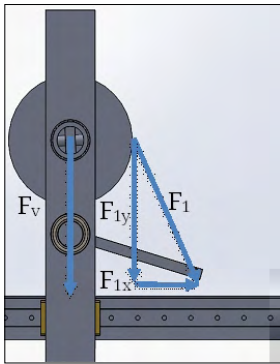


Figure 15. Linear wire's load.

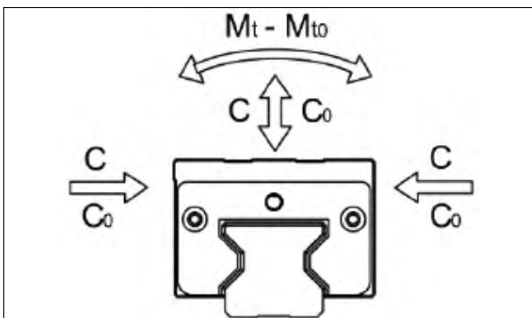


Figure 16. Linear carriage's load capacities. [4]

Maximum load of linear carriage:

$$C_{max} = 53\,000\text{ N} \quad [4]$$

$$F_{1y} = F_1 \cdot \sin \alpha$$

$$\rightarrow F_{1y} = -20\text{ N} \cdot \sin 20^\circ$$

$$\rightarrow F_{1y} = 6.84\text{ N}$$

$$C = (m_{kit} + m_{foil} + m_{other}) \cdot g \cdot F_{1y}$$

$$\rightarrow C = (42.5\text{ kg} + 7.5\text{ kg} + 5\text{ kg}) \cdot 9.81\text{ m/s}^2 \cdot 6.84\text{ N}$$

$$\rightarrow C = 546.39\text{ N}$$

where:

$C_{max}$ : linear carriage's load capacity

$C$ : load

$F_1$ : force required to peel off the foil

$\alpha$ : foil peel-off angle

$m_{kit}$ : specific kit weight

$m_{foil}$ : weight of foil roll

$m_{other}$ : machine components and the weight of the smoothing roller

$g$ : gravity acceleration

$$C < C_{max} \rightarrow C = 546.39\text{ N} < C_{max}$$

Ergo the chosen linear carriage is suitable.

### 4. Ball screw and ball nut sizing

A golyósorsót az elhanyagolható axiális terhelések miatt csak a kritikus fordulatszámra méretezem (katalógusadatok és képletek alapján).

$$n_{max} = f \cdot \frac{dr}{L^2} \cdot 10^7$$

$$\rightarrow n_{max} = 21,9 \cdot \frac{29,825\text{ mm}}{4000\text{ mm}^2} \cdot 10^7$$

$$\rightarrow n_{max} = 408 \frac{1}{\text{perc}} = 6,8 \frac{1}{s}$$

where:

$n_{max}$ : maximum rpm

$f$ : coefficient determined based on the mounting method of the ball screw

$d_c$ : axle core gauge

$L$ : mounting distance

The maximum speed, calculated with 32 mm pitch:

$$v_{max} = n_{max} \cdot P$$

$$\rightarrow v_{max} = 6,8 \frac{1}{s} \cdot 32\text{ mm}$$

$$\rightarrow v_{max} = 217,6 \frac{\text{mm}}{s}$$

The required speed is the one at which the desired productivity is achieved. For this, the time required to wrap one element can be 15 s ( $t_{max}$ ). To calculate the required speed, a 2200 mm ( $l$ ) long door panel is used as a basis.

$$v = \frac{l}{t_{max}} \rightarrow v = \frac{2200 \text{ mm}}{15 \text{ s}} \rightarrow v = 146 \frac{\text{mm}}{\text{s}}$$

$$v < v_{max} \rightarrow v = 146 \frac{\text{mm}}{\text{s}} < v_{max}$$

Ergo the chosen ball screw is suitable.

## 5. Engine selection

To choose the appropriate motor, we first need to determine the maximum load force (Figure 7) [2]. This force is the sum of the friction force resulting from the weight of the specific kit and the force required to peel off the foil. Once we have calculated the load force, we can determine the required torque and choose a suitable motor. For this project, a stepper motor will be the best choice due to its torque retention and provision of additional automation options.

### 5.1. Determination of the forces and torque loading the motor

$$F_v = (m_{kit} + m_{foil} + m_{other}) \cdot g$$

$$\rightarrow F_v = (42.5 \text{ kg} + 7.5 \text{ kg} + 5 \text{ kg}) \cdot 9.81 \text{ m/s}^2$$

$$\rightarrow F_v = 539.55 \text{ N}$$

$$F_s = F_v \cdot \mu \rightarrow F_s = 539.55 \text{ N} \cdot 0.2$$

$$\rightarrow F_s = 107.91 \text{ N}$$

$$F_{1x} = F_1 \cdot \cos \alpha \rightarrow F_{1x} = 20 \text{ N} \cdot \cos 20^\circ$$

$$\rightarrow F_{1x} = 18.79 \text{ N}$$

$$F_t = F_s + F_{1x} \rightarrow F_t = 107.91 \text{ N} + 18.79 \text{ N}$$

$$\rightarrow F_t = 126.9 \text{ N}$$

$$M = d/2 \cdot F_t \rightarrow M = 0.032/2 \cdot 126.9 \text{ N}$$

$$\rightarrow M = 2.0272 \text{ Nm}$$

where:

$F_v$ : force due to the weight of towed elements

$F_s$ : friction force

$\mu$ : sliding friction coefficient

$F_t$ : load

$M$ : torque

$d$ : diameter of ball screw

Since it is necessary to move two kits, double this value must be taken.

Ergo:  $2.0272 \text{ Nm} \cdot 2 = 4.054 \text{ Nm}$

Therefore, the following was chosen: NEMA 34 (6.6 Nm) [6] ( $M_{max} = 6.6 \text{ Nm}$ ) type engine (Figure 18, 19).

## 6. Conclusions

During the verification of the design of the construction, after evaluating the finite element method, it was found that the structure is very over-dimensioned, so in the next period economical production/design will become the focus.

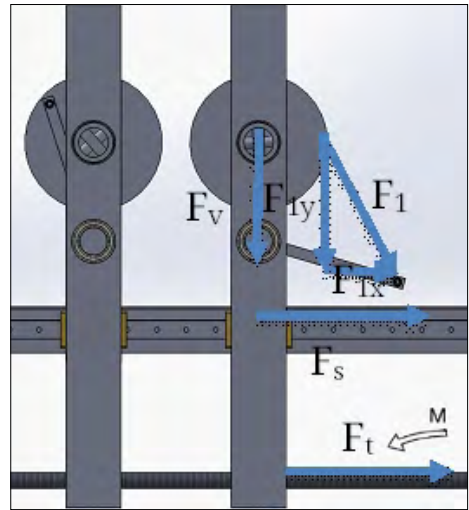


Figure 17. Engine's loads.



Figure 18. NEMA 34 type motor

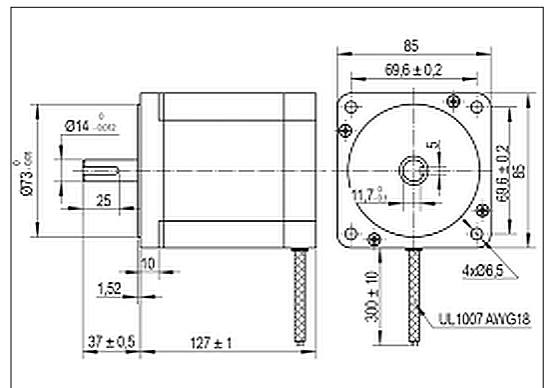


Figure 19. A NEMA 34 type engine drawing [6]

During the selection of the various sub-assemblies, such as the linear line or the linear carriage running on it, it is found that an operator can operate these units with very low utilization, since the loading forces also assume low values. However, during further sizing, it was established that, for example, when determining the maximum speed and RPM, the ball screw and ball nut can be operated with almost maximum utilization, due to the large length.

In future, additional parts of the assembly, inserts and bushings, which are necessary for proper operation, must be designed. As well as the conditions for safe work, the machine must therefore be equipped with light gates, protection against contact and jamming, and protection against overload.

Furthermore, we selected full automation as a development direction. This means that, apart from the replacement of the foil roll and the one-time threading, all operations need to be automated. This requires an automatic cutting system so that the worker only has to do material handling. To cut the film, a cutting system and path must be planned and programmed. Therefore, we would like to introduce an easy-to-use, programmed PLC with a touch screen. With this, it is intended that the worker will be able to perform the foiling with a few touches, in the shortest possible time.

Alternative foiling methods are being investigated, a hot air blowing system has been formulated, with which we could also cover elements with more complex shapes and characteristics with a protective film. The system that provides this still needs to be developed and additional structural solutions have to be found.

### Acknowledgements

Publication of this article was supported by the Scientific Council of University of Nyíregyháza.

### References

- [1] Wittur Hungária Kft. vizuális munkautasítás (letöltve: 2016.03.15)
- [2] Solidworks. <https://www.solidworks.com>
- [3] Solidworks Simulation. <https://www.solidworks.com/product/solidworks-simulation>
- [4] Power Belt: *Rosa Sistemi Hengergörgős megvezetés.* (letöltve: 2022.11.23) [https://www.powerbelt.hu/uploads/source/catalogs/5901\\_recirculating\\_linear\\_rollers\\_and\\_bearings.pdf](https://www.powerbelt.hu/uploads/source/catalogs/5901_recirculating_linear_rollers_and_bearings.pdf)
- [5] Power Belt: *Golyósorsó technikai katalógus.* (accessed on: 2022.11.23) [https://www.powerbelt.hu/uploads/source/catalogs/tbi\\_motion\\_golyosorso\\_technikai\\_katal%C3%B3gus.pdf](https://www.powerbelt.hu/uploads/source/catalogs/tbi_motion_golyosorso_technikai_katal%C3%B3gus.pdf)
- [6] Power Belt: *Bipoláris léptető motorok katalógus.* (accessed on: 2022.11.2) [https://www.powerbelt.hu/uploads/source/catalogs/6746\\_stepper\\_motor\\_catalogue.pdf](https://www.powerbelt.hu/uploads/source/catalogs/6746_stepper_motor_catalogue.pdf)



# VALIDATION AND CALIBRATION OF A MEASUREMENT SYSTEM FOR TESTING ELECTRIC MOTORS

Attila SZÁNTÓ,<sup>1</sup> Henrik András GARAI,<sup>2</sup> Éva ÁDÁMKÓ,<sup>3</sup> Gusztáv Áron SZIKI<sup>4</sup>

<sup>1</sup> University of Debrecen, Faculty of Engineering, Debrecen, Hungary, [szanto.attila@eng.unideb.hu](mailto:szanto.attila@eng.unideb.hu)

<sup>2</sup> DUniversity of Debrecen, Faculty of Engineering, Debrecen, Hungary,, [henrik.andras.garai@gmail.com](mailto:henrik.andras.garai@gmail.com)

<sup>3</sup> University of Debrecen, Faculty of Engineering, Debrecen, Hungary,, [adamko.eva@eng.unideb.hu](mailto:adamko.eva@eng.unideb.hu)

<sup>4</sup> University of Debrecen, Faculty of Engineering, Debrecen, Hungary,, [szikig@eng.unideb.hu](mailto:szikig@eng.unideb.hu)

## Abstract

The authors have been dealing with the modelling and simulation of electric vehicles and motors for many years. Knowing their electromagnetic and dynamic characteristics is essential for the simulation of electric motors. These data have to be determined experimentally because the manufacturers usually do not provide them. In the last two years, we have designed and realised a measurement system for testing electric motors at the Faculty of Engineering of the University of Debrecen. In this publication, we present the validation and calibration of the individual components of the above system, the applied methods and procedures, and the obtained results.

**Keywords:** *measurement system, electric motor, validation, motor test bench, sensors.*

## 1. Introduction

At the Faculty of Engineering of the University of Debrecen, we have been dealing with the simulation of electric vehicles and motors for many years [1, 2]. For the simulation of electric motors, it is essential to know the electromagnetic and dynamic characteristics of the motor. Manufacturers usually do not provide most of these, so it has to be determined experimentally. We have published several papers on this topic [3, 4]. In

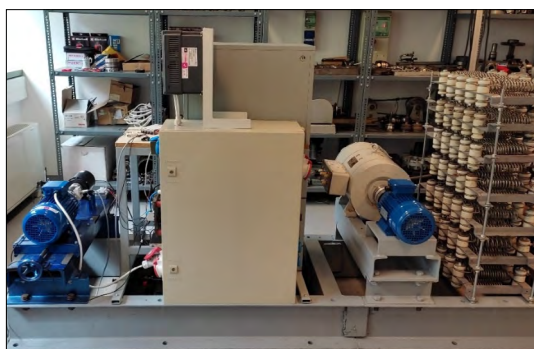


Figure 1. The self-developed measurement system [5]

the last three years, we have designed and built a motor testing measurement system (MS) (Figure 1). A detailed description of the system can be found in [5]. Now, we present the validation and calibration processes and methods regarding individual elements of the system and the results obtained during the research.

Firstly, the optical LED sensor was validated (Figure 2). We measured the RPM of a 2.2 kW

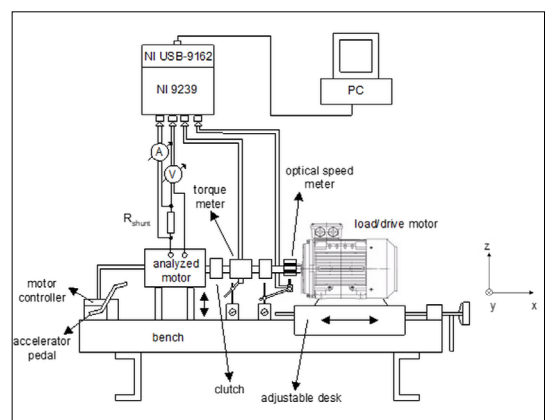


Figure 2. The schematic drawing of the measurement system [5]

three-phase asynchronous motor, which was part of the MS at that time as a drive motor. It should be noted that a motor can operate as a drive motor when fed with three-phase alternating current using a frequency converter or as a load motor when fed with regulated direct current. For the actual validation, on the one hand, we used the inbuilt frequency converter of the MS; on the other hand, a self-made device based on the principle of magnetic induction; additionally, a manual tachometer operating on the optical principle was used. The process is presented in Section 2.

Secondly, we determined the relationship between the intensity of the direct current flowing through a three-phase asynchronous motor – operated as a load motor – and the load torque exerted by it. Results are given in Section 3.

Lastly, we measured the total electrical resistance of the high-performance starting resistor used as the load resistor in the MS. Section 4 provides the details of the last test.

### 2. Validation of the optical LED sensor

In the MS, the angular speed is measured with an optical LED sensor (ROS-P, Monarch Instrument) which operates from 6 V direct current and outputs a voltage signal of 6V or 0V, depending on whether the light beam is reflected from the film strip placed on the rotating surface (the shaft of the motor) to the sensor or not. The maximum angular speed which the sensor can measure is 250000 RPM. Applying more than one strip this maximum value is reduced. The optical LED sensor and its typical output voltage signals can be seen in Figure 3. [5]

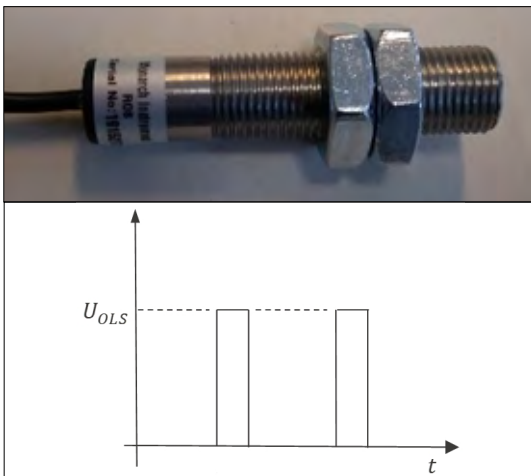


Figure 3. The optical LED sensor and its typical output voltage signals. [5]

The output voltage signals are counted by the software component of the MS [6] implemented by our research group in NI LabVIEW. Simultaneously, the angular velocity is calculated from the number of strips ( $N_{strip}$ ) – placed on the circumference of the shaft – and the voltage signals ( $N_{signal}$ ), detected during a short  $\Delta t$  time with the formula given below [5]:

$$\omega = \frac{2\pi}{\Delta t} \cdot \frac{N_{signal}}{N_{strip}} \tag{1}$$

The device was validated using several independent methods:

- Compare the measured values to the ones that are set and displayed on the frequency converter.
- Compare the measured values to those provided by a homemade device that works on the principle of magnetic induction. We attached a permanent magnet to the shaft of the motor, which then passes in front of a coil and induces a voltage at every turn. The terminals of the coil were connected to the NI 9239 analog-digital voltage module, which measures the induced voltage as a function of time. The RPM can be determined from the number of voltage signals generated during a given period.
- Compare the measured values to those measured by a manual optical angular speed meter (type: DT2234C+, measurement range: 2.5-99999 RPM, accuracy:  $\pm 0.05\% + 1$  digit).

Table 1 contains the rotational RPMs measured by the methods mentioned earlier:

Table 1. The measured RPM values

The values set on the frequency converter:	5 Hz (300 min <sup>-1</sup> )	10 Hz (600 min <sup>-1</sup> )	20 Hz (1200 min <sup>-1</sup> )	30 Hz (1800 min <sup>-1</sup> )	40 Hz (2400 min <sup>-1</sup> )	50 Hz (3000 min <sup>-1</sup> )
The value measured with the optical LED sensor (1/min):	291	585	1187	1789	2390	2983
The value measured using the magnetic induction principle (1/min):	291	587	1188	1788	2390	2992
The value measured with a manual optical tachometer (1/min):	292	587	1187	1789	2390	2991

Based on the measurement results, it can be stated that the RPM values set by the frequency converter – where the accuracy is 0.01 Hz – are slightly higher than the RPM values measured by the other three methods. However, the values measured by the last three methods are consistent. It should be noted that measurements based on the optical principle only result in accurate outcomes if the reflective strip(s) placed to the circumference of the motor's shaft is wholly separated from its surface. A surface that is too bright or uneven can easily distract the sensor. The most significant relative deviation is within 0.5%; thus, it can be concluded that all three methods are suitable for measuring the RPM with sufficient accuracy. The advantage of optical angular speed measurement is that it does not affect the motion of the rotating object being examined in the slightest way.

### 3. Determination of the value of the load resistor

In the MS, the load resistor is a high-power starting resistor used in trams (Figure 4). The coiled resistance wires are mounted on eight separate boards, which are attached to the base of the MS with the help of four threaded rods. Our goal was to determine the electrical resistance of the entire system, that is, the maximum applicable load resistance, which can be later reduced to the desired magnitude.

Measuring the resultant resistance of the entire system (Figure 5), which is a relatively high value, can be accomplished using a digital multime-



Figure 4. The load resistor. [5]

ter. However, when the individual smaller partial resistances within the system are measured, the following measurement setup is recommended. The voltage across the partial resistance is measured, and the current flowing through it is determined from the voltage measured on a shunt resistor. The measured voltage and current ratio gives the value of the sought electrical resistance.

Based on the measurement, the load resistance of the entire system is 7.2  $\Omega$ . The advantage of using a high-power load resistor is that it only heats up to a negligible degree, even at high current levels.

### 4. Determination of the relationship between the torque exerted by the load motor and the intensity of the current flowing through it

Using the asynchronous motor as a load motor, it is fed with a regulated direct current. The intensity of the direct current can be regulated by the control panel of the MS. As the intensity of the current increases, the loading torque of the motor increases proportionally. However, it is essential to ensure that the current intensity does not exceed the rated current intensity of the motor for an extended period, as this can cause damage to the motor.

Our goal was to determine the loading torque associated with different current values. During the experiments, the load motor was connected to a torque sensor via a rotating shaft and was driven by another motor (Figure 2.). Afterwards, we increased the current flowing through the load motor in small steps, and for each current value,

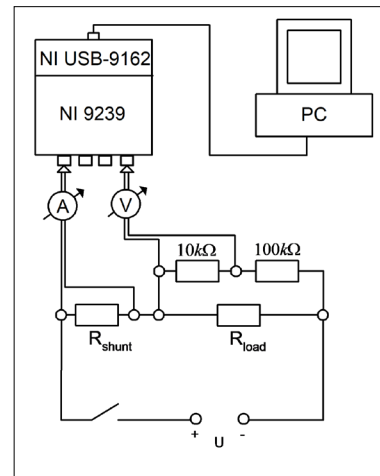


Figure 5. Measurement setup for measuring low partial load resistances.

we read the value indicated by the torque sensor attached to the rotating shaft. In this way, we determined the torque-current characteristic of the load motor.

Unfortunately, due to the failure of the torque meter, we could not perform the measurements yet.

## 5. Conclusions

We validated the MS's built-in optical angular speed meter using two independent methods during the above-described experiments. The relative deviation of the RPMs measured by different devices was less than 0.5%. Thus, the device we installed can be used with appropriate accuracy to measure the angular speed of electric motors in the tested range of 0-3000 RPM.

We determined the total electrical resistance of the starting resistor used as a load resistor and provided a procedure for precisely measuring its partial resistances.

We provided a procedure for measuring the current-load torque characteristic of the load motor. However, unfortunately, due to the failure of the torque meter, the measurements cannot be finished.

## Acknowledgement

„Supported by the ÚNKP-22-3 New National Excellence Program of the Ministry for Culture and Innovation from the source of the national research, development and innovation fund.”

"The research was supported by the thematic excellence programme (TKP2020-NKA-04) of The Ministry for Innovation and Technology in Hungary."

## References

- [1] Szántó A., Hajdu S., Sziki G. Á.: *Dynamic Simulation of a Prototype Race Car Driven by Series Wound DC motor in Matlab-Simulink*. Acta Polytech. Hung, 17/4. (2020) 103–122.
- [2] Sziki G. Á., Szántó A., Mankovits T.: *Dynamic Modelling and Simulation of a Prototype Race Car in MATLAB/Simulink Applying Different Types of Electric Motors*. International Review of Applied Sciences and Engineering, 12/1. (2021) 57–63.
- [3] Sziki G. Á., Sarvajcz K., Kiss J., Gál T., Szántó A., Gábora A., Husi G.: *Experimental Investigation of a Series Wound Dc Motor for Modeling Purpose in Electric Vehicles and Mechatronics Systems*. Measurement, 109. (2017) 111–118.
- [4] Szántó A., Kiss J., Mankovits T., Sziki G. Á.: *Dynamic Test Measurements and Simulation on a Series Wound DC Motor*. Applied Sciences, 11/10. (2021) 4542.
- [5] Sziki G. Á., Szántó A., Kiss J., Juhász G., Ádámkó É.: *Measurement System for the Experimental Study and Testing of Electric Motors at the Faculty of Engineering University of Debrecen*. Applied Sciences, 12/19. (2022) 10095.
- [6] Ádámkó É., Szántó A., Sziki G. Á.: *Software Developments for an Electric Motor Test Bench Developed at the Faculty of Engineering of the University of Debrecen*. In IOP Conference Series: Materials Science and Engineering. 1237/1. (2022) 012012.



# CASE STUDIES FROM THE LAST 5 YEARS' RESTORATION PROJECTS OF HISTORIC MONUMENTS IN SOPRON

Sándor TÁRKÁNYI

*University of Sopron, Faculty of Wood Engineering and Creative Industries. Sopron, Hungary.  
tarkanyi.sandor@uni-sopron.hu*

---

## Abstract

During the period between 2017 and 2022, the facades of 25 buildings were renovated within the framework of the Modern Towns Program in Sopron. Due to the development supported by the Hungarian Government, the Lenck House was born again and a Museum Quarter was established by the joint opening of the buildings at 6-7-8 Fő tér. This study describes the restoration process of the facades of three historic buildings, giving an insight even into the processes of authorization and execution. The aim is to present the work of the Hungarian authorities in the field of the protection of historic monuments (with special regard to Sopron), and to highlight the results of such renovations of historic buildings that have been carried out lately.

**Keywords:** *historic monuments, Sopron, Modern Towns Program, restoration.*

---

## 1. Introduction

Among Hungary's towns, Sopron has the largest number of nationally protected monuments, which includes more than 400 pieces of real estate. Between 1945 and 1975, high quality research and restoration projects took place in the historic downtown, which received the Golden Prize for Monument Preservation from the F.V.S. foundation in 1975 [1]. The European quality, scientific monument preservation activity, managed by Ferenc Dávid art historian, continued up to the early 1990's.

Starting from 2001, the National Office of Cultural Heritage assumed authority over monument affairs, which was taken over by the local government agencies ten years later. Ferenc Dávid's and his followers' approach to the direction and methodology of local heritage protection is influential to this day.

From 2017 to 2022, the facades of 25 buildings were restored on Sopron as part of the Modern Cities Program. My study aims to briefly introduce and evaluate the restorations of the last five years through three examples.

## 2. Achievements of the Modern Cities Program in Sopron

The Modern Cities Program (henceforth: MCP) is a prioritized development program for major cities that provides a total of 4200 billion HUF for funding projects in 23 cities in Hungary. In Sopron, Prime Minister Viktor Orbán launched the MCP scheme on March 15, 2015. The footstone for the Sopron project was laid in 2017 at the mouth of Kolostor street.

The goal of the project is to guide the priorities of development in major cities. The restoration of historic buildings, esp. of the facades facing the streets, in the downtown area is an important element of the project in Sopron. Among the various projects, this study focuses on the restoration of historic buildings. [2]

The main criterion for choosing the buildings to be restored through the MCP was that they shall be municipal properties. At the outset of the program another scheme was suggested where private real estate renovation would also be financed by a third part state and third part municipal funding, but unfortunately this option was discarded due to the increased costs of the ongoing renovations.



The 25 buildings whose (mostly) street-facing façades were renovated through the program were, as follows: 1 Fő square, 2 Hátsókapu, 5 Orsolya square, 3 Petőfi square, 7 and 9 St. György street, 2, 4, 7, 15, 21 and 26 Templom street, 4, 8, 11, 12, 14, 16, 22-24, 26 and 28 Új street, 54-56 Várkerület. (see [Figure 1](#)).

In case of 22-24 Új street, which are the hospital building and the temple keepers building, on the right and left of the medieval community synagogue located in the courtyard, respectively, in addition to the street-facing façade, the two lateral façades visible from the street were also renovated, as per my suggestion. The MCP also financed the renovation of the Lenck villa (Deák square 1), currently housing a museum, and the creation of the Museum quarter (6-8 Fő square).

Based on wood preservation experts' reports, the roofing materials and roof structure of the buildings in 2 Fegyvertár street, 2 Hátsókapu, 4 Petőfi square and 56 Várkerület were in a very poor condition. Based on the decision of Sopron City's Municipality, the roof structure was fortified and the roofing replaced in 2 Hátsókapu and 56 Várkerület only. In case of 2 Hátsókapu, roofing replacement was limited to street-facing roof surfaces and chimneys.

In the following analysis, I will describe three building renovation examples, introducing the MCP process and achievements. I tried to choose examples that include roofing renovation. In the second example, earlier façade renovations were amended, and in the third house, earlier renovation results were revised and the façade appearance changed.



**Figure 1.** A MCP Building restorations within the baroque downtown area of Sopron. Bold lines represent the restored façades. (Drawing made by András Veöreös and Sándor Tárkányi).

### 3. Examples of MCP restorations in Sopron

#### 3.1. Façade renovations and partial roof- ing renovations in 2 Hátsókapu street, Sopron

The request for the Heritage Renovation Permit regarding the street-facing façade of the building was submitted by the Sopron City Municipality to the Government Agency of Győr-Moson Sopron County (henceforth: Government Agency) on February 13, 2017. The ARCHI.DOC Architectural Studio prepared the renovation documents in September 2016, coordinated by architect Dávid Józsa. The designs showed the existing and proposed street façades (both those facing Hátsókapu and St. György street), with details of the damages shown on the existing façades.

The following renovations were proposed for the building in 2 Hátsókapu:

- chimney renovations (7 instances);
- remedial chemical waterproofing of the wall footing;
- renovation of the street-facing portion of the roof, changing the roofing and flashings;
- plastering replacement in the ground floor, where it has separated from the wall, as well as reinforcing, repairing or replacing of the rest of the plastering;
- introducing repair (WTA) plaster on surfaces affected by soil moisture;
- repainting the façades;
- cleaning, reinforcing, complementing and treating the surface of the stonework on the façade to make them more hydrophobic;
- replacing the damaged roofing.

The Government Agency granted the Permit under the following four conditions:

- submitting the detailed designs, including the site inventory of the street-facing façades, prior to starting the renovation;
- colours, materials, structures and fixtures to be used during the renovation are to be pre-approved by the Agency, based on material or surface samples;
- designer to supervise the works during construction;
- stone fragments (gothic and baroque) on the façade are to be restored based on official stone restoration notices.

The contractor submitted the detailed designs and the site inventory on April 20, 2017, and the Government Agency approved them under

the condition that the original wall sections and stonework exposed earlier must be preserved (designs did not show all of these fragments.) The renovations did not start within a year and the owner did not ask for an expansion. Thus, the Municipality applied for another permit on March 5, 2018, with the earlier approved designs attached.

The new permit included three conditions:

- renovations require designer supervision and researcher guidance;
- sample plastering and colouring should be created on the façade surfaces and approved by the designer;
- restoration of the original façade stonework requires official stone restoration notices in each case.

On December 18, 2018, the Municipality gave heritage protection notice regarding the wall diagnostics of the building. Architect and historical and structural diagnostics expert Heléna Szecskó created the research plan. The Government Agency recognized the notice on December 19, and issued an official certificate.

On January 24, 2019, stonemason and restorer József Sütő submitted a stone restoration proposal regarding the stonework on the façade. In the 14-page proposal, the restorer describes the present state and the proposed cleaning, exposing, desalination, reinforcement, complementing, colouring and water repellent treatment processes. He also complemented the photographic documentation by a damage map of the stone surfaces of the façade. The Government Agency accepted the stone restoration notice on January 28, 2019.

The Municipality submitted the heritage renovation permit request for the a posteriori waterproofing of the façade of the 2 Hátsókapu building on February 25, 2019. Building renovation and insulation expert Erika Luthár prepared the renovation proposal, endorsed by Heléna Szecskó. The expert proposed that Oxal HSL siloxane micro-emulsion to be injected into the wall as horizontal water barrier. This requires a single row of drill-holes, spaced at 12 to 15 cm and drilled at an angle of 30 to 45°. The footing should receive an insulation coating of Oxal DS-HS sulphate resistant insulation sludge.

There was a heritage protection art historian and wall researcher inspection on February 20, 2019, with a reminder created. Art historian and wall researcher András Nemes, construction supervisor Tibor Eszes and structural engineer Richárd Degovics were present at the inspection. The researcher requested keeping a 50 to 60 cm

wide vertical strip of the original surface (witness strip) on the striated portion of the shorter façade section, from the level of the corner balcony, between the first and second windows. He also asked for 50 to 60 cm wide witness strips on the longer façade (Hátsókapu street) on the left and righthand side of the gate. The researcher also instructed that, except for the cement plaster of the footing, plastering must be removed by hand only, and that a 0.9 to 1.0 m wide witness plaster strip should be left in the upstairs lesene and parapet zone. Plastering replacement of the witness surfaces was possible on the go, in stages. András Nemes wanted to research the original colouring and paint in the plastered console surfaces of the enclosed balcony and the plastered mirror fields under the windowsills. To his knowledge, the building was painted with green engobe in the 1960's. The developer gave notice of commencing the renovation on February 26, 2019.

On the request of the contractor Szabó and co. Ltd., structural engineer Richard Degovics created a structural assessment of the roof structure and cracks in the façade and fascia. The assessment exposed problems in the roof structure and wall cracks, and suggested wall stitching to stop wall cracking, detailing the method to be applied.

Regarding the queen post trusses, the following recommendations were made:

- tying the lookouts to the wall plate using cramp irons;
- tying the rafters to the purlin using inverted cramp irons;
- incorporating a ridge beam and collar ties, as well as a collar beam for each roof truss;
- creating chimney trimmers;
- intermediate rafters wherever rafters are spaced at more than 85 cm;
- hacking away the top part of and strengthening rotted rafters;
- replacing the roofing materials.

Roofing included grooved tiles and rounded roof tiles on the courtyard wing and street facing roof, respectively. The assessment suggested using single grooved tiles on the street facing roof, for structural reasons (creating symmetric snow load instead of the earlier asymmetric situation.)

The contractor gave notice of eliminating the construction zone to the Government Agency on March 13, 2019. This was followed by another heritage protection inspection on March 13, requested by the authority in order to use traditional methods for plastering. According to the report, the contractor created the authentic façade col-

ouring, as identified by the art history research, based on the samples and designs recommended by the architectural designer, within one week.

Art historian András Nemes submitted his report regarding the colour investigations of downtown buildings 2 Hátsókapu, 9 St. György street and 54-56 Várkerület to the Government Agency, on April 9, 2019. Regarding the real estate in question, the researcher stated that the historical name of the building is 'Green House'. The house received ochre green colouring in the renovations of 1963/64, presumably based on its earlier colour. During this renovation, the house was stripped of its earlier plastering, and thus the exact colour before the 20th century is unknown. He suggested that the colours used in 1963/64 should be used again, as it appears presently.

The contractor submitted an alteration notice on March 11, 2019, regarding the roofing materials. Based on consultation with the heritage protection administrator, instead of the rounded tiles named in the budget and technical description, grooved Creaton "Róna" tiles were approved in natural (33%), antique (33%), and copper (33%) colours, laid randomly, using battens spaced at 26 cm. The heritage protection administrator approved the roofing after creating a sample surface of 2 square meters.

On March 28, 2019, the contractor submitted another alteration notice, this time regarding the plaster system to be applied. Instead of the Keim Porosan repair plaster named in the budget, he wanted to use the MC OXAL DS-HS insulation sludge up to a height of 1.5 metres (or 20 cm of above the adjacent terrain). Above this level, he wanted to use the LB-Knauf Eurosan plaster system. Above 1.5 m, LB-Knauf Kontakt sprinkle sub-plastering and Premium base were to be used. The administrator approved the alteration notice (Figure 2).

On April 11, 2019, the heritage protection administrator viewed the colour samples painted on the façade. Earlier, the Municipality requested a deep ochre colour to be used. After the viewing, the representative of the customer, chief architect Gergely Németh also discarded this concept. Eventually, the heritage protection administrator chose the base and insert colours from the various sample shades. On this they, the colour of the cast stone footing was also chosen. The pattern structure and colour of the cast stone footing was finalised and approved on April 29, 2019.

An official record regarding the façade painting and dismantling the scaffolding was created



**Figure 2.** Moulding the fascia of the St. György street façade of 2 Hátsókapu, using a mould knife (author's photograph).

on June 7, 2019, overseen by the representative of the Agency and that of the contractor. The heritage protection administrator inspected the completed façade paint and roofing materials from the scaffolding. The contractor has done first rate work, and thus the scaffolding could be dismantled (see **Figure 3**). The Agency's representative asked that pigeon spikes would be installed on the sill of the medieval stone window frames. The contractor accepted this job.

On May 7, 2020, the Municipality submitted a request to the Government Agency regarding the final acceptance of the street facing façade and roofing renovations of 2 Hátsókapu. The Agency issued the acceptance certificate on June 2, 2020.

### 3.2. Façade renovations of 16 Új street, Sopron

The Municipality submitted the permit request to the Government Agency regarding the street-facing façade of 16 Új street on December 5, 2016. Renovation plans were created by the A2 Architectural Studio, coordinated by architect Szilárd Fekete. In addition to the site layout, the design documents also included the assessment drawing of the existing façade (with damage map) and the renovation plans.

The architect proposed the following procedures as part of the façade renovation:

- replacing the damaged footing;
- remedial waterproofing against ground water by injection;
- removing the stucco above the footing and re-plastering using WTA plaster up to the windowsill level;



**Figure 3.** A section of the restored façade of the 2 Hátsókapu building, as seen from St. György street. (author's photograph)

- scraping the paint from the façade, creating a new skim coat layer using a tinted stone powder rub, followed by red lime plaster;
- painting the gutters;
- painting the street-facing window frames;
- replacing the bottom row of the roofing tiles and the mortar on the ledge and connections;
- staining the dormer window siding brown;
- stone structure renovations based on special restoration permit.

In the heritage protection permit, the Government Agency named five conditions:

- creating a construction plan and site inventory;
- renovations require designer supervision and researcher guidance;
- final colour selection should be based on colour samples;
- façade stonework restoration requires special restoration notice to be submitted.

The Municipality submitted the construction details, façade site inventory and scientific architectural history documentation on March 16, 2017. The Government agency approved the plans on April 3, 2017. Since the work didn't start within a year, the heritage protection permit expired.



A new request was submitted on March 6, 2018, and the Government Agency issued the heritage protection permit on March 9. The conditions were, as follows:

- providing designer supervision and researcher guidance;
- creating colour samples for final colour selection;
- submitting special restoration notice for façade stonework restoration.

The Municipality submitted the façade stonework restoration notice on October 4, 2018. Stonemason and restorer József Sütő prepared the stone restoration documentation, proposing that the stonework be cleaned, reinforced, and water repellent-treated. In the case of the bottom stone pillars of the gate, he proposed replacing them with identical stone blocks due to extensive salt damage. The Government Agency recognized the notice on October 8, 2018.

The Municipality gave notice of starting the renovations on February 22, 2019. The work zone was also created on the same day, documented by an official record.

The Municipality submitted the heritage protection request for the remedial waterproofing of the street-facing façade of 16 Új street on March

19, 2019. Building renovation and insulation expert Erika Luthár prepared the renovation proposal, endorsed by Heléna Szecsskó. The Agency approved the remedial waterproofing notice on April 11.

Approval of the wall colour, wooden door and window frame and hardware colouring transpired on July 31, 2019. The Municipality gave notice of completing the street facing façade renovations of 16 Új street on April 27, 2020. The Government Agency issued the official recognition certificate of completion on May 5, 2020.

The contractor deviated from the approved construction plan during the renovations on two occasions. Instead of using a tainted skim coat on the façade, they used white plaster, and instead of lime plaster they used paint. Due to the white skim coat, small façade damages show very prominently. The other deviation was a positive one, namely, installing new gutters instead of painting the old ones (Figure 4).

### 3.3. Façade renovations of 8 Új street, Sopron

The Municipality submitted the permit request to the Government Agency regarding the street-facing façade of 8 Új street on December 5, 2016. Renovation plans were created by the A2 Architectural Studio, coordinated by architect Szilárd Fekete. In addition to the site layout, the design documents also included the assessment drawing of the existing façade (including a damage map) and the renovation plans.

The architect proposed the following procedures as part of the façade renovation:

- replacing the damaged footing and installing a higher, ventilated footing, up to the level of the top of the basement windows' stone framing;
- remedial waterproofing against ground water by injection;
- removing the stucco above the footing and re-plastering using WTA plaster using flesh-coloured smooth stone dust plastering and textured stone dust plastering, up to and above the top of the windows, respectively;
- repainting the imitation s graffito corner stone details on the two edges of the building;
- witness surfaces will remain untouched on the façade;
- painting the gutters;
- replacing the bottom row of the roofing tiles and the mortar on the ledge;
- staining the dormer window siding brown;



**Figure 4.** The restored street-facing façade of 16 Új street (author's photograph)



–stone structure renovations based on special restoration permit.

In the heritage protection permit, issues on December 16, 2016, the Government Agency named five conditions, the same as listed for 16 Új street. The Municipality submitted the construction details and site inventory on March 6, 2017 to the Government Agency, which approved it on March 24.

Due to the expiration of the heritage protection permit, the Municipality submitted a new permit request on March 5, 2018. In the new permit, the Government Agency included three conditions:

- providing designer supervision and research-er guidance;
- creating colour samples for final colour selection;
- submitting special restoration notice for façade stonework restoration.

József Sütő prepared the stone restoration documentation, proposing that the stonework be cleaned, reinforced, and water repellent-treated. In case of the stone pillars of the gate, he proposed replacing them with identical stone blocks. The Government Agency recognized the notice on October 1, 2018. The Municipality gave notice of commencing the construction on October 8, 2018.

The Municipality submitted the heritage protection request for the remedial waterproofing of the street-facing façade of 8 Új street on March 19, 2019. Building renovation and insulation expert Erika Luthár prepared the renovation proposal, endorsed by Heléna Szecskó. In the documentation, the experts made the same recommendations regarding the methods and materials as for 16 Új street. The Agency recognized the remedial waterproofing notice on April 11.

Art historian András Nemes wrote an expert's report describing the witness surfaces on the façade on June 13, 2019. Ten days earlier, the author viewed the site along with contractor Gábor Baranyai, and researcher András Nemes. The report states that “Earlier created site inventory shows that the present stucco was created in 1961. So-called witness surfaces were created at that time, conserved for posterity. At the time of the 1990 façade renovation, witness surfaces were unfortunately not handled professionally. In addition to reinforcing them, they received a azure paint, which compromised their originality. Borders created around the edges of the original surfaces produced a map-like pattern. Their current appearance is rather distracting, since it interrupts the harmony of the façade. The very

understated harmony of the façade, ornamented with sgraffiti on the edges and in the window ledge zone, is disrupted by the witness surfaces.

In the expert report, the researcher makes the following suggestions:

- renovation (cleaning, conservation, restoration, minimal supplementing where needed) of the sgraffito-ornamented surfaces;
- after conservation, amorphous witness façade surfaces should be covered with the help of an expert restorer, to create an uninterrupted façade surface. This will create a pleasing façade appearance.

Based on the report, the contractor modified the materials and technologies to be used for the renovation, which was approved by the Agency. On July 10, 2019, the final colours of the façade were chosen based on the sample colouring applied to the façade earlier. This included the base colouring, as well as sgraffito, stone framework and main ledge colours.

The Municipality gave notice of completing the street facing façade renovations of 8 Új street on April 27, 2020. The Government Agency issued the official recognition certificate of completion on May 5, 2020.

Based on the results, errors and flawed decisions made in the earlier renovation of the building were corrected during the recent restoration. The street-facing façade went through exemplary restoration due to the contractor's conscientious and circumspect work and co-operation with the authorities and experts (**Figure 5**).



**Figure 5.** The restored street-facing façade of 8 Új street. (author's photograph)

#### 4. Conclusions

This study introduced three examples of the façade renovations completed in Sopron in the MCP program. The case studies show that the renovations, although mostly limited to street-facing façades, were properly prepared and expertly executed. Contractors co-operated with the authorities as well as experts during the renovations. Whenever the condition of the buildings required, they made extra efforts to get the de-

sired outcome. Thus, MCP façade renovations were successful from a heritage protection point of view.

#### References

- [1] Dercsényi Dezső: *Sopron műemlékvédelmi Európa-díja*, Soproni Szemle XXX/1. (1976) 39–46.
- [2] Gajzágó Gergő: *Modern városok programja: új fejezet a magyar várospolitikában*, Tér és Társadalom 33/3. (2019) 29–48.  
<https://doi.org/10.17649/TET.33.3.311>



# THE BAROQUE RENOVATION OF THE MEDIEVAL FRANCISCAN CHURCH OF JÁSZBERÉNY

Olivér TURI

*University of Debrecen, Faculty of Technology, Debrecen, Hungary. turioliver25@gmail.com*

---

## Abstract

This study discusses the Franciscan church in Jászberény, originally built in the Middle Ages. The methods of *Bauforschung*/building archaeology were used in the attempt to create a theoretic reconstruction of the church's former appearance, involving laser scanning and point cloud data. The re-search focused mainly on the attic space, more specifically, on the question of the former vaults of the church.

**Keywords:** *Baroque, Franciscan order, laser scanner, Jászberény, Gothic.*

---

## 1. The Investigation of the church

### 1.1. Historical background

The church that was examined in this research is the Friars' church of Jászberény, Hungary, which was originally part of the former Franciscan monastery. The town where the church is located is in the centre of the Jászkun region, which is now part of Jász-Nagykun-Szolnok county. The last part of the county's name likely comes from Ispan Szaunik (ispán), who is known as the companion of Gerard bishop in the Legend of Saint Gerard. Also, the first two components of its name could be derived from the Jász and Kun tribes, who were resettled in the area along the river Zagyva. [1] The Franciscan order supposedly began to convert the pagan people at the same time as the Dominican order. Evidence, such as the bulla of October 7th 1278 written by Pope Nicholas III supports this theory. This bulla entails the Franciscan order's work amongst the Kun tribes. Eventually, the Franciscan order achieved outstanding success in the integration of the Jász and Kun people. The construction of the church was feasible partially because of the economic growth during the reign of King Matthias I. Before starting the construction of the church, the Jász people asked King Matthias I for permission to build the church. This is proven by a copy of an authorised letter from the time. The letter is now preserved in the Vatican archives, it was sent by

King Matthias I to Pope Sixtus IV, and it was delivered in 1472 by a high-ranking figure of the Hungarian province of the Franciscan order, Fábíán Igali. Although there are no direct data available related to the construction of the church, recent art historical research suggests that there was a Franciscan construction workshop in Hungary, which also enjoyed the support of the royal court of Visegrád. [2] 15–17. p.

### 1.2. On-site inspection of the church

#### 1.2.1. The selection of the topic

Besides the personal connection, an important question played a main role in the selection of this church as a topic. The question came up several times in the related literature, and has not been answered in its entirety until now therefore this became the main question of my research. The question was, whether the church nave was originally vaulted, covered with a horizontal wooden slabs or had an open roof. Reviewing many of the publications related to the construction history, revealed no clear answer to this question. Therefore, it became the main starting point of this research. The research was conducted with the *Bauforschung*/building archaeology method, during which the building was considered the primary source of the study. The former Franciscan church of Jászberény has a single nave, with a polygonal sanctuary narrower than the nave,

with medieval walls that are supported from the outside by large stepped buttresses.

### 1.2.2. The medieval vaults

The most important observable trace in this regard is the plastering of the nave wall at a height of 2.15 m above the connection line of the current vault in the attic. We can treat it as a fact that in the Middle Ages, the church attics were not plastered. This leads to the conclusion, that the interior height of the nave was originally higher. This statement is also supported by the remains of a Gothic lancet window which was found on the South wall of the nave.

Moving towards the west side of the building the remains of two additional windows can be found. This makes it probable that the nave of the medieval church was illuminated by three windows from the southern side. Additionally, this makes it clear that the ceiling height of the church was indeed higher compared to its current state. Following this, a search was conducted for imposts and other signs on the wall that could indicate the past existence of vaults. However, there was no evidence to support the existence of these. Therefore, we can accept that the ceiling height of the church was 2.15 metres higher previously, but there are no indicators of former existing vaults.

In conclusion, it can be stated that the church indeed did not have vaults, there is another observation also supporting this. The space of the attic between the nave and the sanctuary is divided by a solid stone wall. This wall could have served as a firewall, to prevent the spreading of fire between the two spaces. Although when the whole body of the church is vaulted, this structure is not

absolutely necessary in this place. Since there were no remains of beams in either the North or in the South wall, the possibility of an open timber structure is more plausible. Although, there was no direct evidence to prove this assumption.

### 1.2.3. The examination of the western gable wall

During further examination of the attic, the building's west side gable wall was observed. It is known from the *Historia Domus* of the church, that the edges of the wall originally had a steeper angle, the top of the gable wall was blown off in the 18th century. Although the wall did not suffer major damages, the roof's angle of inclination had to be less steep, this also reduced the height of the walls.

While observing the gable wall several remarkable things can be noticed. First, there were three holes where beams might have been previously on both ends of the wall. What is more interesting, two bigger holes can be found under these. Above one of these bigger holes, a typically carved stone can be seen, which at first glance, looks like a lintel. On closer inspection, a wooden beam can be observed running through both holes in the West wall's Southern side. It is possible, that the bigger holes in the walls functioned as light sources for the attic.

### 1.2.4. The structural reinforcements of the walls

In the attic space tie rods can be observed, connecting the church's northern and southern walls and the transverse arches of the vault, to prevent the further outward shifting of the walls. On July



**Figure 1.** *The remains of the walled-up Gothic lancet windows located in the attic.*



**Figure 2.** *The three smaller holes and one bigger hole with a stone functioning as a lintel in the attic's gable wall.*



21<sup>st</sup> 1868 an earthquake caused immense damage to the building, then later in July, August and September further earthquakes shook the church.

According to contemporary descriptions, the building was on the verge of collapse. On the basis of the contract signed by the Franciscan order with the architect József Szódy, the installation of the tie rods began in October 1868, so repair of the suffered damages could begin with the contraction of the walls. These reparations were finished by the 10th of October.

### 1.2.5. The southern portal

A Gothic portal was discovered in the Southern wall of the nave in 1925. The portal's bottom is located 1.4 m deeper than the current floor level of the church. Later inspection revealed that the portal did not serve as an entrance to the crypt, as was originally assumed. Instead, the portal provided access from the monastery to the nave. [2] 35–51. p. The floor level had to be raised presumably because of its proximity to the Zagyva river. Since the monastery was built on a swampy area by the river, it had to be protected from groundwater, which might have been the reason for the raising of the floor level. In the issue of *Jász Hírlap* published on 30th December, 1939, József Komáromi published an article about the church. In that, he mentions that the newly discovered gate, which was found in good condition, was plastered by an enthusiastic painter working in the confessional corridor of the church. As a result, the gate suffered damages that could not be repaired even with restoration methods. [3]



**Figure 3.** *The tie rods connecting the walls, the vaults and the roof structure.*

## 1.3. The history of the church

### 1.3.1. The historical background of the Baroque renovation

Following the Ottoman conquest of Hungary and the Rákóczi War of Independence, the population of the Kingdom of Hungary did not show a large decrease - compared to the growth of other European countries it remained stagnated. Nationalities spread throughout the country during the resettlement policy of Leopold II Holy Roman Emperor and King of Hungary and Maria Theresa. However, an important aspect of the resettlement was that all the settled nationalities were Christian. This led to the growth of church communities, which entailed the need to expand churches.

### 1.3.2. Baroque reconstruction

The reconstruction of the church began in the 18th century. The reconstruction was influenced by the 95 theses nailed on the gate of the All Saints' Church of Wittenberg by Martin Luther on 31st October 1517. This act served as an indicator in the development of the reformation movement which swept across Europe. From an architectural point of view an important part of Luther's teachings was the preservation of medieval Puritan values. As a response, the Catholic Church launched a counter-reformation movement, which in its values was closer to the luxury represented by the Baroque. The transformation of the medieval parts of the church was mainly due to its ruin and destruction, but some elements were transformed due to integration into the Baroque style. Three respectively two large windows were installed on the North side of the nave and of the sanctuary, to let more light in. The importance of light played a major role in the new Baroque period, but because the interior's height was reduced due to the vaulting, the three Gothic windows on the south side of the nave had to be walled up. Smaller oval windows were installed in their place. The Gothic portal was walled up because the floor level had to be raised. In order to allow access, a new gate was built between the 2nd and 3rd pillars of the South wall facing West. According to the *Historia Domus*, the reconstruction of the tower started at the same time as the construction of the organ loft before 1715. The Baroque tower, built on medieval foundations, was probably completed in 1720, as the baroque tower spire was put on it at that time. Finally, the most characteristic Baroque transformation was



the creation of the organ loft, because the organ played an important role during ceremonies. The design of the organ loft is parallel to almost all medieval churches still in use today. In 1769, the vault of the sanctuary was replaced with a barrel vault, similar to that of the nave. In 1780, it attained the imposing baroque appearance expected by the Counter-Reformation. [2] 65–72. p.

## 1.4. The examination of the church

### 1.4.1. Laser scanner survey

3D laser scanning was conducted on the interior of the church building. This inspection was done with a Stonex laser scanner owned by the University of Debrecen Department of Civil Engineering. The scans were recorded from two positions in the sanctuary and from two positions in the nave, each of these produces recordings in 360° around the device.

During this process the scanner is mounted to a levelled stand, the device then emits laser beams around itself to its surroundings. These beams are projected back from the surface of the surrounding objects. From the time of the rebound, the device calculates the distance of the points, from which it can create a point cloud. Therefore, it is important to take scans from several different locations, because the system cannot obtain points from objects covered by others. These blind spots would lead to empty holes in the created point cloud. Following this, the recorded points are converted into PTX. format by using the scanner's system. After that a complete point cloud is created by piecing together the four partial point clouds in the software, CloudCompare. Further modifications were performed on the point cloud with the software Meshlab. Lastly, the completed model was cut in half with the use of the software Blender 3D, and the church interior's negative image was placed into a right prism to be prepared for 3D printing.



**Figure 4.** A three-dimensional model created by merging the points recorded with the scanner into a point cloud.

## 2. Conclusion

Based on the observations, the Baroque transformations of medieval churches can be divided into two groups: the transformations resulting from restoration, and those resulting from modernization. In addition, we can also talk about additive transformations, which involve expansion. Possibilities for research include the examination of other similar churches using the methodology developed here.

### Acknowledgement

I would like to thank Dr Zoltán Bereczki and Anita Bíró Edina for contributions, without them this article would not have been possible.

### References

- [1] Kristó Gy.: *Fejezetek az Alföld középkori történetéből*. Szeged: Dél-alföldi Évszázadok. Csongrád Megyei Levéltár, Szeged, 2003. 104–110.
- [2] Szántó K.: *A jászberényi ferences templom története*. Ecclesia. Budapest, 1974.
- [3] Komáromi J.: *Jász Hírlap*. In: Műemlékek Országos Bizottsága, 20/1940.

**SZERZŐK JEGYZÉKE**  
**LIST OF AUTHORS**

**A–B**

ASZTALOS GERGŐ TAMÁS 14  
ÁDÁMKÓ ÉVA 51  
BAKAI NÁNDOR 1  
BAKOS LEVENTE ATTILA 6

**D**

DIÓS SZABOLCS SÁNDOR 14  
DÓSA JÁNOS 22

**G–H**

GÁL KÁROLY-ISTVÁN 37  
GARAI HENRIK ANDRÁS 51  
GERGELY ATTILA LEVENTE 32  
HILLEBRAND PÉTER 1  
HUSI GÉZA 14

**K–R**

KERESZTES KRISTÓF 32  
MÁTÉ MÁRTON 37  
RÁK OLIVÉR 1  
REZES GÁBOR 44

**S–SZ**

SZÁNTÓ ATTILA 51  
SZIGETI FERENC 44  
SZIKI GUSZTÁV ÁRON 51

**T–Z**

TÁRKÁNYI SÁNDOR 55  
TOLVALY-ROSCA FERENC 37  
TURI OLIVÉR 63  
ZAGORÁCZ MÁRK BALÁZS 1

